THE EMERGENCE OF COLLECTIVE BEHAVIOR ON SOCIAL AND BIOLOGICAL NETWORKS

by

Adam Troy Charles Wilander

A dissertation submitted in partial fulfillment
of the requirements for the degree

of

Doctor of Philosophy

in

Mathematics

MONTANA STATE UNIVERSITY
Bozeman, Montana

November 2018

DEDICATION

This dissertation is dedicated to my parents, Steve and Patty Wilander, without whom this would not be possible. I also dedicate this to my daughter, Charlotte; I hope you find an academic or nonacademic pursuit you can live with. I love you!

ACKNOWLEDGEMENTS

This finished product would not have been possible without the advice, encouragement, and (often overwhelming) knowledge of my committee: Dr. Scott McCalla, Dr. Tomas Gedeon, Dr. Jack Dockery, Dr. Mark Pernarowski, and Dr. Dominique Zosso. I would like to extend special gratitude to my committee chair, Dr. Scott McCalla, for his steadfast support over the last few years, and also to Dr. Mark Pernarowski, with whom I had my first experience in editing and publishing a research paper over several long summers.

I also want to express my appreciation for the math department at MSU and the broader area of Bozeman; this has been a truly unique and rewarding place to be for this seven-year chapter of my life. This includes my fellow graduate students of the math department: Dan Perry — whose extensive movie knowledge is only second to my own — I hope to one day complete the movie Pi under your motivation. Also, thanks to Katie Banner (who doubled as my landlord during these challenging times), friends we lost to job offers and other departments — Doug Anderson, Chris Taddiken — and others I have bonded with over the pain of comprehensive exams like Tony Gaussoin and Anna Cepek.

Finally, I want to thank my family for their emotional (and monetary!) support and especially Liz, who has grounded me in recent months. I wish all of you the best.

TABLE OF CONTENTS

TABLE OF CONTENTS – CONTINUED

LIST OF FIGURES

Figure Page

LIST OF FIGURES – CONTINUED

Figure Page

LIST OF FIGURES – CONTINUED

Figure Page

LIST OF ALGORITHMS

ABSTRACT

In this thesis, we broadly examine collective behaviors in various social and biological contexts. Aggregation, for instance, is a natural phenomenon that occurs in a variety of contexts; it is observed in schools of fish, flocks of birds, and colonies of bacteria, among others. This behavior can be found in some agent-based models, where it is typically assumed every pair of individuals interact according to a simple set of rules. In the first half of this thesis, we study a particular, well-understood aggregation model upon relaxation of the assumption that every individual interacts with every other. We review prior results on this topic — when the underlying structure of interactions is an Erdős–Rényi graph. Seeking to incorporate community structure into the network, we establish the analogous problem under a class of networks called stochastic block graphs; a particular aspect of the system's metastable dynamics is explored upon varying the graph's connection densities. Finally, we evaluate the potential to leverage this system's dynamics in order to recover community structure (given a known graph as input).

In the second half of this thesis, we similarly explore the aggregate behaviors of synchronization and desynchronization, appearing in diverse settings such as the study of metabolic oscillations and cell behaviors over time, respectively. Previous studies have leveraged a model in which repressilator entities are connected by a diffusive quorum sensing mechanism; these have shown (numerically) that the complex composition of observable behaviors depends upon the insertion point of the upregulating protein in the feedback loop. We rigorously prove a version of this; for negative feedback, negative signaling (Nf-Ns) systems we find only a unique stable equilibrium or a stable oscillation is possible. Additionally, we observe (numerically) the complex multistable dynamics that arise when a positive signal is included in the feedback loop and characterize this shift as a saddle node bifurcation of a cubic curve.

1

INTRODUCTION

Networks play an integral role in describing and understanding myriad complex systems in the sciences; they have been used to explain flocking behavior in starlings [38], chasing dynamics in predator-prey interactions [4], the spread of epidemics [23], and the effect of personal relationship structures on the formation of gangs [21]. Coupled with powerful results in fields such as graph theory, networks grant us a window into understanding how we interact with one another and how that affects our state in the broader group.

At its heart, a *network* consists of a collection of individuals (nodes) with a prescribed set of interactions (edges). Individuals can be biological units, such as birds, fish, bacteria, humans, and so on, but they can also be inanimate — web pages on the Internet, for instance. Interactions, similarly, can take many forms, but are usually some exclusive behavior or quality between pairs of individuals (something that can definitively be assigned one pair at a time). Among fish, birds, and the like, this interaction structure connects members of the same social group; an individual animal is connected to those who directly influence its behavior. In social networks, humans are linked to those whom they are friends with, such as colleagues from work. A web page is connected to other web pages through hyperlinks.

These interactions are generally first thought of in the binary sense: existence or absence thereof. In this case, the structure of individuals and edges can be recorded in a 2D structure, an adjacency matrix, in which a given index pair represents a grouping of two individuals, and the entry (0 or 1) whether or not there exists a link between them. Sometimes, this network is interesting in itself, and matrix theory

may reveal important aspects of its structure that lie hidden beneath the surface. The original PageRank algorithm [24], for instance, accepts this foundation of web pages and hyperlinks to define an adjacency matrix, which for the entire Internet is an enormous collection of data, and leverages theory relating to the spectra of such matrices to extract a single vector (the PageRank vector) that can be thought of as representing the probability a surfer, following links at each step at random, will end up at a given site as time evolves [24, p. 5]. This plays a vital role in the search engine's determination of the relative "importance'' of websites for search engine rankings.

In certain applications, the network is simply a surrogate for a grouping of inhomogeneous individuals, each attached to a subset of the system's agents, with a prescribed response to changes in some measurable aspect of their identity, their state vector. This is particularly the case with biological networks, for instance designer cells with levels of quantities (enzymes, proteins, and the like) that can be stimulated or inhibited, and affect the concentrations of other quantities at the cellular level. Here, the interaction structure between comparable units is the focus rather than network structure alone.

At other times, interaction potentials are layered atop a rich node and edge structure. Agents may interact with each other in a pairwise sense; provided there is an edge between two units, a given function describes (for instance) how the individual's state evolves as a function of its state relative to its attached partner's state. In collections of fish, individuals (fish) might be connected to other individuals by social group; this defines the system's *network*. In addition to that, a simple set of rules are followed:

1. Don't get too close to other fish. If you do, move away.

2. Don't stray too far from other fish. If you do, move closer.

Each fish, in trying to maximize its own utility through its interactions with other individuals, gives rise to complex, large-scale dynamics (schooling) that seem as though they must be guided by a central conductor.

In this work, we present two unrelated projects along these lines; we categorize each under the broad banner of "Dynamics on networks." In Chapter 2, we look at a familiar ordinary differential system, describing the evolution of aggregation behavior in e.g. fish, birds, bacteria and the like, and examine its dynamics when its pairwise interactions occur (or not) according to an underlying, random network. The network we use is particularly interesting, as it is broad enough to allow for inhomogeneities between certain individuals. As an example, individuals *within* a friend group are rather likely to see each other as friends, while a pair of individuals from different friend groups are considerably less likely to.

In Chapter 3, we study a coupled cellular circuit [15]. Here, the structure of connections and relationship between agents across such links creates oscillatory and (at times) synchronous behavior, either as a concerted effort to address a threat, or as a way to consistently vary some necessary output relative to a waxing and waning need. As alluded to before, the individuals are qualitatively different; each represents a protein and mRNA concentration pair that affects the other protein/mRNA pairs in a unique way. A final quantity is allowed to diffuse through the cell and medium outside the cell, indirectly allowing each cell's intracellular quantities to affect those of neighboring cells. This network structure is intriguing because it represents a sort of multiscale network (unlike that of Chapter 2). On the large scale, cells interact with cells due to the free motion of an autoinducer quantity. On the small, intracellular scale, proteins interact with other proteins as a result of defined relationships.

Our ultimate goal throughout this work is to depict some of the unique ways networks can be used to model real-world phenomena. We build upon the previous

literature in several ways – either through generating new knowledge from present systems or extending extant systems to new applications. We characterize the behavior of solutions to these, taking care to connect such dynamics back to the structure of the original networks, where possible. Finally, we identify possible veins along which future research may take place.

5

SWARMING ON BLOCKS

Introduction

Aggregation is a type of macroscopic behavior observed in myriad biological systems; for example, it is seen among flocks of birds and schools of fish. This behavior is most readily reproduced in the broad class of first-order "aggregation models." Such models describe the motion of individuals, where it is assumed agents interact with the collective according to a set of pairwise rules. Even a simple set of assumptions – like agents attract over great distances and repel over small distances – can generate these complex arrangements of individuals on the large scale.

The most basic aggregation models often assume all-to-all interactions; that is, each particle affects and is affected by every other particle in the system. One such model is the following, wherein individuals are coupled through an interaction kernel, F:

$$\frac{\mathrm{d}x_i}{\mathrm{d}t} = \frac{1}{N}\sum_{j=1}^{N} F(|x_i - x_j|)\frac{x_i - x_j}{|x_i - x_j|}, \tag{2.1}$$

where the $x_i : \mathbb{R} \to \mathbb{R}^d$ describe a particle's position as a function of time $t \geq 0$ and for $i \in [N] := \{1, 2, \ldots, N\}$.

We take a brief detour to contrast these first-order models with other descriptions of swarming behavior like Cucker-Smale (C-S) [6]. Letting x_i and v_i be the position and velocity coordinates of the i^{th} particle, the C-S model is as follows:

$$\frac{\mathrm{d}x_i}{\mathrm{d}t} = v_i, \tag{2.2}$$

$$\frac{\mathrm{d}v_i}{\mathrm{d}t} = \frac{\lambda}{N}\sum_{j=1}^{N} \psi(|x_j - x_i|)(v_j - v_i), \tag{2.3}$$

for $t > 0$, $i \in [N]$, $\lambda \geq 0$ a coupling strength, and ψ an interaction kernel between pairs

of agents. Of course, the form of the C-S model (2.2)-(2.3) is very reminiscent of the aggregation equations (2.1), though the former come with the added sophistication of the coupling parameter and allow for changes in phase (momentum in movement of the flock over time). That is, such equations allow for a more diverse array of observable behaviors.

Preliminaries

We return to the aggregation equations (2.1). To exhibit certain behaviors (though, at this point, we have not yet established behaviors of interest), we may impose simple restrictions on F. One such requirement is for this function to be "weakly repulsive-attractive." This denotes $F(0) = 0$ (to ensure self-interactions are neutral to system behavior), $F(r) > 0$ for small r, and that $F(r) < 0$ for large r. The last two requirements amount to a statement that particles repel each other over short distances and attract each other over large distances. We note the following:

Proposition 2.0.1. *Suppose* $y \in \mathbb{R}^d, \mathbf{x} \in \mathbb{R}^{N\times d}, F : \mathbb{R}^d \to \mathbb{R}^+$. *The equations* (2.1)*:*

1. *form a* ***gradient system*** *for integrable* F*; that is, there exists* Φ *so that* (2.1) *can be written as*

$$\mathbf{x}' = -\nabla\Phi(\mathbf{x}),$$

2. *are* ***isotropic****, in the sense that the magnitude of the component forces of* (2.1) *do not depend on direction, or*

$$\left\| F(|x_i - x_j|)\frac{x_i - x_j}{|x_i - x_j|} \right\| = F(|x_i - x_j|),$$

3. are ***invariant*** *under translations; that is, letting*

$$\zeta\left(y, \mathbf{x}\right) = \frac{1}{N}\sum_{j=1}^{N} F(|y - x_j|)\frac{y - x_j}{|y - x_j|},$$

we have

$$\zeta\left(y + \alpha, \mathbf{x} + \mathbf{1}_N \otimes \alpha\right) = \zeta\left(y, \mathbf{x}\right),$$

where $\mathbf{1}_N$ *is the length-*N *vector of ones,* $\alpha \in \mathbb{R}^d$*, and* $\otimes$ *denotes the vector outer product.*

Remark 2.0.2. *The latter property 2.0.1–3 yields a natural equivalence between solutions:*

$$\mathbf{x}(t) \sim \mathbf{y}(t) \iff \exists\, \alpha \in \mathbb{R}^d : x_i(t) = y_i(t) + \alpha \quad \forall t, i \tag{2.4}$$

One such kernel function that satisfies our aforementioned restrictions on F (to exhibit collective behaviors), used in [35], is the piecewise linear

$$F(r) = \min(\kappa r, 1 - r), \quad r \geq 0 \tag{2.5}$$

for $\kappa > 0$. We stress this form of F is not meant to be seen as wholly descriptive of *all* possible repulsive-attractive kernels, but rather it is a particularly simple example of one that can lead to the macroscopic behavior of aggregation (that is, a nontrivial equilibrium state).

In this system and with such a function, it is well-established (cf. [29], cited in [35]) that solutions may tend to steady states consisting of many clusters; a *cluster* denotes a configuration of the system's N particles into a finite number of locations in space. For the given choice of F and system dimension $d = 1$, we observe a two-cluster

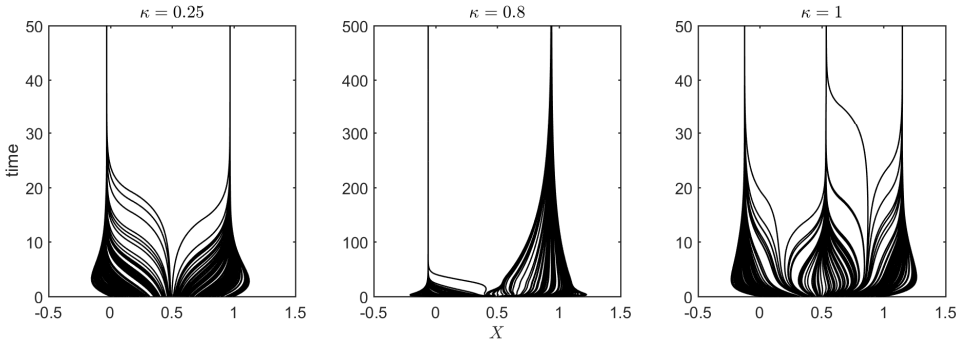

Figure 2.1: A plot of solutions $\mathbf{x}(t)$ to the all-to-all connected equations (2.1) with kernel F as in (2.5). We used uniformly random initial conditions on $[0, 1]$ and took the repulsion parameter $\kappa \in \{0.25, 0.8, 1\}$.

steady state of the form

$$\tilde{x}_i(t) = \begin{cases} -1/2 & : \quad 1 \leq i \leq \lfloor N/2 \rfloor \\ 1/2 & : \quad \lfloor N/2 \rfloor + 1 \leq i \leq N \end{cases} \tag{2.6}$$

Here, we use the bold $\tilde{\mathbf{x}}$ to denote the steady state (2.6) across all particles $i = 1, 2, \ldots, N$; note also that the specific form of (2.6) arises from our typical usage of random, uniformly-distributed initial conditions for a given trajectory, $\mathbf{x}$. Accordingly, we ask the following question.

Question 1. *How does a trajectory* $\mathbf{x}$ *near* $\tilde{\mathbf{x}}$*, in the sense (for some given quantity,* $\delta > 0$*)*

$$\|\tilde{\mathbf{x}}(0) - \mathbf{x}(0)\| < \delta,$$

evolve as $t \to \infty$*?*

To answer Question 1, we first define stability in the asymptotic sense (cf. [2, p. 24]).

Definition 2.0.3. *(Asymptotic stability). A trajectory* $\mathbf{x}^0(t)$ *is said to be asymptotically stable if there exists a* $\delta_{\max}$ *such that, for* $\delta < \delta_{\max}$ *and a trajectory* $\mathbf{x}(t)$ *satisfying*

$\|\mathbf{x}(t_0) - \mathbf{x}^0(t_0)\| < \delta$, *we have* $\lim_{t\to\infty}\|\mathbf{x}(t) - \mathbf{x}^0(t)\| = 0$.

In other words, any sufficiently small perturbation of an asymptotically stable trajectory vanishes as $t \to \infty$. With the terminology 2.0.3 in hand, we recall this important fact ([10], as cited in [35]):

Theorem 2.0.4. *Let* $x_i : \mathbb{R} \to \mathbb{R}$ *denote (for* $i = 1, 2, \ldots, N$*) the location of particle* i *at time* t*, given by the all-to-all aggregation equations* (2.1)*:*

$$\frac{\mathrm{d}x_i}{\mathrm{d}t} = \frac{1}{N}\sum_{j=1}^{N} F(|x_i - x_j|)\frac{x_i - x_j}{|x_i - x_j|},$$

with $F : [0, \infty) \to \mathbb{R}$ *defined by* $F(r) = \min(\kappa r, 1 - r)$.

Then, the two-cluster steady state (2.6) *is asymptotically stable for* $0 < \kappa < 1$ *(up to equivalence under translations* (2.4)*), and it becomes unstable as* $\kappa \geq 1$.

As the system (2.1) is translation invariant, we take Equation (2.6) as a representative for all similar (in the sense of Equation (2.4)) two-cluster steady state solutions.

In Figure 2.2, we revisit the character of the force F as a function of the repulsion parameter κ. An increase in κ directly increases the rate of change (with respect to r) of the repulsive force for small r; the rate of change of $F(r)$ for large r (repulsive *and*, for r large enough, attractive) is, of course, fixed at -1. Up to a rescaling of the variable r, Equation (2.5) adequately characterizes a piecewise linear function with a zero at $r = 1$ and *any* slope for the upward and downward components, as κ can simply be chosen to match the ratio of upward to downward slope. Further, κ determines the critical value for r at which the domains of the piecewise's components overlap; by a simple calculation this is at

$$r_c = \frac{1}{1 + \kappa}.$$

Thus, on the interval $[0, 1]$, we have $F(r) \to 1 - r$ in a pointwise sense as $\kappa \to 0^+$. This form of F, particularly the location of its zeroes at $r = 0$ and $r = 1$, allows for many of the "clustered" steady states we observe. The derivative of each particle's position is a mere average, weighted by the presence or absence of an edge between the aforementioned particle and other system particles. Accordingly, if all single-pair forces are zero (due to all individuals coexisting at two locations, separated by one), then this derivative must equal zero and we are in equilibrium. We do, however, mention that values of $\kappa > 1$ can allow for clustered states that occur at distances *not* coinciding with zeroes of F (see Figure 2.1).

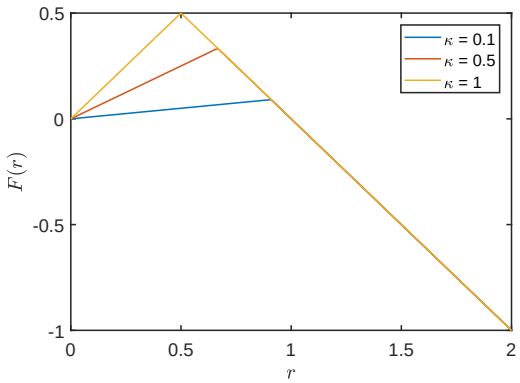

Figure 2.2: A graph of $F(r)$, taking the repulsion parameter $\kappa \in \{0.1, 0.5, 1\}$.

The piecewise-linear form of F is, of course, convenient for computation and some analysis. For instance, suppose we are examining (2.7) on some small perturbation of the two-cluster steady state, where half the system's particles are centered at an average of $-1/2$ and the other half are centered at an average of $1/2$; that is, $x_i = -1/2 + \epsilon_i$ for $i \leq N/2$ and $x_i = 1/2 + \epsilon_i$ for $i > N/2$ (for small $\epsilon + i$). Then, for large N, linearity of the expected value operator [27] implies the particle-particle average of (2.7) (of the form $\frac{1}{N}F(r)$) can instead be replaced with the kernel evaluated at the average particle-particle distance. This will be useful (later) to perform some

analysis on a substitute equation in center of mass coordinates.

Graphs and Random Graph Generation To more precisely model real-world systems like starling flocks (in which individual starlings consider the relative positions of a selection of nearest neighbors when adjusting their position relative to the flock [38]) or voters' policy positions (where input is gathered from a sparse network of friends, family, and colleagues), it is necessary to adjust the typical assumption of all-to-all connectivity. As such, the standard aggregation model is replaced by the aggregation model on a network. This underlying network may be fixed (or not) with respect to time, sparse or densely connected, and may have one of the many different sets of structural properties generation methods like Erdős–Rényi, nearest neighbor, and Watts-Strogatz imbue them with.

To accommodate this need, we first define some preliminary concepts.

Definition 2.0.5. *(Graph). A graph (also: network) is an ordered pair,* $\mathcal{G} = (V, D)$*; the set* $V \subseteq \mathbb{N}$ *are the* ***nodes****, and the set* $D \subseteq V \times V$ *are the* ***edges****.*

Each edge in D is a two-element, ordered subset of V, which we can think of as a starting point and an ending point. Graphs can be undirected or directed; an undirected graph conveys a certain degree of symmetry, as an (i, j) edge can exist if and only if a (j, i) edge exists. Finally, a *weighted* graph supplements this organization with a list of weights, wherein each edge receives an additional value representing the "strength" of the link.

In this chapter, we concentrate on unweighted and undirected graphs.

Definition 2.0.6. *(Adjacency matrix). Let* $\mathcal{G} = (V, D)$ *be an unweighted graph on*

N nodes. Then the adjacency matrix $E \in \{0,1\}^{N\times N}$ is given by the following:

$$E(i,j) = \begin{cases} 1 & : \quad (i,j) \in D \\ 0 & : \quad (i,j) \notin D \end{cases}$$

Accordingly, from this point on we use $E(i,j) = 1$ or $E(i,j) = 0$ interchangeably with the existence (or not) of the edge (i,j) in D, respectively.

Remark 2.0.7. *If a graph $\mathcal{G}$ is undirected, then its corresponding adjacency matrix, E, is symmetric ($E^T = E$).*

In easing the assumption of all-to-all connectivity in (2.7), one might imagine replacing a fully-connected graph, in which E is the matrix of ones, with one generated in the following manner: instead of connecting each distinct pair of particles with probability 1, we would independently connect them with probability p, for $0 \leq p \leq 1$. This simple random method of graph generation is the Erdős–Rényi approach. Specifically,

Definition 2.0.8. *(Erdős–Rényi graph) Let $N = |V|$ be the number of nodes and $p \in [0,1]$ represent an independent, pairwise probability of connection between nodes. The edges of the graph $\mathcal{G}$ are then sampled randomly, according to*

$$e_{ij} = \begin{cases} 1 & \textit{with probability} \quad p, \\ 0 & \textit{with probability} \quad 1-p, \end{cases}$$

for $1 \leq i,j \leq N$. We denote a graph generated in this matter by $\mathcal{G} \sim ER(N,p)$.

If an undirected graph is instead desired, we only sample the entries of the adjacency matrix, E^+, above and including the main diagonal. That is, e_{ij} is determined by Definition 2.0.8 for $j \geq i$, and the remaining entries are filled in

via the restriction $e_{ij} = e_{ji}$. Numerically, we generate the full (symmetric) adjacency matrix by

$$E = E^+ + \left(E^+\right)^{\mathrm{T}} - \mathrm{diag}(E^+),$$

where E^+ is the sampled top half of connections and $\mathrm{diag}(E^+)$ is the matrix containing only the entries of E^+ along the main diagonal. Finally, though the meaning is the same, it is our convention to use e_{Nij} rather than e_{ij} to denote the i, j entry of the adjacency matrix E. This is to explicitly stress the dependence of the network (and thereby the aggregation equations (2.7)) on the number of system particles, N.

Aggregation on Erdős–Rényi Graphs

We summarize the key research questions of [35] here.

Question 2. *How do key dynamical features of the system* (2.1) *change as we adjust* p *within* $[0, 1]$ *and multiply the interaction kernel by* e_{Nij}*? Do stable cluster states lose stability as we decrease* p*, and do other states gain stability? Do solutions remain close to the solution under the all-to-all connected system?*

The corresponding system used by the authors in [35] is (2.1) weighted by the existence of graph edges.

Definition 2.0.9. *(E–R aggregation model). Let* $x_i : \mathbb{R} \to \mathbb{R}$ *(for* $i = 1, 2, \ldots, N$*) denote the position of particle* i *at time* t *and* F *the interaction kernel of* (2.5)*. Further, suppose the graph* $\mathcal{G} \sim ER(N, p)$ *defining the interaction topology is undirected, unweighted, and generated initially (at* $t = 0$*) but fixed in time. Then, the aggregation equations (E–R) are given by*

$$\frac{\mathrm{d}x_i}{\mathrm{d}t} = \frac{1}{N} \sum_{j=1}^{N} e_{Nij} F(|x_i - x_j|) \frac{x_i - x_j}{|x_i - x_j|}. \tag{2.7}$$

Again, p is treated as a parameter that changes the output system (2.7). Yet, one may observe that this result isn't deterministic; it is, for instance, possible (though exceedingly unlikely for large N) to generate the all-to-all connected graph – represented by a matrix of 1's – with a $p \ll 1$. It has been established ([10, 17], as cited in [35]) that the all-to-all graph can consist of a two-cluster state, stable if $0 < \kappa < 1$. Despite this, we may initialize (2.7) with a thousand different networks by the same parameter p and discover not a single one yields a stable two-cluster steady state! Hence it is clear that the classical stability of Definition 2.0.3 fails us. Indeed, for any p and finite N it may be *possible* to achieve both stable and unstable results across many runs. Thus, we require a modified definition of stability:

Definition 2.0.10. *(Asymptotic stability almost surely (E-R)). Denote by* $\tilde{\mathbf{x}}(t)$ *the two-cluster steady state* (2.6) *of* (2.7)*. We say* $\tilde{\mathbf{x}}(t)$ *is asymptotically stable almost surely if*

$$\mathbb{P}\left\{\tilde{\mathbf{x}}(t) \text{ is asymptotically stable} : \mathcal{G} \sim ER(N,p)\right\} \to 1$$

as $N \to \infty$*.*

In this sense, for fixed p, (2.6) is asymptotically stable almost surely if the proportion of generated graphs leading to an unstable two-cluster state in (2.7), each weighted by its probability of being generated, gets vanishingly small as N tends to infinity. In Figure 2.3, we provide a picture summary of the large-N dynamics of (2.7), taking $\mathcal{G} \sim \mathrm{ER}(N,p)$.

Interestingly, under this choice of network, the following result was proven in [35].

Theorem 2.0.11. *Let* F *be defined by* (2.5) *for* $0 < \kappa < 1$*. Then the steady state* (2.6) *to the system* (2.7) *is asymptotically stable almost surely if*

$$p \geq \epsilon \frac{\log^{3/2} N}{N} \tag{2.8}$$

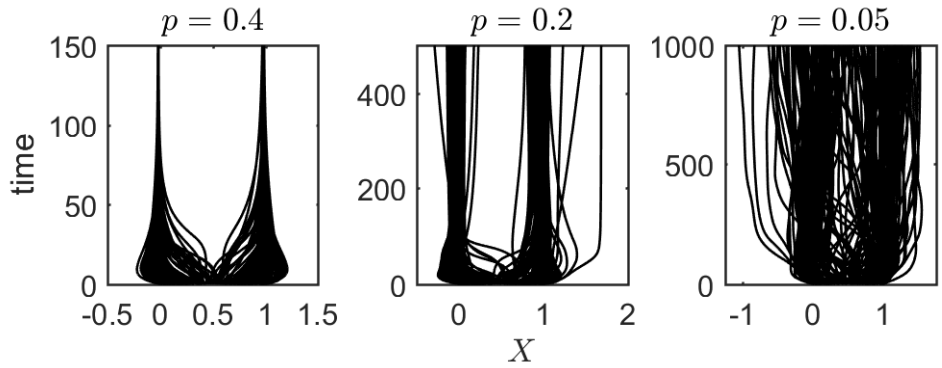

Figure 2.3: Dynamics of the aggregation model (2.7) on a simple random graph (for various probabilities of connection between pairs of particles, p and $N = 500$ particles). Note the apparent destabilization of the two-cluster state as p is decreased.

for some $\epsilon > 0$. *The steady state* (2.6) *is asymptotically unstable almost surely if*

$$p \leq 2(1-\epsilon)\frac{\log N}{N} \tag{2.9}$$

for some $\epsilon > 0$.

The threshold (2.9) is greater than, and reminiscent of, the $\log N/N$ scaling yielding a connected or disconnected Erdős–Rényi graph, implying that connectivity of the network is necessary but not sufficient to attain a stable two-cluster state (2.6).

As noted in [35], the system (2.7) can be interpreted in any dimension $\mathbb{R}^d$, $d \geq 1$ without any modification. We simply let each x_i be a function from $\mathbb{R}$ to $\mathbb{R}^d$, as such; both sides of the equation (2.7) make complete sense if x_i is a d-dimensional vector quantity rather than a scalar. Additionally, we make the following modification to the kernel F from (2.5):

$$F(r) = \min\left(ar + b, 1 - r\right), \quad a \geq 0, b \in [0, 1]. \tag{2.10}$$

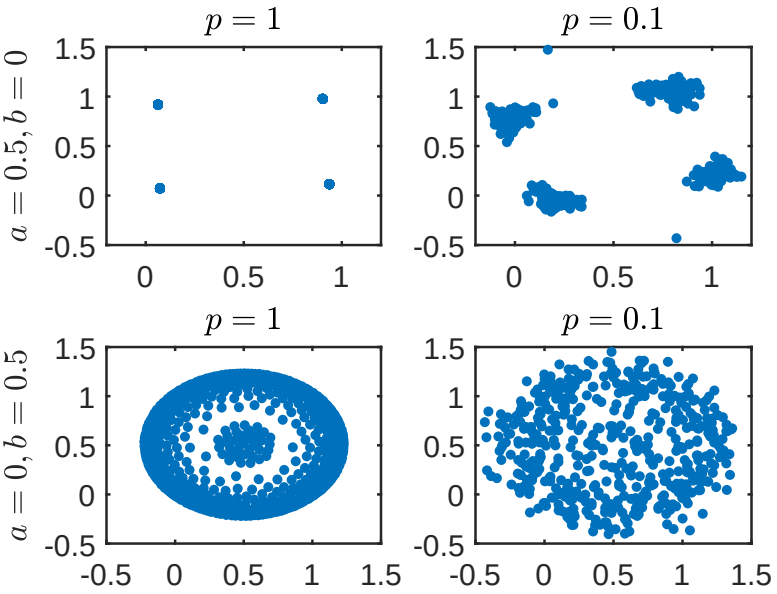

Figure 2.4: A plot of 2D aggregation dynamics with $N = 500$, using the altered interaction function (2.10). The probability of connection between pairs of particles, p, is specified on top of each panel; the interaction function's parameters, a and b, are specified on the left. Again, note the apparent deterioration of the stable state as $p \to 0$.

We determine the domain's overlap r value of the function (2.10) to be

$$r_c = \frac{1-b}{a+1}, \tag{2.11}$$

hence the added parameter, b, uniformly increases output F values, relative to (2.5), across all $r < r_c$ for r_c as in (2.11). Such a change does not appear to add any noteworthy complexity to the 1-dimensional system but allows for interesting structures in higher dimensions. We provide some examples in Figure 2.4.

In the top panels of Figure 2.4, we see a clear analog of the 1D clustered state (2.6). On the left, our system's particles arrange themselves into four groups, separated in space and with particles belonging to the *same* group sharing the same

location in $\mathbb{R}^2$ as $t \to \infty$. On the right, decreasing the probability of connection of the underlying network eventually destabilizes this state, though it still persists in an approximate sense. In the bottom panels, we see a much more complicated stable structure that does not have a clear analog in the 1D system. As p is decreased this state destabilizes immediately, and all that remains for small p is a loose ring around a grouping of particles. The analysis of equilibria like those in the top row (those that permit an analytical description for a range of p near 1) is the subject of papers like [36].

In this chapter, we first develop a more general choice of network topology than the basic Erdős–Rényi approach. Specifically, we seek to directly encode the latent community structure observed in many natural and human systems (like individuals' political affiliation relative to the party line, networks of friends, family, and colleagues, and the like). In such systems, we can often separate individuals into communities, wherein there is a homogeneous structure in connectivity among "in-members" that is markedly different from those connections between members of different groups. This desire motivates our development and usage of the stochastic block model to generate networks.

With this framework in hand, we then apply it to the 1D variant of system (2.7). We deviate from typical treatments of similar problems in a fundamental way; we focus on a specific sort of metastable dynamics rather than classic linear stability of equilibria. We look to assess how communities, well-separated in space at one point in time, then evolve as $t \to \infty$. To do this, we first introduce a convenient change of coordinates. Rather than dealing with communities in terms of their individual members, separately, we represent each with a single variable – a "center of mass." We then show this bit of information is connected to the system's metastable dynamics in a fundamental way, leveraging accurate approximations (in certain regimes) and

heuristic arguments to relate the system to a simple, "competing timescales" problem. Last, we offer a novel application of our aggregation equation's dynamics to the field of community detection.

The Stochastic Block Model

We again note that, as seen in Figure 2.3, the system (2.7) sorts (within a certain parameter regime) particles into clusters separated in space – in the sense that each x_i, $i = 1, 2, \ldots, N$ tends to one of a finite number of locations. Motivated by this observation, we seek a class of graphs that can be directly imbued with such cluster structure. That is, we want to specify different probabilities of connection between and within groups of particles in our random graph. As a simple application, this will allow us to represent a network in which two groups are densely connected amongst themselves, but sparsely connected between groups (for example, networks of friendships between two "cliques" of individuals).

To accommodate this need, we adopt one of the simplest methods that generates such graphs – the stochastic block model. We define this below:

Definition 2.0.12. *(Stochastic block model). Let N and k be positive integers representing the number of vertices and planted communities, respectively. Let P be a k-by-k symmetric matrix with entries valued in $[0, 1]$ (the probabilities of connection). Let the $C_1, C_2, \ldots, C_k$ denote the community set partitions of $\{1, 2, 3, \ldots, N\}$. X, the community labeling vector of length N, is determined as follows: for $v \in C_j$ (for some j)*

$$X_v = j. \tag{2.12}$$

Then the graph $\mathcal{G}$ is drawn from $SBM(N, C, P)$ if, independent of other vertex pairs,

$$e_{Nij} = \begin{cases} 1 & \textit{with probability} \quad P(X_i, X_j), \\ 0 & \textit{with probability} \quad 1 - P(X_i, X_j). \end{cases} \tag{2.13}$$

We write $\mathcal{G} \sim SBM(N, C, P)$ for short.

As in [35], we only consider undirected network topology – each connection is symmetric. Appropriately, we only sample the entries above the main diagonal of the adjacency matrix E. The bottom half of the matrix is then filled in via equating it to the matrix transpose, $E^T = E$. Self-interactions are irrelevant to the equations (2.7) (as $F(0) = 0$), so the value of the entries along the main diagonal of E have no impact on the system. By convention, we thus set all diagonal entries $E(i, i) = 0$.

Remark 2.0.13. *We note that, if the probability matrix $P = p\mathbf{1}_{k,k}$ for some $0 \leq p \leq 1$ and $\mathbf{1}_{k,k}$ the k-by-k matrix of ones, then*

$$SBM(N, C, P) \cong SBM(N, V, p) \cong ER(N, p),$$

in the sense that $\mathbb{P}\{e_{ij} = 1\} = p$ under all three methods and for any i, j.

This is intuitive; there is no distinction between the particles inside and outside a given community. Accordingly, we recover the Erdős–Rényi network structure on a graph of N particles with probability parameter p. This reveals the stochastic block model structure as a simple gluing of k Erdős–Rényi graphs together at a between-community link density prescribed by the off-diagonal entries of P. Thus the connectivity threshold for graphs generated by the stochastic block model method can be described analogously.

Proposition 2.0.14. *Let $\mathcal{G} \sim SBM(N, C, P)$ be a randomly generated stochastic block network on k communities, with N particles, and with probabilities of connection specified by the $k \times k$ matrix P. Additionally, assume the proportion of system particles belonging to each community remains fixed, that is*

$$\lim_{N\to\infty} \frac{|C_i|}{N} = \alpha, \quad i = 1, 2, \ldots, k \tag{2.14}$$

for some $\alpha \in (0, 1)$. Then, $\mathcal{G}$ is connected almost surely as $N \to \infty$ if, for each $1 \leq i \leq k$, there exists a $\gamma(i) > 1$ such that

$$P(i, i) > \gamma \frac{\log N}{N} \tag{2.15}$$

and for each $j \neq i$ we have

$$P(i, j) > \delta \tag{2.16}$$

for some $\delta > 0$.

Proof. Denote by $\mathcal{G}_i = (V_i, D_i)$ the subgraph of $\mathcal{G}$ containing only nodes from C_i and edges between members of C_i. That is, $V_i = C_i$, and

$$D_i = \{(x, y) \in D : x, y \in C_i\}.$$

By [9] and due to (2.15), $\mathcal{G}_i, i = 1, \ldots, k$ is almost surely connected as $N \to \infty$. By (2.16),

$$\mathbb{P}\left[\{(x, y) \in D : x \in C_i, y \in C_j\} = \emptyset\right] \to 0$$

for each $1 \leq i, j \leq k$ and as $N \to \infty$. Hence, letting

$$D_{i,j} = \{(x, y) \in D : x \in C_i, y \in C_j\},$$
$$V_{i,j} = \{x \in V : (\{x\} \times V) \cap D_{i,j} \neq \emptyset\},$$

we have that

$$\hat{\mathcal{G}} = \left(\bigcup_i \mathcal{G}_i\right) \cup \left(\bigcup_{i \neq j} (V_{i,j}, D_{i,j})\right)$$

is connected almost surely in the large N limit. As $D_{\hat{\mathcal{G}}} \subseteq D_{\mathcal{G}}$, then $\mathcal{G}$ is connected almost surely. □

The conditions (2.15)–(2.16) are, of course, equivalent to requiring each "Erdős–Rényi subgraph" be connected and for there to be at least *one* connection between the community subgraphs. We incorporate this network topology into the equations (2.7).

Definition 2.0.15. *(SBM aggregation model). Let $x_i : \mathbb{R} \to \mathbb{R}$ (for $i = 1, 2, \ldots, N$) denote the position of particle i at time t and F the interaction kernel of (2.5). Further, suppose the graph $\mathcal{G} \sim SBM(N, C, P)$ defining the interaction topology is undirected, unweighted, and generated initially (at $t = 0$) but fixed in time. Then, the aggregation equations (SBM) are given by*

$$\frac{\mathrm{d}x_i}{\mathrm{d}t} = \frac{1}{N} \sum_{j=1}^{N} e_{Nij} F(|x_i - x_j|) \frac{x_i - x_j}{|x_i - x_j|}. \tag{2.17}$$

Hence, without respect to network topology, the equations (2.17) are precisely the same as (2.7); we are seeking to ascertain the additional complexity imposed on those equations under a different method of network generation.

Last, we note here and explain more in detail later that the choice of the

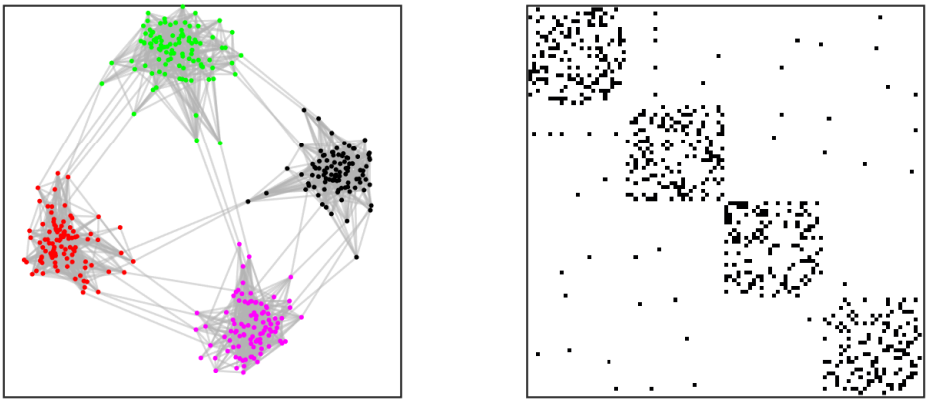

Figure 2.5: Left panel: a representative example of a network generated from the stochastic block model method. Here, we have $N = 400$ particles (equally distributed to each of the four communities). Probability parameters: $p_{\text{in}} = 1/10$ and $p_{\text{out}} = 1/2000$. Right panel: a pixel picture of the adjacency matrix of a stochastic block network generated from the same probability parameters but on $N = 100$ particles (each community: 25 particles).

parameter κ is deeply enmeshed with the dynamics of the system (2.7). As a rule of thumb, the system (2.7) can only tend toward stability as $\kappa \to 0^+$, and toward unstable behavior as $\kappa \to 1^-$, in the sense that we can find a stable state like (2.6) (in the asymptotic sense) for $\kappa \approx 0$ that destabilizes as $\kappa \to 1^-$, but not necessarily vice versa. We characterize the reason for this shift in a later section. Unlike the case in which our network topology is a simple Erdős–Rényi graph, we also provide a simple basis of reasoning for the system attaining stability asymptotically almost surely (in the limit as $N \to \infty$) for a particular threshold value of κ that may, perhaps, be greater than unity. For the given network structure, this suggests a clean division between stability and instability as a function of the system's probability parameters.

Methods

Before presenting our results, we begin with a discussion (and justification) of our methods used in generating them. Unless otherwise specified, in this chapter we take networks on $N = 200$ nodes for the purpose of simulation. Our deterministic system has a considerable amount of inherent variation – not only in the form of initial conditions, but also in the individual equations themselves (as the e_{Nij} coefficients change for the network). Indeed, one of the ways in which the e_{Nij} coefficients can change most drastically in system (2.7) is through changes in community size. If our connectivity structure is set so that

$$P(i,j) = \begin{cases} p_{\text{in}} & : \quad i = j \\ p_{\text{out}} & : \quad i \neq j \end{cases}$$

and $p_{\text{in}} \gg p_{\text{out}}$, then there will likely be a rather large difference in the resulting system if we specify, say, many small communities versus a handful of large ones. This will be the case even without regard to initial conditions.

We would like to pick N to be very large; this would reduce the magnitude of variation in the nodes' degrees relative to N itself. For example with $N = 200$ and a connection probability p for all particle-particle pairs close to 0 (like $p = 0.2$), one standard deviation is about 14% of the mean in total number of connections. For $N = 2000$, one standard deviation is about 4.5% of the mean in total number of connections. As we increase N, the degree of each particle is increasingly likely to cluster near its mean; assuming links are generated independently, this implies that each $\dot{x}_i$ (being an average of individual interactions) increasingly clusters near a mean, as well. This is more or less a restatement of de Moivre-Laplace theorem, which qualifies the convergence of the binomial distribution to the normal distribution with

mean $\mu = np$ and variance $\sigma^2 = npq$ as $N \to \infty$ [27, pp. 62-63]:

Theorem 2.0.16. *(De Moivre-Laplace Integral Theorem). Let* $0 < p < 1$, $q = 1 - p$, *and* C_n^k *the binomial coefficient from* k *choices of a set of* n *elements:*

$$C_n^k = \frac{n!}{(n-k)!\,k!}.$$

Also, let

$$P_n(k) = C_n^k\, p^k q^{n-k},$$
$$P_n(a,b] = \sum_{a<x\leq b} P_n(np + x\sqrt{npq}).$$

Then,

$$\sup_{-\infty\leq a<b\leq\infty} \left| P_n(a,b] - \frac{1}{\sqrt{2\pi}} \int_a^b e^{-x^2/2}\,\mathrm{d}x \right| \to 0, \quad n \to \infty.$$

Accordingly, the random impact of generating adjacency matrices as we have described is mitigated in the asymptotic limit, as $N \to \infty$. Of course, N can be small in many real-world instances of networks; in such cases, we are unable to fine-tune N, and must accept (and manage) the system's stochastic behavior.

When we do have control over N, we must balance our desire to pick it very large with the increasing computational demands of doing so. The two main ways a larger N expands our computing load are in increased processing time and increased memory utilization. Directly, a larger N increases processing time through repeated evaluation of the equations (2.7) for each particle x_i. Each equation consists of roughly N floating point operations, and there are N equations, hence we would expect computational complexity to scale like $O(N^2)$, at least. That is, magnifying N from 200 to 2000 may increase the time it takes to resolve the equations (2.7) nearly 100-fold! Additionally, our code makes heavy use of MATLAB's *meshgrid* to fully realize the N^2 possible

$F(r)$ values over all x_i and x_j pairs; this is done to leverage MATLAB's efficient parallelization of basic matrix operations for rapid computation of the equations (2.7). As such, large values of N will quickly begin to stress the limits of conventional, end-user memory and necessitate a different coding approach.

The coefficients e_{Nij} are randomized as described in the beginning of this section, with initial conditions for the x_i at time $t = 0$. Though certain graph topologies (cf. [3]) allow for the adjacency matrix E to vary as a function of time, this introduces unnecessary complexity into our system and as such is beyond the scope of this chapter; accordingly, E does not change over time during a single run, only between initializations. Practically, this assumption is eminently sensible due to the fact that many of the real-world networks we have cited are static in time; one's network of friends, for instance, does not change much outside certain large life events (new job, moving to a new area, changed relationship status). Initial conditions for the x_i – denoted by $x_i^0 = x_i(0)$ – relay large separations between communities, meaning an initial separation is chosen (often $S = 200$ here), and particles are seeded so that, on average, particles from one community are at an initial distance of S from particles of the next community. With two communities, our initial state is

$$x_i^0 = \begin{cases} -S/2 + \mathcal{U}(-1/2, 1/2) & : \quad 1 \leq i \leq |C_1| \\ S/2 + \mathcal{U}(-1/2, 1/2) & : \quad |C_1| + 1 \leq i \leq N \end{cases}$$

A small, uniform random variable on $(-1/2, 1/2)$ has been added to the initial condition; this random component is to avoid seeding sparsely-connected particles in equilibrium at $t = 0$ (as $F(0) = 0$).

A note on our choices of parameters for evolution of (2.7)**:** as we are only concerned with *undirected* graphs, the relevant information to take from P (and more directly, the adjacency matrix E) lies on the main diagonal or above. With M total

communities, this is a total of $(M^2 + M)/2$ entries, which grows rather quickly – like M^2 – as M gets large. As such, the difficulty in collecting and presenting data makes managing larger community numbers rapidly unfeasible. We escape the grasp of this problem in two key ways: first, by only considering dynamics on two communities, and second, by varying the main diagonal ("inner") entries and off-diagonal ("outer") entries as two groups, where each element varies in lockstep with the others. In the first instance, the choice of only two communities is natural, as the prevalence of a two-cluster steady state for a large range of repulsion parameters κ lends itself to this perspective. Additionally, as the sums in (2.7) can be split into pairwise, community-to-community interactions, there is inherent, general value in knowing how shifting system parameters can affect transitions in the two-community case. Additionally, as we will see under the next subsection, "Dynamics unfolding on communities," the behavior of the system (2.7) is rich and complex despite the simplification.

In the second instance, the advantage of such an approach is that it reduces P to a two-parameter family of matrices:

$$P(i,j) = \begin{cases} p_{\text{in}} & : \quad i = j \\ p_{\text{out}} & : \quad i \neq j \end{cases}$$

where p_{in} and p_{out} are probability parameters in $[0, 1]$. Of course, this is only a minor simplification (and thus a minor potential loss of information) for $M = 2$, as we supplant 3 parameters with 2 parameters, but it is much larger as $M \to \infty$. Yet, we suspect that even such simplifications do not blur the complexities of our system much. It is one of our ultimate goals in this chapter to try to connect the attracting nature of the two-cluster steady state with a simple ratio of a pair of these probabilities. Allowing these other elements of P to vary independently, as such, may only change our position relative to a threshold in a way that can be expressed as a

change in probability ratio.

Generally, we evolve the equations (2.7) in time with the simple, first-order, forward Euler method. We note the equations (2.7) are not stiff; accordingly, the superior stability properties of implicit or multistep Runge-Kutta schemes are not necessarily desirable when considering their greater cost in computation. Similarly, our limited need for higher-order truncation error leads us away from higher-order methods upon considering their greater cost in computation (cf. [19] for a consideration of these and other issues). We evolve our solution from previous timesteps by taking a step of size Δt, two steps of size $\Delta t/2$, and then applying Richardson extrapolation [39] to the result to attain an estimate of our local truncation error. This number allows us to automatically choose a step size so that at t_{n+1} we have a local truncation error that does not exceed a certain tolerance, ϵ_{tol}. Accordingly, this adaptation of Euler's method lets us navigate intervals where the actual solution is changing rapidly in time with a small Δt, while taking great leaps across time when the actual solution is *not* changing rapidly in time. We do note that for particular applications where direct control over our step size is necessary – for example, later discussion on the system's convergence timescales – we revert to forward Euler with a fixed Δt step size.

As data must be presented over a large number of initializations (due to the inherent variance in graph structure due to Definition 2.0.15), we have only found it practical to evolve (2.7) with a moderately-sized N rather than one much larger (like $N = 2000$). This mitigates the processing advantage of a smaller N while retaining any advantage in memory utilization, as runs can be performed and data stored separately. Generally, to visualize our data we simply average it across initializations at a given set of parameters; this can be especially useful if the underlying outputs of interest vary linearly with inputs. For example, one of the most prevalent pieces

of information we provide throughout the chapter is "center of mass" data per community; later we will see that differences in centers of mass between communities acts as a "sorting number" that tells us what proportion of particles from one community get mixed with particles from the other community. A difference of 0 implies 50% of a community ends up mixed in with another community, a difference of 1 implies *no* sorting occurs, and this varies in a linear way between. An average difference of 0.50, then, would indeed suggest that 75% of a community (on average) is mixed in with the other community.

Dynamics Unfolding on Communities

We revisit the aggregation model on stochastic blocks (2.17) of Definition 2.0.15:

$$\frac{\mathrm{d}x_i}{\mathrm{d}t} = \frac{1}{N}\sum_{j=1}^{N} e_{Nij} F(|x_i - x_j|)\frac{x_i - x_j}{|x_i - x_j|},$$

with

$$F(r) = \min(\kappa r, 1 - r)$$

for $\kappa > 0$. Recall the e_{Nij} are edges drawn from a stochastic block graph on N nodes, $\mathcal{G} \sim \mathrm{SBM}(N, C, P)$. We seek to answer the following:

Question 3. *1. How do the full particle dynamics of* (2.7) *change as the graph's outer connection probability varies?*

2. How can we reduce the dimensionality of the system (2.7) *to more readily describe its large-N dynamics?*

3. Finally, what is the complete picture of (2.7)*'s dynamics as the inner and outer connection probabilities vary jointly?*

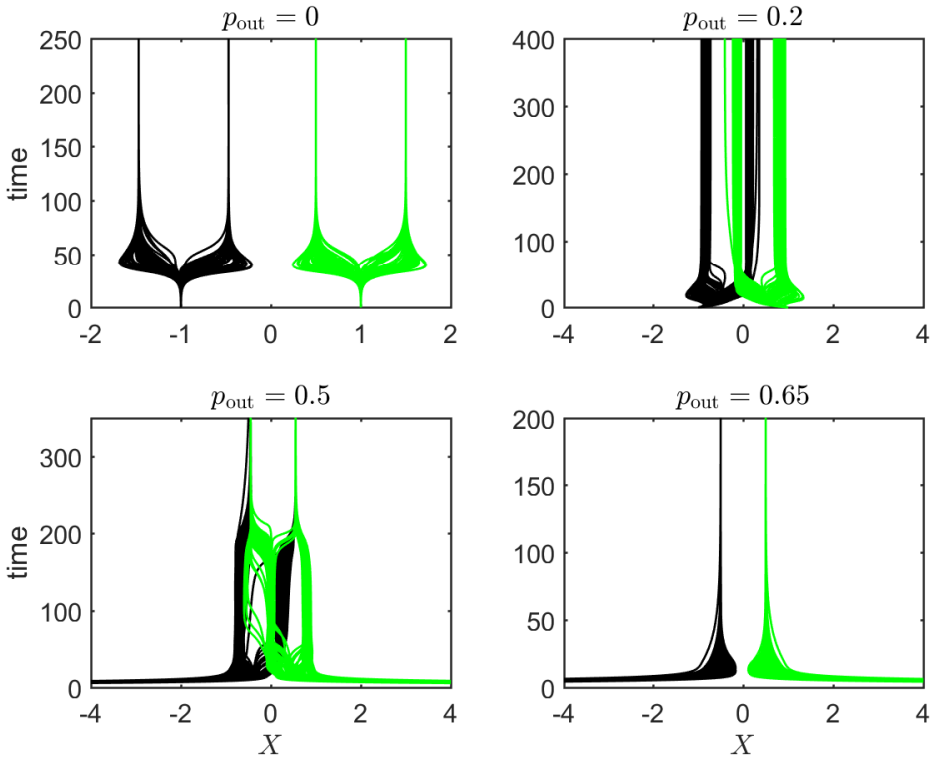

Figure 2.6: A space-time plot of the aggregation model (2.17) on a stochastic block network with two communities; $p_{\text{in}} = 0.8$ is fixed, but outer connectivity (p_{out}) varies. Lines of the same color represent trajectories of particles from the same community. Here, $p_{\text{in}} = 0.8$ throughout. Parameters: $\kappa = 0.5, N = 200$ particles (equally distributed to both communities).

We explore the first part of Question 3; Figure 2.6 depicts the nonlinear dynamics of (2.7) as P varies. Typically, though there is no particular justification beyond ease of presentation, we vary the diagonal entries P_{ii} (which represent the probability of two particles from the *same* community being connected) under the restriction that $P_{ii} = P_{jj}$ for each i, j and vary the off-diagonal entries – the outer connectivities – freely. In the two-community case, this allows us to present our results as a function of two rather than three variables. Later in the chapter, we show that for $0 < \kappa < 1$, the threshold for stability requires a significantly larger inner connection probability

relative to the outer connection probability. Motivated by friend groups, professional relationship networks, and the like, we note that these structures often exhibit dense connections between same-group members and relatively sparse connections otherwise. Accordingly, it is instructive to pick P_{ii} large and then let P_{ij} (for each $i \neq j$) vary continuously from $(0, 1)$ to observe how the relative sparsity of between-community connections changes the system's behavior.

We traverse Figure 2.6 in increasing p_{out}. When $p_{\text{out}} = 0$, we observe (for $1 \leq i, j \leq N$)

$$X_i \neq X_j \Longrightarrow e_{ij} = 0.$$

Accordingly, the particles of each community tend to, independently, a respective two-cluster state. Next, as the outer connection probability is increased to $p_{\text{out}} = 0.2$, we see mixing take place, meaning there are some i, j for which

$$|x_i - x_j| \to 0$$

despite i, j belonging to different communities. However, this seems to occur over a much larger timescale than the previous panel and without, perhaps, the asymptotic stability of the underlying two-cluster state (2.6). As we increase this probability again to $p_{\text{out}} = 0.5$, we find our trajectory tending to the two-cluster state, so that there appear to exist $x \in C_1, y \in C_2$ with $|x - y| \to 0$ as $t \to \infty$. Finally, as the outer connection probability is increased again, to $p_{\text{out}} = 0.65$, the sample trajectory still tends to the two-cluster state, $\tilde{x}$, although we no longer observe mixing behavior. Based on these observations, we presume the following:

Conjecture 1. *Let $p_{\text{in}} \gg \log N/N$ be fixed, with $0 < \kappa < 1$ and N the number of system particles. Assume initial conditions for the x_i respect community structure;*

that is, for any i, j with $X_i \neq X_j$,

$$|x_i(0) - x_j(0)| \gg 1.$$

Then the aggregation model (SBM) of Definition 2.0.15 undergoes the following qualitative changes in behavior as $p_{\text{out}} \in [0,1]$ varies. For some $\gamma, \delta > 0$,

- *If $p_{\text{out}}/p_{\text{in}} > \gamma$, then $\mathbf{x}(t)$ tends to the **unmixed two-cluster state** (up to translations), $\tilde{\mathbf{x}}_u = (\tilde{x}_{i,u})_i$, with high probability:*

$$\tilde{x}_{i,u} = \begin{cases} -1/2 & : \quad i \in C_1 \\ 1/2 & : \quad i \in C_2 \end{cases}. \tag{2.18}$$

- *If $\delta < p_{\text{out}}/p_{\text{in}} < \gamma$, then $\mathbf{x}(t)$ tends to a **mixed two-cluster state** (up to translations), $\tilde{\mathbf{x}}_m$, with high probability:*

$$\tilde{\mathbf{x}}_m = \pi\left(\tilde{\mathbf{x}}_u\right)$$

for some permutation $\pi \in S_N$ satisfying $\pi(i) = j$ for some $i \in C_1$ and $j \in C_2$.

Center-of-Mass Coordinates

We continue towards our goal by providing an answer to the second part of Question 3.

Definition 2.0.17. *(Center-of-mass coordinates for the aggregation equations (SBM)). Let $\mathcal{G} \sim SBM(N, C, P)$, and let $k = |C|$ be the number of components of our partition to V. Let*

$$n_i = |C_i|\,.$$

Then m_i, the center-of-mass coordinate corresponding to community i, is given by

$$m_i = \frac{1}{n_i} \sum_{k \in C_i} x_k. \tag{2.19}$$

Additionally, we define the system's center-of-mass coordinate by

$$m_0 = \frac{1}{N} \sum_{k=1}^{N} x_k. \tag{2.20}$$

Given the Definition 2.0.17, we prove some basic facts relating to these center-of-mass coordinates.

Proposition 2.0.18. *Let the center-of-mass coordinates, m_i, to the aggregation model (SBM) of Definition 2.0.15 be defined as in Definition 2.0.17. Then, the following statements are satisfied.*

1. *Conservation of mass:* $\mathrm{d}m_0/\mathrm{d}t = 0$ *for all* t.
2. *Specifically, if* $k = 2$, $|C_1| = |C_2|$, *and* $m_0(0) = 0$ *(that is* $m_1(0) = -m_2(0)$*), then* $m_1(t) = -m_2(t)$ *for all* t.

Proof. For the first statement, let G be the function from (A.1) in Appendix A:

$$G(j,k) = e_{Njk} F(|x_j - x_k|) \frac{x_j - x_k}{|x_j - x_k|}.$$

Given the definition (2.20) and the derivatives of x_k in the equations (2.7), we find

$$\begin{aligned} \frac{\mathrm{d}m_0}{\mathrm{d}t} &= \frac{1}{N} \sum_{k=1}^{N} \sum_{j=1}^{N} G(k,j) \\ &= \frac{1}{N} \left(\sum_{j=k} G(k,j) + \sum_{j>k} G(k,j) + G(j,k) \right). \end{aligned}$$

Given $G(j,k) = -G(k,j)$ (established in Appendix A) and $G(j,j) = 0$, the first statement follows.

For the second statement, assume the first statement holds. Then the definitions (2.19)–(2.20) and $|C_1| = |C_2|$ imply

$$m_0 = 2\left(m_1 + m_2\right) \Longrightarrow 0 = \frac{\mathrm{d}m_0}{\mathrm{d}t} = 2\frac{\mathrm{d}}{\mathrm{d}t}\left(m_1 + m_2\right).$$

In particular,

$$\frac{\mathrm{d}}{\mathrm{d}t}\left(m_1 + m_2\right) = 0, \quad \text{for all } t. \tag{2.21}$$

We conclude

$$m_1(t) + m_2(t) = \left(m_1(t) + m_2(t)\right) + \left(m_1(0) + m_2(0)\right) = \int_0^t \frac{\mathrm{d}}{\mathrm{d}t}\left(m_1(t) + m_2(t)\right)\,\mathrm{d}t,$$

where equality of the first and second quantities is due to the assumption $m_1(0) + m_2(0) = 0$. As, directly, the third quantity is equal to zero due to (2.21), the result in the Proposition follows. □

Corollary 2.0.19. *The second statement of Proposition 2.0.18 implies, if*

$$\lim_{t\to\infty} m_1(t) = -\frac{1}{2}\hat{p} + \frac{1}{2}\hat{q},$$

then

$$-\lim_{t\to\infty} m_1(t) = \lim_{t\to\infty} m_2(t) = -\frac{1}{2}\hat{q} + \frac{1}{2}\hat{p}.$$

In particular, if each x_i tends to $\pm 1/2$, then $\mathbf{x} \to \pi(\tilde{\mathbf{x}})$, where $\tilde{\mathbf{x}}$ is the two-cluster steady state (2.6) *and π is a permutation in S_N.*

The result of Corollary 2.0.19 suggests the only attracting two-cluster state is a permutation of $\tilde{\mathbf{x}}$.

Remark 2.0.20. *Note that, upon substitution of the aggregation equations* (2.7) *into* (2.19)*, we find*

$$\frac{\mathrm{d}m_i}{\mathrm{d}t} = \frac{1}{n_i}\sum_{k\in C_i}\frac{\mathrm{d}x_k}{\mathrm{d}t} = \frac{1}{Nn_i}\sum_{k\in C_i}\sum_{j=1}^{N} e_{Nkj}F(|x_k - x_j|)\frac{x_k - x_j}{|x_k - x_j|}. \tag{2.22}$$

However, the formulation (2.22) is not immediately useful for solving the aggregation equations (2.7) due to its $\mathbf{x}$ coupling. Still, we note the difference between the centers of mass of a community pair is a simple and useful "sorting number" that, under some reasonable parameter assumptions, indicates how well-mixed two communities are. To see this, assume we have an equal number of particles converging to one of two locations (separated by 1). Again, let $\hat{p}$ denote the proportion of first-community particles at, say, $x = -1/2$, while $\hat{q} = 1 - \hat{p}$ is the proportion of first-community particles tending toward the *second* location ($x = 1/2$). If the two communities have an equal number of particles, and since (by assumption) we have an equal number of particles in each cluster location, this implies the second community has $\hat{q}$ and $\hat{p}$ of its particles at the first and second locations, respectively. A simple computation gives us the difference between centers of mass of $d = 2\hat{p} - 1$. Hence, as expected, $d = 1$ implies total separation of communities and $d = 0$ implies perfectly mixed communities.

Assuming Conjecture 1, the validity of the sorting number immediately and clearly holds over a large swath of parameter space. As Figure 2.6 suggests, the two-cluster state – mixed or not – tends to only lose its broad ability to attract when p_{in} greatly exceeds p_{out}. Hence the assumption that particles tend to one of two locations is sound provided this is not the case (as $t \to \infty$). We formalize our argument here.

Proposition 2.0.21. *Let* $\mathbf{x}$ *be a trajectory of the aggregation equations (SBM) of Definition 2.0.15. Additionally, assume* $\mathbf{x} \to \pi(\tilde{\mathbf{x}})$ *for some* $\pi \in S_N$*, where* S_N *is the*

permutation group on N elements and $\tilde{\mathbf{x}}$ is the two-cluster steady state (2.6)*. Then, the sorting number*

$$s = \lim_{t\to\infty} |m_1(t) - m_2(t)| \tag{2.23}$$

satisfies the following:

1. *We have $s = 1$ if and only if $\mathbf{x}$ tends to the unmixed state* (2.18) *as $t \to \infty$.*

2. *We have $s = 0$ if and only if $\mathbf{x}$ tends to the perfectly-mixed state as $t \to \infty$: for some $S, T \subset C_1$ satisfying $S \sqcup T = C_1$ and $|S| = |T| = C/2$,*

$$i \in S \Longrightarrow \tilde{x}_{i,p} = -1/2,$$
$$i \in T \Longrightarrow \tilde{x}_{i,p} = 1/2.$$

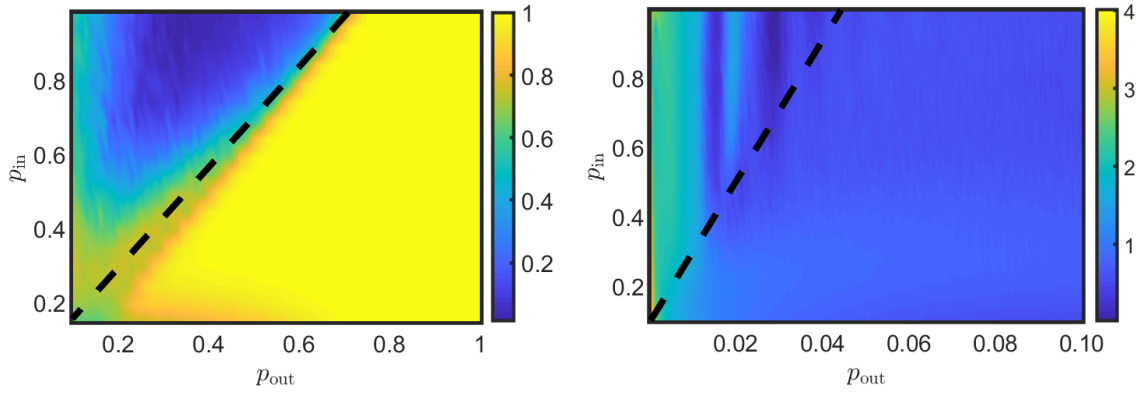

Figure 2.7: A numerically-simulated bifurcation graph of our model in terms of $(p_{\text{in}}, p_{\text{out}})$; the color bar indicates the value of the sorting number, s, as in (2.23). Parameters as in 2.6. Left panel: $p_{\text{out}} \in [0.1, 1]$, right panel: $p_{\text{out}} \in (0, 0.2]$; in both, $p_{\text{in}} \in (0, 1]$. Results averaged over 100 runs with point-source initial conditions about -100 and 100. Adjacency matrices generated randomly but with specified proportions of connectedness. Observe that the color bars in the left and right panel are not equivalent.

We now seek to describe the system's dynamics in terms of inner and outer connection probabilities. In Figure 2.7, the center of mass equations are examined in

place of (2.7); that is, though we still solve the full model (2.7), we use the center-of-mass coordinates (2.19) for visualization. Here, we record each community's center of mass when we have determined each particle has settled into an approximate steady state (at a large time value, $t = T$). Our observations from the numerics depicted in the left panel of Figure 2.7 are summarized in Result 1, a partial validation of Conjecture 1.

Result 1. *Let the repulsion parameter, κ, and the number of particles, N, be fixed. Experimentally, we find there exist a, b so that*

1. $p_{\text{in}} < ap_{\text{out}} + b$ *implies*

$$|\bar{m}_1(T) - \bar{m}_2(T)| \approx 1.$$

   By Proposition 2.0.21, this suggests the unmixed state (2.18) *is attained with high probability* ≈ 1.

2. $p_{\text{in}} > ap_{\text{out}} + b$ *implies*

$$|\bar{m}_1(T) - \bar{m}_2(T)| \not\approx 1,$$

   suggesting the unmixed state is not attained with high probability ≈ 1.

We discuss each of these in turn. For Result 1–1, choosing an inner connection probability below the threshold value of $ap_{\text{out}} + b$ led to, averaged over many (100) runs, an average mean difference of

$$|\bar{m}_1(T) - \bar{m}_2(T)| \approx 1. \tag{2.24}$$

Over these runs, the maximum value of the above quantity (2.24), similarly, did not exceed 1, hence we can conclude each run yielded an approximate value of 1. For T

large, we interpret that as an approximate statement regarding

$$d_{\text{final}} = \lim_{t\to\infty} |m_1(t) - m_2(t)|,$$

the actual value each community tends to. In our simulations, provided

$$p_{\text{in}}, p_{\text{out}} \gg \log N/N,$$

we did not observe a difference in centers of mass near 1 without $\mathbf{x}$ appearing to tend to $\tilde{\mathbf{x}}$. Accordingly, we arrive at Result 1–1. Of course, Result 1–1 suggests little information is lost asymptotically by passing the system in $\mathbf{x}$ to a simple, two-particle interaction in m_1, m_2, which will motivate our later discussion of a "center-of-mass approximation." Our interpretation of Result 1–2 follows directly from Proposition 2.0.21–1. We are careful to avoid suggesting Result 1–2 implies a mixed state is attained with probability not near zero, as the later discussion of the right panel of Figure 2.7 will illustrate.

As a side concern, our results also indicate $(p_{\text{in}}, p_{\text{out}})$ pairs at which

$$|\bar{m}_1(T) - \bar{m}_2(T)| \approx 0.$$

Given the smallest value possibly attainable by such a quantity is zero, again this implies $m_1(T) - m_2(T) \approx 0$ over a proportion of runs close to 1. Assuming the two-cluster state attracts these trajectories, this would indicate the system attains a nearly perfectly-mixed state with high probability. However, individual runs over these pairs, such as the one that yielded the $p_{\text{out}} = 0.2$ panel of Figure 2.6, suggest such an assumption may be premature. In some of these cases, we observe trajectories tending to banded steady states, for which there exist i such that $|x_i - x_j| \neq 0$ for

any j.

The Transition Between Mixed and Unmixed States In both panels of Figure 2.7, we have added a bold dashed line to emphasize the threshold between regimes. In the left panel, where $p_{\text{out}} \geq 0.2$, the line distinguishes the area in parameter space in which our initial states tend to the community-separated, two-cluster state with high probability. For $(p_{\text{out}}, p_{\text{in}})$ pairs lying to the right of the line, particles tend to remain well-separated in space from initial states where this is true as $t \to \infty$. For pairs lying to the *left* of the line, particles mix between communities to varying degrees. We note that, in this later regime and for p_{in} especially large relative to p_{out}, communities approach near-complete mixing; that is, for communities of equivalent size, half of each community's particles tend to each cluster location as $t \to \infty$. In the lower-outer-connectivity case (right panel), the line splits the pictured region in parameter space into an area in which the two-cluster, albeit mixed, state prevails (pairs to the right of the line) and an area in which a degenerate state consisting of more than two clusters dominates. We explain the origins of this phenomenon later.

We stress the importance of community-separated initial conditions here. We are largely concerned with metastable dynamics in this case rather than classic (linear) stability. Specifically, we want to determine the tendency of particles to sort themselves into clusters upon initialization at a large distance. One application of this, later, is in using this information to determine community structure based upon observed, real system behavior; this applies provided the system obeys our simple aggregation laws and we begin to observe particle pairs at very small or very large distances.

As such, the general tendency reflected in Figure 2.7 for smaller p_{out} values to result in larger community-to-community separations in centers of mass – to the

right of the well-mixed (deep blue) portion of the graph – does not indicate that the two-cluster unmixed state (2.18) approaches stability in the sense of Definition 2.0.3. Instead, it just indicates that, with high probability, it is attractive enough to draw in particles seeded from our particular set of initial conditions: communities individually clustered tightly, but at extremely large distances from one another. A more standard numerical treatment would examine relatively small perturbations of the two-cluster state for numerical stability.

We move on to discussing the bifurcations in Figure 2.7. The intuition for the phenomenon observed here arises from the following fact: for a kernel $F(r)$ as in (2.5), the tendency of a connected, two-particle system is clearly to converge to a fixed distance of 1. The system of N particles, for N large, is governed by many such interactions. We now imagine two communities seeded at a given distance apart, with particles from either community being tightly grouped. An abundance of connections between these two communities – large outer connectivity probability – is a strong attractive force between the centers of mass when r is large, and is a repulsive force otherwise. The resulting system dynamics rely on the "push" and "pull' between these two tendencies. For large inner and outer connectivities, the tendency of each community to split into two clusters is mitigated by the repulsive/attractive forces of the neighboring community. Yet, as the outer connectivity decreases, the latter force becomes weaker, so that particles from one community can join other nearby communities.

As it appears in the figure, the transition between these two behaviors appears rather sharp. We refer to the location of the shift as $p_{\text{out}} = p_c(p_{\text{in}})$ for each inner connection probability, p_{in}. We note that this formulation, strictly speaking, only makes sense on average, not on a run-to-run basis. For a graph randomly generated from a given edge probability or edges randomly picked from a required proportion of

connections, it is possible that variance in the graph structure may lead to a number of behaviors. That is, even if we record $p_c(1) = 0.68$, generating a graph with a finite number of nodes from the inner/outer probability pair of $(1, 0.65)$ could lead to the entirely separated state. In some sense, then, our proxy for the limiting $p_c(p_{\text{in}})$ strongly relates to the centers of mass picture. If the average separation found over a large number of runs is close to 1, then we can infer an individual run has a high probability of being separated. Thus, it is acceptable to include that inner/outer pair in the separated regime.

System Behavior for Very Small p_{out} For completeness, we here include a similar panel for extremely low connection probabilities in Figure 2.7. Somewhat surprisingly, we observe yet another change in the centers of mass; they begin to tend upward to a large (greater than 1) separation. This is perhaps an artifact of a low average-p state when $\kappa = 0$, that is when there is only attraction and repulsion imposed by the second piece of (2.5) over large distances. In that case, it is possible to find a solution close to a "four-cluster" steady state, with each cluster separated by a distance of 1 from the next, despite the existence of only two communities.

We offer some additional precision to this claim below.

Definition 2.0.22. *(Outer-connected and outer-disconnected community subsets). Take $\mathcal{G} = (V, D)$ and let C_1, C_2 be a partition of V. We define the outer-connected and outer-disconnected subsets of community i, respectively $C_{i,c}$ and $C_{i,d}$, as follows:*

$$C_{i,c} = \{v \in C_i : \exists\, v' \notin C_i \ni (v, v') \in D\} \tag{2.25}$$

$$C_{i,d} = \{v \in C_i : \forall v' \notin C_i \ni (v, v') \notin D\} \tag{2.26}$$

Remark 2.0.23. *Clearly,* (2.25) *and* (2.26) *imply $C_i = C_{i,c} \sqcup C_{i,d}$ for $i = 1, 2, \ldots, k$.*

The sets of Definition 2.0.22 are directly used to specify the four-cluster steady state $\mathbf{x}_4(t) = (x_{i,4}(t))$, where

$$x_{i,4}(t) = \begin{cases} -3/2 & : \quad i \in C_{1,d}, \\ -1/2 & : \quad i \in C_{1,c}, \\ 1/2 & : \quad i \in C_{2,c}, \\ 3/2 & : \quad i \in C_{2,d}. \end{cases} \tag{2.27}$$

(We do observe that particles in $C_{i,d}$ can also coexist with particles in $C_{i,c}$ at $\pm 1/2$, respectively.) This is well-defined due to Remark 2.0.23. We next show it is actually a solution of (2.7).

Proposition 2.0.24. *Let $\mathcal{G} = (V, D)$, with suitable outer-connected and outer-disconnected sets, $C_{i,c}$ and $C_{i,d}$, as in Definition 2.0.22. Then, the four-cluster steady state* (2.27) *is a solution to the aggregation equations* (2.7)*.*

Proof. Take t arbitrary, and let G be the function of Appendix A (as in (A.1)):

$$G(i,j) = e_{Nij} F(|x_i - x_j|) \frac{x_i - x_j}{|x_i - x_j|}.$$

Supposing $i \in C_{1,d}$, then $j \in C_{1,d}$ implies $G(i,j) = 0$, as $|x_i - x_j| = 0$ by definition (2.27). If $j \in C_{1,c}$, then $G(i,j) = 0$ due to $F(|x_i - x_j|) = F(1) = 0$ by the definition of F from (2.5). If $j \in C_{2,c} \cup C_{2,d}$, then $G(i,j) = 0$ as $e_{Nij} = 0$ due to definition of the outer-disconnected subset from (2.26).

Supposing $i \in C_{1,c}$, then $j \in C_{1,d}$ implies $F(|x_i - x_j|) = F(1) = 0$. If $j \in C_{1,c}$, then $|x_i - x_j| = 0$. If $j \in C_{2,c}$, then $F(|x_i - x_j|) = F(1) = 0$. Finally, if $j \in C_{2,d}$, then the definition (2.26) again implies $e_{Nij} = 0$. In all four cases, we must have $G(i,j) = 0$. Repeating the logic above for $i \in C_{2,c}$ or $i \in C_{2,d}$, the Proposition follows. □

Remark 2.0.25. *Note that we can infer the difference between two communities' centers of mass given the state* (2.27)*:*

$$|m_1 - m_2| = \frac{3}{2}\frac{|C_{2,d}|}{|C_2|} + \frac{1}{2}\frac{|C_{2,c}|}{|C_2|} + \frac{3}{2}\frac{|C_{1,d}|}{|C_1|} + \frac{1}{2}\frac{|C_{1,c}|}{|C_1|} \tag{2.28}$$

It is clear from Definition 2.0.22 that $|C_{i,d}|/|C_i| \to 1$ *(for each* i*) implies* $|C_{i,c}|/|C_i| \to 0$*. Accordingly,* (2.28) *yields*

$$|m_1 - m_2| \to 3.$$

Conversely, as (for each i*)* $|C_{i,c}|/|C_i| \to 1$*, then* $|C_{i,d}|/|C_i| \to 0$*. Accordingly* (2.28) *yields*

$$|m_1 - m_2| \to 1.$$

A difference of $|m_1 - m_2| = 3$ is thus what we expect to see as outer connections become sparse, that is $O(N)$. Broadly, Remark 2.0.25 reveals the familiar two-cluster state as a simple evolution from the four-cluster state; while the disconnected component exists, particles are layered into four clusters equidistant from each other. As the number of outer connections grows, the disconnected component and thus the associated cluster at $\pm 3/2$ loses members to the connected cluster at the closer-to-0 values of $\pm 1/2$, respectively. Thus $|m_1 - m_2|$ moves closer to 1. Once nothing remains of the disconnected components, the associated state is simply the two-cluster state, $\tilde{\mathbf{x}}$, and $|m_1 - m_2| = 1$.

We provide a plot of a trajectory converging near the state (2.27) in Figure 2.8 for illustrative purposes; every trajectory tending to the position we have labeled with $C_{i,c}$ or $C_{i,d}$ (for some i) belongs to that respective set. We ask a natural question:

Question 4. *As a function of the system's parameters, how do trajectories near the four-cluster steady state* $\mathbf{x}_4$ *evolve as* $t \to \infty$*?*

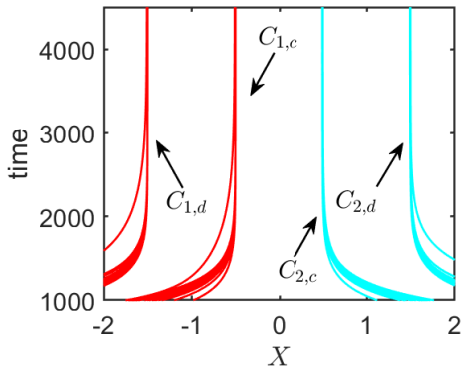

Figure 2.8: A plot of a trajectory tending to the 4-cluster state (2.27) as $t \to \infty$. Trajectories of particles from the outer-connected and outer-disconnected subsets of each community, $C_{i,c}$ and $C_{i,d}$, $i = 1, 2$ are labeled.

We assume the system's outer connection probability is sufficiently small for the state to exist meaningfully, with $C_{i,d} \neq \emptyset$. That is, we have $|D_{\text{out}}| = O(N)$. Note also from the right panel of Figure 2.7 that such a state appears to not heavily depend on p_{in}, hence we focus on the repulsion parameter, κ alone.

In Figure 2.9, we provide a sample plot of numerical trajectories of the aggregation equations (2.7) with $N = 200$ particles. We use a sufficiently small p_{out} for the four-cluster steady state to exist. We consider the centers of mass of each community's connected/disconnected component; for $i = 1, 2$, let

$$m_{i,c} = \frac{1}{|C_{i,c}|} \sum_{j \in C_{i,c}} x_j,$$
$$m_{i,d} = \frac{1}{|C_{i,d}|} \sum_{j \in C_{i,d}} x_j.$$

Then, define

$$\epsilon = \max\left(|m_{1,c} - m_{1,d} - 1|, |m_{2,c} - m_{1,c} - 1|, |m_{2,d} - m_{2,c} - 1|\right). \tag{2.29}$$

We use the quantity (2.29) as a quick measure of the deviation between low-p_{out} trajectories to (2.7) and the four-cluster steady state (2.27). Varying $\kappa \in [0, 1]$, we offer a few discrete observations for κ in this range:

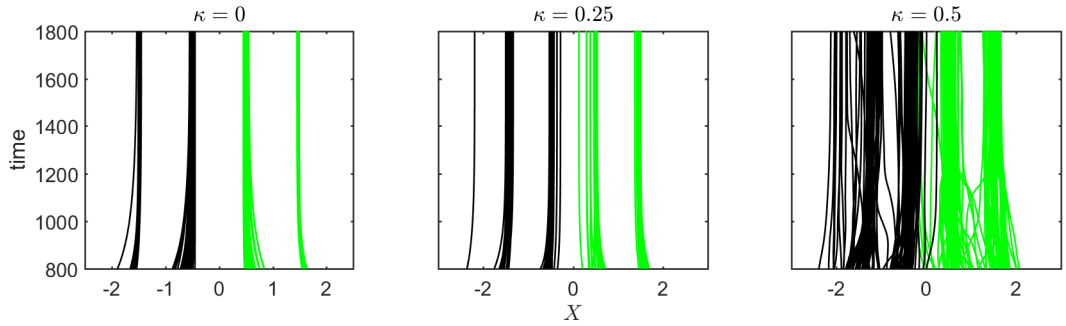

Figure 2.9: A plot of the degenerate 4-cluster state under different repulsion strengths, κ. Note the shadow of the four-cluster steady state remains as κ is increased, though the clusters become wider bands as κ is increased.

- For $\kappa = 0$, we find $\epsilon = 0.03$; that is, each cluster's center of mass strays no more than 3% past the prescribed separation of 1 from the next. Of course, in this case we expect such a difference to approach 0 as $t \to \infty$.
- For $\kappa = 0.25$, we find $\epsilon = 0.04$.
- For $\kappa = 0.5$, we find $\epsilon = 0.12$.
- For $\kappa = 0.99$ (not depicted in Figure 2.9), we find $\epsilon = 0.12$.

The last result above is interesting, as this value of κ is very near the critical threshold for instability of the two-cluster state in the all-to-all aggregation equations (as per Theorem 2.0.4). In attempting to answer Question 4, our numerical results (though not exhaustive) are suggestive of a κ threshold before which ϵ is very nearly zero, and past which ϵ increases more rapidly as a function of κ (though it remains small relative to 1). Accordingly, as we see limited deviation from the predicted location of

each center of mass regardless of κ, we believe the centers-of-mass difference (2.28) for the four-cluster steady state (2.27) can be used to well-approximate the actual centers-of-mass difference $\lim_{t\to\infty} |m_1(t) - m_2(t)|$ in this regime of probability values.

For what probabilities are we assured either a disconnected component or the absence of one? The thresholds for connectedness *within* Erdős–Rényi clusters are well-established. For connectedness between communities — in the sense that each particle from each community has at least one link to a particle from the other community, we establish some simple probabilities. For a given particle, the probability of having at least one link to a particle from the other community is the probability of having *no* links, subtracted from unity. Here, X_i denotes the random variable for particle x_i's degree. Thus, for a particular outer probability p_{out},

$$\begin{aligned}\mathbb{P}\{X_i > 0\} &= 1 - \mathbb{P}\{X_i = 0\} \\ &= 1 - (1 - p_{\text{out}})^{|C_j|}.\end{aligned}$$

Hence,

$$\mathbb{P}\left\{\bigcap_i X_i > 0\right\} = \left(1 - (1 - p_{\text{out}})^{|C_j|}\right)^{|C_i|}. \tag{2.30}$$

These yield the following result:

Proposition 2.0.26. *Suppose we have two equivalently-sized communities to partition V, that is $|C_1| = |C_2| = N/2$. Then, the community C_i of the graph $\mathcal{G} \sim SBM(N, C, P)$ almost surely (as $N \to \infty$) has an empty outer-disconnected component, $C_{i,d}$, if there exists a $\delta > 0$ such that*

$$p_{\text{out}} > (2 + \delta)\frac{\log N}{N}. \tag{2.31}$$

Conversely, if there exists a $\delta > 0$ *such that*

$$p_{\text{out}} < (2-\delta)\frac{\log N}{N}, \tag{2.32}$$

then the graph $\mathcal{G}$ *almost surely has a nonempty outer-disconnected component,* $C_{i,d}$.

Remark 2.0.27. *Though we omit a rigorous proof, the observation of Proposition 2.0.26 stems from recalling*

$$\lim_{N\to\infty}\left(1-\frac{1}{N}\right)^N = e^{-1}.$$

As $\log N \ll N$, *we substitute* $p_{\text{out}} = (2+\delta)\log N/N$ *and replace*

$$(1-p_{\text{out}})^{N/2} = \left(1-\frac{(2+\delta)\log N}{N}\right)^{N/2} \approx N^{-(2+\delta)/2} = \frac{1}{N^{1+\delta/2}}.$$

Then, the limit

$$L = \lim_{N\to\infty}\left(1-\frac{1}{N^{1+\delta/2}}\right)^{N/2} \tag{2.33}$$

tends to one (indicating each particle almost surely has one link to the other community as $N \to \infty$*). Upon replacing* δ *with* $-\delta$, *we find the limit* (2.33) *tends to zero (indicating at least one particle almost surely has no links to the other community as* $N \to \infty$*).*

The scalings (2.31) and (2.32) of Proposition 2.0.26 are, of course, suggestive of the classic Erdős–Rényi result. There, it was found that for an simple random graph of N nodes, the sharp threshold for connectivity was centered about $\log N/N$. Of course, our stochastic block graph (in the easiest case) is simply a gluing of two Erdős–Rényi graphs of size $N/2$, in the sense that connections within each community have uniform density (on average). Accordingly, the threshold for connectivity in each,

independently, scales like $2\ln(N/2)/N$. Noting $\ln(N/2) = \ln(N) - \ln(2)$ and that $\ln(2) \ll \ln(N)$, they must share the same (sharp) threshold as for the classic Erdős–Rényi graph. In this capacity, the scaling for connectivity between communities is precisely that of the threshold for connectivity within communities; this aspect remains the same despite the added structure of the stochastic block graph.

The Location and Character of the Transition Point In this section, we seek to describe how the location of the transition point between mixed (with high probability) and unmixed states (2.18) varies as our system parameters vary. Particularly, motivated by Figure 2.7, we attempt to describe how varying inner probabilities affects the location of this point. We also vary the system's repulsion parameter, κ, to show how that affects the transition point. We begin with a suitable definition.

Definition 2.0.28. *(Transition point). Let $\mathcal{G} \sim SBM(N, C, P)$, where C is a fixed two-community partition of $\{1, 2, \ldots, N\}$ and*

$$P = \begin{bmatrix} p_{\text{in}} & p_{\text{out}} \\ p_{\text{out}} & p_{\text{in}} \end{bmatrix}$$

for $p_{\text{in}}, p_{\text{out}} \in [0, 1]$. Additionally, define the aggregation system in terms of center-of-mass coordinates through (2.22)*. Then the transition point, an outer connection probability value denoted $p_{\text{out}} = p_c$ satisfies*

$$p_c = \sup \left[p_{\text{out}} : \mathbb{P}_{\mathcal{G}} \left\{ |m_1(t) - m_2(t) < 1| \right\} = 1 \right]. \tag{2.34}$$

Of course, for finite N any graph $\mathcal{G}$ is possible with finite (though perhaps extremely small) probability, hence the Definition 2.0.28 bears no fruit. Additionally,

even for probability values for which we are guaranteed an unmixed state (2.18), integration error in our numerical scheme often leads to a cluster separation of ≈ 1, but not exactly 1. Accordingly, we replace the exact requirement (2.34) with a small tolerance, ϵ, and infer probabilities via an average of $|m_1(T) - m_2(T)|$ values over many runs, varying $(p_{\text{in}}, p_{\text{out}})$ throughout $[0,1] \times [0,1]$ and realizing graphs $\mathcal{G} \sim \text{SBM}(N, C, P)$ at each pair a large number of times.

In Figure 2.10, we offer a slice of the full bifurcation diagram 2.7. For illustrative purposes, we have fixed the inner probability at $p_{\text{in}} = 0.8$; our graphs have $N = 200$ with evenly-sized communities. For each data point, we have run the system to large time, T, recorded $|m_1(T) - m_2(T)|$ for each run, and then averaged these values over many graph realizations of $\mathcal{G} \sim \text{SBM}(N, C, P)$. For Figure 2.10, we have additionally decomposed the difference in centers of mass data into its two parts, $m_1(T)$ and $m_2(T)$, to emphasize the prior point of Proposition 2.0.18–2; here, we noted that $m_1(t) = -m_2(t)$ for all time t provided $|C_1| = |C_2|$ and $m_1(0) = -m_2(0)$.

For $\kappa = 0.5$, we notice a rich set of behaviors for the slice.

- We see, for $p_{\text{out}} > p_c$, values of

$$\bar{d}_{\text{final}} = |\bar{m}_1(T) - \bar{m}_2(T)|$$

  very near 1, indicating the unmixed state (2.18) is attained with high probability.

- For $p_{\text{out}} \in (p_c - \delta, p_c)$ (here $\delta < 1$ is a certain small number), the quantity $\bar{d}_{\text{final}}$ attains values less than one, and it changes rapidly in this region as a function of p_{out}.

- There appears to be a "midpoint," which we here denote as p_m, satisfying

$p_m \approx p_c/2$. Near this value, $\bar{d}_{\text{final}}$ attains a minimum.

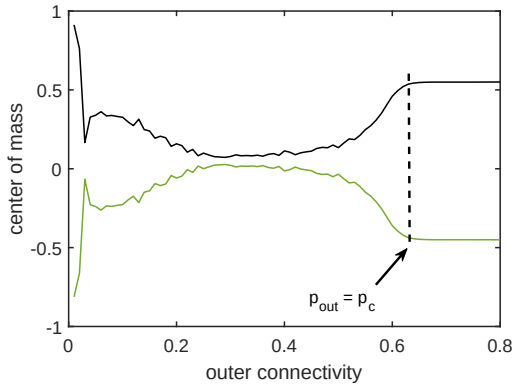

Figure 2.10: A slice of the full bifurcation graph of Figure 2.7 at $p_{\text{in}} = 0.8$. Note the symmetry in the center-of-mass data about $x = 0$ and the critical outer connection probability at which the unmixed state (2.18) is no longer attained with high probability.

We explore how the character of these slices changes as κ is varied first. In Figure 2.11, we illustrate the effect of κ on the crucial behaviors mentioned above. Specifically, we take $p_{\text{in}} = 0.8$ (as in the slice Figure 2.10), $\kappa \in [0.5, 1]$, and $p_{\text{out}} \in [0.2, 1]$ on an evenly-spaced grid. Each data point comes from the averaged results of 100 initializations of $\mathcal{G} \sim \text{SBM}(N, C, P)$ with a given $p_{\text{in}}, p_{\text{out}}$ pair. A summary of our experiment's results, is provided below in Result 2 with an associated depiction for $\kappa \in \{0.5, 0.7, 0.9\}$ in Figure 2.11.

Result 2. *Throughout our regime of tested parameter values for κ, we find:*

- *All else being equal, the location of the transition point, p_c, is an increasing function of κ.*
- *For fixed p_{in}, the smallest value of $\bar{d}_{\text{final}}$ attained is generally an increasing function of κ.*

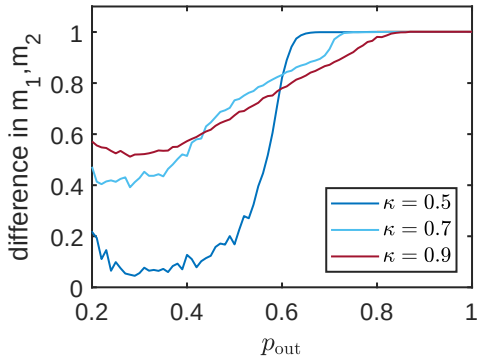

Figure 2.11: A plot of $\lim_{t\to\infty} |m_1(t) - m_2(t)|$ (estimated at large t) as a function of p_{out}. Various repulsion strengths $\kappa \in \{0.5, 0.7, 0.9\}$ and an inner connection probability of $p_{\text{in}} = 0.8$ were used.

Result 2–1 is an intuitive one, and we provide a more detailed heuristic argument for it in Appendix D. However, we briefly summarize such arguments here. For the unmixed two-cluster state (2.18) to attract, inner-community repulsive forces (dictated by the value of κ for a nearly-converged trajectory and, indirectly, by p_{in}) cannot be so strong as to overwhelm the outer-community repulsive forces (indirectly determined by p_{out}). Hence, a secular increase in κ increases such inner-community repulsive forces, and, accordingly, increases the requirement on our outer forces of connection to compensate and retain attraction. For $N \to \infty$, this balance may be simply expressed as

$$\kappa p_{\text{in}} = p_{\text{c}},$$

which explains why we would expect to see the transition point vary not only as an increasing function of κ, but a linear function (for p_{in} fixed, or vice versa, as a linear function of p_{in} for κ fixed). For finite N, though, variance in the connection structure of $\mathcal{G}$ appears to erode this relationship. For particularly high values of κ (depicted in Figure 2.11: $\kappa = 0.9$), the transition point location, p_c, may even exceed the inner probability of connection. This occurrence, of course, would run contrary

to our oft-stated assumption that outer connection structure is sparse relative to inner connection structure, hence such κ values with natural choices of probability parameters may only lead to mixing-type behaviors with high probability.

Next, we focus on Result 2–2. Here, we notice that larger values of κ tend to result in larger minimum d_{final} values over a fine grid (with grid points in $\mathbf{p}_{\text{grid}}$), defined by

$$\mathbf{p}_{\text{grid}}(i) = p_{\min} + (i-1)\Delta p, \quad \Delta p = \frac{1 - p_{\min}}{n_{\text{grid}}}. \tag{2.35}$$

Typically, $n_{\text{grid}} \geq 100$ in (2.35). Assuming trajectories are still attracted by the two-cluster state (2.6), Proposition 2.0.21 implies our system's particles tend to less well-mixed states (as $t \to \infty$) for larger values of κ. In this sense, values of κ closer to 1 perhaps limit the extremes of behavior in our system; there are less suitable $(p_{\text{in}}, p_{\text{out}})$ pairs for unmixed states and nearly perfectly-mixed states.

Of course, we cannot necessarily interpret the d_{final} values attained from small p_{out} values or $\kappa \approx 1$ in the same way as those gathered from κ not near 1. This is due to our observation that, for $p_{\text{in}} = O(1)$ and κ not close to 1, a permutation of (2.6) appears to be broadly attracting even for relatively small p_{out}; conversely, for $\kappa \approx 1$, it is our experience that a permutation of (2.6) attracts for a much smaller set of outer probability values or over a much longer timescale. Accordingly, as per Proposition 2.0.21, we suspect the implications of d_{final} as a "sorting number" are relevant to the former case but not necessarily the latter. However, as our experience indicates, asymptotic destabilization of (2.6) tends to lead to trajectories like the $p_{\text{out}} = 0.2$ (top-right) panel of Figure 2.6 over long stretches of time. In this case, we do not observe sorting as a binary phenomenon (particle tending to one of two fixed locations in space as $t \to \infty$) unless we loosely re-interpret cluster 1 and 2 as, for

instance,

$$C_1 = \{i \in V : x_i(T) \leq \text{median}(\mathbf{x})\}, C_2 = \{i \in V : x_i(T) > \text{median}(\mathbf{x})\},$$

Under this interpretation, a trajectory like the top-right panel of Figure 2.6 (persisting for all time) would be nearly perfectly-mixed, as about one-half of each community's particles fall to the left of the median at time T; yet we still observe a value of $d_{\text{final}} > 0$. We must keep this in mind to avoid treating $\bar{d}_{\text{final}}$ as a sorting number in regions of parameter space in which a permutation of the two-cluster state (2.6) does not attract our initial states with high probability or in which such a state is attracting over excessively large convergence times (that is not captured by our numerical scheme).

We return to our previous discussion of Figure 2.7. Of particular interest to us is the location of the transition point, p_c; again we refer to our modification of Definition 2.0.28. How does it change as we adjust our within-community connection probability? To answer this numerically, we simply traverse each slice in fixed p_{in} over the p_{out} grid (2.35) until we find a probability associated with a center-of-mass separation notably less than 1. That is, for a certain ϵ tolerance,

$$\tilde{p}_c(\epsilon) = \max\left\{p_{\text{out}} \in \mathbf{p}_{\text{grid}} : \bar{d}_{\text{final}} < 1 - \epsilon\right\}. \tag{2.36}$$

As error in our numerical integration scheme leads to slight deviations from a cluster-to-cluster separation of 1, even for parameters for which the unmixed state (2.18) is assured, we use the parameter ϵ in (2.36) to incorporate this error. Our data for $N = 200$ and $\kappa = 0.5$ is presented in Figure 2.12. We have fit the data to a linear curve; note the extremely tight linear relationship between p_c as a function of p_{in}. The curve's coefficients, $a = 0.637$ and $b = 0.1019$ directly correspond to the coefficients

mentioned in Result 1.

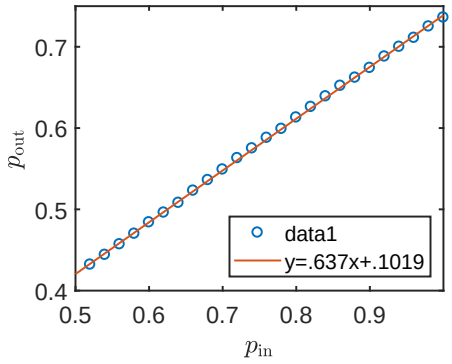

Figure 2.12: A plot of the estimated value of the transition point, p_c. Note the clear linear relationship of input to output; we have highlighted this by fitting the data to a linear equation.

We explore this in the context of sorting behavior in Figure 2.13. To align this more closely with the full graph in both inner and outer connection probabilities of Figure 2.7, we reverse the axes of Figure 2.12 to match. Given a $(p_{\text{in}}, p_{\text{out}})$ lying on the curve in Figure 2.12, our results suggest:

- an increase in the ratio of $p_{\text{in}}/p_{\text{out}}$ will lead to mixed two-cluster states $\pi(\tilde{\mathbf{x}})$ for some $\pi \in S_N$ with probability not near zero;
- a decrease in the ratio of $p_{\text{in}}/p_{\text{out}}$ will lead to an unmixed two-cluster state (2.6) with high probability.

The inner community connectivity also changes the behavior of the masses' centers in another important way; a higher inner-community connectivity limits the disorder of system behavior over time. We quantify this effect here.

Definition 2.0.29. *Let* $\mathbf{x} \in \mathbb{R}^N$. *Then the Euclidean norm of* $\mathbf{x}$ *(or* 2*-norm for short) is*

$$\|\mathbf{x}\|_2 = \sqrt{x_1^2 + x_2^2 + \cdots + x_N^2}.$$

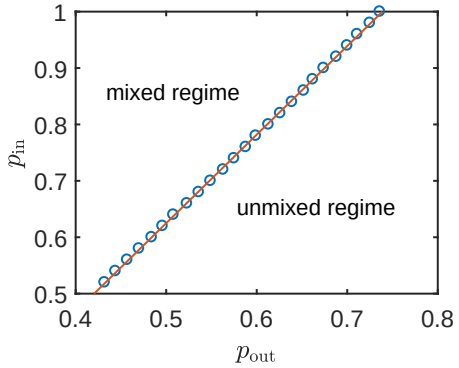

Figure 2.13: A plot of the qualitative shift in behavior (with high probability) as the transition point curve in $(p_{\text{out}}, p_{\text{in}})$ is crossed. Data is the same as in Figure 2.12.

We use Definition 2.0.29 to define a quantity representing a community's spread:

Definition 2.0.30. *For convenience, we let $\hat{C}_i$ be the vector of length $n_i = |C_i|$ containing elements of the partition arranged in ascending order. Also, define the vector $\mathbf{x}_{C_i}$*

$$x_{C_i}(j) = x\left(\hat{C}_i(j)\right).$$

Then, the inner-community distance of community C_i at time t, denoted $\sigma(C_i)(t)$, is

$$\sigma(C_i)(t) = \|x_{C_i}(t) - m_i(t)\mathbf{1}_{n_i}\|_2, \tag{2.37}$$

where m_i is the center-of-mass coordinate for community i of Definition 2.0.17 and $\mathbf{1}_{n_i} = (1, 1, \ldots, 1)$ is the length-n_i vector of ones.

Clearly, (2.37) is equivalent for any ordering of the partition.

We explore the maximum inner-community distance observed (numerically) for fixed p_{in}, as a function of p_{out}. As before, at each $(p_{\text{in}}, p_{\text{out}})$ pair, we initialize the adjacency matrix/starting positions of the particles and then evolve the system until large T. For each run, we record the maximum computed value of $\sigma(C_i)(t)$ over our

grid of time values. Our results are presented in Figure 2.14.

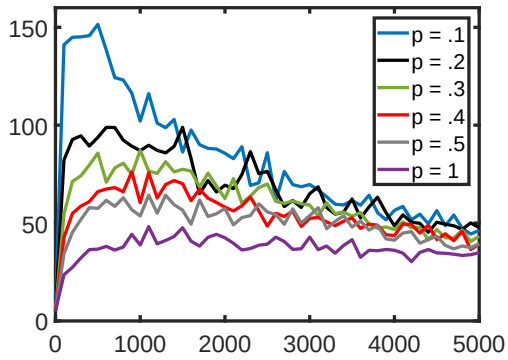

Figure 2.14: A plot of the maximum inner-community distance (2.37) over a large time interval. Legend denotes $p_{\text{in}} \in \{0.1, 0.2, 0.3, 0.4, 0.5, 1\}$. The x-axis is outer community connectivity (out of 10000 possible connections). Non-probability parameters as in Figure 2.6. Results averaged over 100 runs with point-source initial conditions at -100 and 100 and random adjacency matrices A.

We summarize our experience here.

Result 3. *On average, for all system parameters other than p_{in} fixed, the maximum computed value (in time) of $\sigma(C_i)$ is a decreasing function of p_{in} at each p_{out} connectivity value.*

This occurs somewhat disproportionately for large p_{out} rather than small p_{out} – to the point where, as we see in Figure 2.14, an inner connection probability of 1 leads to nearly-indistinguishable values of $\sigma(C_i)$ across p_{out} not near zero. For smaller values of p_{in}, it appears $\sigma(C_i)$ attains a maximum and then decreases as $p_{\text{out}} \to 1$.

System Convergence Times In Figure 2.15, we illustrate some average total convergence times over many values of p_{in} and p_{out}.

Definition 2.0.31. *The total system convergence time, $t_{\text{conv,tot}}$ (to tolerance ϵ) is defined by*

$$t_{\text{conv,tot}} = \inf \left\{ t : \lim_{z \to \infty} |x_i(t) - x_i(z)| < \epsilon \quad \forall i \right\}.$$

Of course, in practice we eschew the infimum of Definition 2.0.31 for a minimum over a fine grid of time values and replace the infinite-time limit with a system state at very large T.

Again, we have included a dashed line to indicate our separation of parameter space into unmixed (with high probability) and generally mixed states; this is the threshold from Result 1. We observe:

1. For $p_{\text{out}} > p_c(p_{\text{in}})$, trajectories likely tend to an unmixed state. In this case, individual particles rapidly tend to one of two cluster locations, separated by 1.

2. For $p_{\text{out}} < p_c(p_{\text{in}})$, trajectories often tend to mixed states. In this case, $t_{\text{conv,tot}}$ is relatively large.

Changing the balance of these probabilities in a way that leads to mixing thus increases $t_{\text{conv,tot}}$.

Holding our other parameters constant, we can reduce the likelihood of attaining an unmixed state in two countervailing, independent manners: by decreasing p_{out} or by increasing p_{in}. The latter affects convergence time more indirectly, simply by upsetting the balance between short- and large-distance repulsive forces to enable mixing. The former does this, as well, but also elongates the first observed timescale; decreasing p_{out} reduces the initial strength of repulsion between communities' centers of mass (which for large S tends to be the dominant force). This is clear from (2.7), particularly upon splitting the equations into an "inner" and "outer" component (the force exerted upon a community by its own particles and by the other community's particles) in (2.43)–(2.44). A smaller value of p_{out} has no effect on the inner force (2.43), yet it increases (on average) the outer force (2.44).

The graph 2.15 suggests, interestingly, that increasing p_{in} only tends to increase the system's convergence time if doing so takes us nearer to the given threshold; this

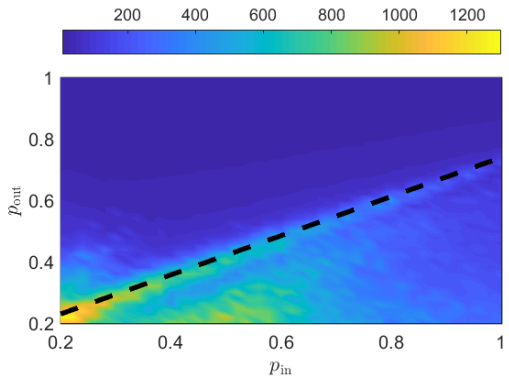

Figure 2.15: A plot of total convergence times (see Definition 2.0.31) as a function of inner and outer probabilities of connection. Each data point comes from an average of 25 runs.

should match our intuition. Increasing p_{in} from a point where the two-cluster unmixed state is attained with high probability (as indicated in Result 1) may drive the system into mixing behavior, elongating the overall timescale to converge, but increasing p_{in} *again* from this point tips the scales further in favor of mixing – small-distance repulsion – over the chief resistance to mixing, long-distance repulsion. Hence, it is difficult to predict the effect of increasing p_{in} on the system's convergence without first knowing where we are in relation to the critical "transition point" threshold. Decreasing p_{out}, on the other hand, tends to have a nearly universally neutral-to-increasing effect on t_{conv}. The direct channel it affects convergence through is a simple lengthening of the community-wide timescale, but as we shall explore later in this subsection, the increase we observe there cannot explain all, or even much, of the increase. Accordingly, we conclude that decreases in p_{out}, unlike p_{in}, tend to extend the mixing timescale *regardless* of our location in $(p_{\text{in}}, p_{\text{out}})$ space.

We now seek to decompose the data of Figure 2.15 into two key components in order to offer a heuristic for the existence of a transition point between the two-community unmixed state (2.18) (in which particles remain separated by community)

and a mixed variant (in which particles from different communities may coexist at a single location in space) here. To do so, we introduce two quantities: $t_{\text{conv},1}(p_{\text{in}}, p_{\text{out}}; \epsilon)$ and $t_{\text{conv},2}(p_{\text{in}}, p_{\text{out}}; \epsilon)$. We define them as follows.

Definition 2.0.32. *Let $\mathcal{G} \sim SBM(N, C, P)$ with N, κ fixed, $|C| = 2$, and $\epsilon > 0$. Additionally, suppose $\mathbf{x}$ is a solution to (2.7) with associated center of mass coordinates m_1, m_2 as in (2.19). Let*

$$T_{1,i} = \left\{ t : \lim_{z \to \infty} |x_i(t) - x_i(z)| < \epsilon \right\},$$
$$T_{2,i} = \left\{ t : |m_1(t) - m_2(t)| < 1 + \epsilon \right\}.$$

Then, the 1-community and 2-community time quantities, $t_{\text{conv},1}$ and $t_{\text{conv},2}$ are defined by

$$t_{\text{conv},1} = \inf \left(\bigcap_{i \in C_k} T_{1,i} \right), \tag{2.38}$$

$$t_{\text{conv},2} = \inf \left(\bigcap_{i \in \{1,2\}} T_{2,i} \right). \tag{2.39}$$

Remark 2.0.33. *Numerically, we replace the limit of Definition 2.0.32 with a function evaluation at large t – that is we assume*

$$\lim_{z \to \infty} x_i(z) = x_i(T), \quad T \gg 1.$$

In words, (2.38) is a measure of the time taken for a single colony (*with external edges removed*) to converge. Similarly, (2.39) is a measure of how long, for initially well-separated colonies, to arrive within a small tolerance of the ordered equilibrium separation of 1.

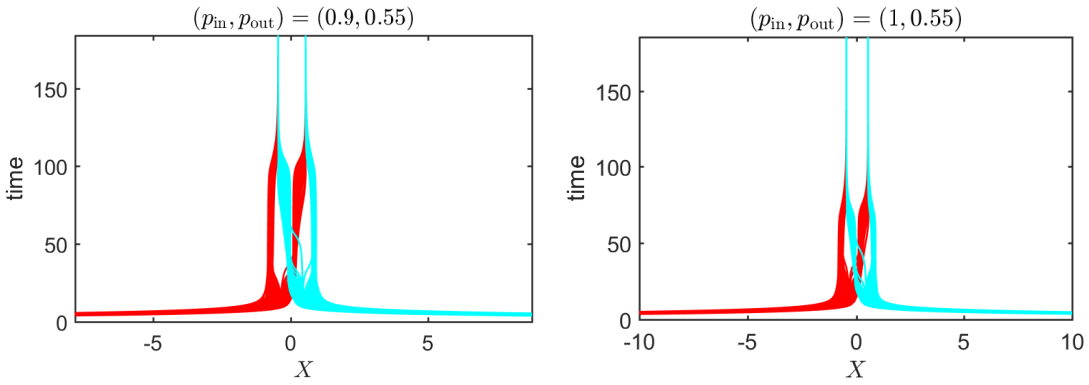

Figure 2.16: A full-particle plot for $p_{\text{out}} = 0.55$ and p_{in} near the critical transition point threshold. The inner connection probability is increased past the threshold in the right panel.

In Figure 2.16, we show this effect of increasing p_{in}. We generate plots from identical initial conditions $\mathbf{x}(0)$ and κ, only changing our $(p_{\text{in}}, p_{\text{out}})$ pair from $(0.9, 0.55)$ to $(1, 0.55)$. The network generated from each pair is very dense, though the latter pair yields a fully-connected inner connection structure. Moreover, each pair is obviously well outside the regime in which unmixed dynamics dominate. The pre-mixing timescale, $t_{\text{conv},2}$, is virtually unchanged. While this can change with p_{in}, we will see later that this change is limited on very dense graphs. The mixing timescale, the other component of $t_{\text{conv},1}$, is considerably reduced from the first (smaller p_{in}) initialization to the second (fully-connected) one.

Intuitively, we see the stochastic block structure in (2.7) as contributing two basic, generalized forces to its dynamics. The first, which the quantity $t_{\text{conv},1}$ hopes to capture, is the tendency of a given colony to split itself into the two-cluster steady state independent of other forces; this was observed, for instance, in the first panel of figure 2.6. In a sense, underlying each colony itself is an Erdős–Rényi structure, and this quantity communicates the contribution of that structure to the ordered behavior. Second, the quantity $t_{\text{conv},2}$ communicates the tendency (on the macroscopic scale) of

two colonies to draw in and repel each other based on the specific kernel $F(r)$. Our kernel forces a separation of 1, of course.

As a heuristic argument, the reason we might expect dynamics such as those seen in Figure 2.7 is this: for a high proportion of connected pairs of particles inside a single colony (p_{in} large), the inner-community forces dominate. Thus, $t_{\text{conv},2}$ ought to be small relative to $t_{\text{conv},1}$. As the inner and outer-community timescales – $t_{\text{conv},1}$ and $t_{\text{conv},2}$, respectively – are not comparable, long-term behavior of the system is dictated primarily by the two-community center-of-mass dynamics. That is, particles that begin separated in space are able to remain separated in space. As we decrease the strength of the bonds repelling and attracting particles within a single community, the single- and two-community timescales begin to equalize, in the sense that $t_{\text{conv},1} \approx t_{\text{conv},2}$. We surmrise the long-term, macroscopic dynamics are governed by a mix of the two.

In Figure 2.17, we explore this idea numerically. To generate the right panel, we

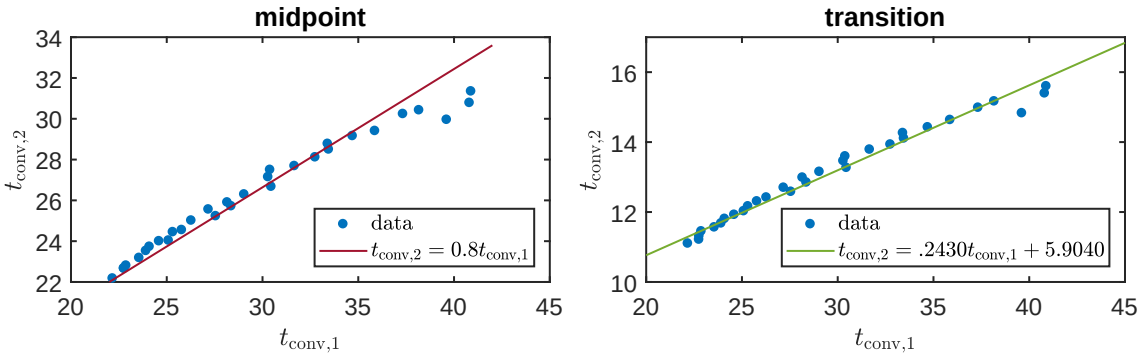

Figure 2.17: A plot of the approximate relationship between $t_{\text{conv},1}$ and $t_{\text{conv},2}$ at the computed value of the transition point and midpoint. Data points generated from an average of 25 runs each and for varying $p_{\text{in}} \in [0.7, 1]$.

traversed the bifurcation slices (for fixed p_{in}) like Figure 2.7 until we determined the first p_{out} value at which $|m_1(t) - m_2(t)| \to L < 1 - \epsilon$, indicating a loss of metastability of the unmixed two-cluster state (2.18). Note that we only considered relatively

large p_{in} slices, particularly those in the range $[0.7, 1]$. This is due to the generally degenerate small-p behavior (emerging from, among other factors, greater variation in network structure). We then recorded these critical probability values. For the left panel, as a simple estimate for the p_{out} value at which $\lim_{t\to\infty} |m_1(t) - m_2(t)|$ is smallest, we simply took each transition point pair (p_{in}, p_c) and halved the second coordinate to yield $(p_{\text{in}}, p_c/2)$; accordingly, we referred to this pair as the midpoint. Given the general structure of slices like Figure 2.7, it is a reasonable assumption that a great degree of mixing would likely occur at such a pair. For each panel, at this point, we generated random matrices with the prescribed connectivity values and determined $t_{\text{conv},1}$ and $t_{\text{conv},2}$ in the manner of Remark 2.0.33. To minimize variability, we performed this many (25) times and averaged our t_{conv} results over these runs.

As we can see, our heuristic offers a potentially useful characterization of the system dynamics provided p_{in} is not near zero. Despite the relationship not being entirely tight and the fact this link deteriorates as our connection probabilities tend to zero, there still appears to be a clear disparity in the relative sizes of $t_{\text{conv},1}$ and $t_{\text{conv},2}$ at the midpoint and at our computed value for the transition point comparatively.

Result 4. *Let $t_{\text{conv},1}$ and $t_{\text{conv},2}$ be as in Definition 2.0.32. We refer to $p_{\text{out}} = p_c(p_{\text{in}})$ as the transition point at a given inner probability value and $p_{\text{out}} = p_c(p_{\text{in}})/2$ as the midpoint. Letting p_{in} vary, we find*

1. ***Midpoint**: there is an approximately linear relationship between $t_{\text{conv},1}$ and $t_{\text{conv},2}$; that is,*

$$t_{\text{conv},2} = c_1 t_{\text{conv},1} + c_2.$$

   Moreover, our numerics find $c_1 \approx 1$, so that $t_{\text{conv},1}$ and $t_{\text{conv},2}$ are comparable in size.

2. ***Transition point**: there is an approximately linear relationship between $t_{\text{conv},1}$*

and $t_{\text{conv},2}$; that is,

$$t_{\text{conv},2} = d_1 t_{\text{conv},1} + d_2.$$

Moreover, our numerics find $c_1 \approx 0$, so that the quantities are not comparable in magnitude.

As the quantities $t_{\text{conv},1}$ and $t_{\text{conv},2}$ appear comparable in the region in $(p_{\text{in}}, p_{\text{out}})$ leading to the greatest probability of observing mixing behavior, we presume this indicates the relative importance of each component of the system's dynamics – large-scale convergence of centers of mass and particle-particle behaviors over relatively short distances. Conversely, past the transition point of Result 1, the quantities $t_{\text{conv},1}$ and $t_{\text{conv},2}$ appear to not be close in size, perhaps indicating the relative importance of one over the other. Of course, the unmixed state (2.18) lends itself to a characterization of being dominated by such large-scale behaviors; accordingly, we surmise the convergence of independent clusters to a separation of 1 dominates the scope of behaviors observed near this point. We do note, however, that while there is some uncertainty surrounding the precise location of this critical point, we believe the t_{conv} quantities to vary continuously near it, and thus a relationship similar to that expressed in Result 4 should hold if we are reasonably close in our estimation of the point. The link between these quantities, though very suggestive in the left panel of Figure 2.17, would likely be even tighter (that is, c_1 would be closer to 1) if we located a $(p_{\text{in}}, p_{\text{out}})$ pair at which the sorting number $|m_1(T) - m_2(T)|$ (for large T) is even smaller.

Center of Mass Approximation

In this section, we revisit the center-of-mass approach used for Figure 2.7. Our goal is one of dimensionality reduction; we seek to (at least in an approximate

sense) replace the system of N equations with a system of $M \ll N$ equations while still retaining some of the descriptive power of the original system. As established previously, center of mass coordinates are rather convenient in describing the broad behaviors of mixing or converging to a community-separated state, hence we use them here. Clearly, representing the system in center of mass coordinates represents a significant reduction in complexity – going from a system of N equations to a system of $|C|$ equations, where $|C|$ is simply the number of communities we have established in the stochastic block model. As is our general practice in this chapter, $|C|$ is typically 2.

We reiterate our previous definition of the center-of-mass coordinate system.

Definition 2.0.34. *(Center-of-mass coordinates for the aggregation equations (SBM)). Let $\mathcal{G} \sim SBM(N, C, P)$, and let $k = |C|$ be the number of components of our partition to V. Let*

$$n_i = |C_i| .$$

Then m_i, the center-of-mass coordinate corresponding to community i, is given by

$$m_i = \frac{1}{n_i} \sum_{k \in C_i} x_k. \tag{2.40}$$

For two communities, we may express our coordinate system as

$$m_1(t) = \frac{1}{n_1} \sum_{i \in C_1} x_i$$
$$m_2(t) = \frac{1}{n_2} \sum_{i \in C_2} x_i,$$

where m_1 and m_2 are the centers of mass of communities 1 and 2, respectively.

Remark 2.0.35. *Suppose $m_1 < m_2$, with $|x_i - x_j| > (1+\kappa)^{-1}$ for all $i \in C_i$ and $j \in C_2$. Additionally, suppose $n_1/N \to \tilde{p}_1$ and $n_2/N \to \tilde{p}_2$. After a Taylor expansion (see Appendix A), $m_1(t)$ and $m_2(t)$ admit a first-order approximation*

$$\frac{\mathrm{d}m_1}{\mathrm{d}t} \sim \frac{n_2 p}{N} \frac{(m_1 - m_2)(1 - |m_1 - m_2|)}{|m_1 - m_2|} = -\frac{n_2 p}{N}(1 + (m_1 - m_2)), \tag{2.41}$$

$$\frac{\mathrm{d}m_2}{\mathrm{d}t} \sim \frac{n_1 p}{N} \frac{(m_2 - m_1)(1 - |m_1 - m_2|)}{|m_1 - m_2|} = \frac{n_1 p}{N}(1 + (m_1 - m_2)), \tag{2.42}$$

where $\sim$ refers to an asymptotic relationship as $N \to \infty$.

Of course, in the event $n_1/n_2 \to 1$, then n_1/N and n_2/N both tend to $1/2$, and our approximation to m_1, m_2 satisfies $\dot{m}_1 = -\dot{m}_2$.

At first glance, the previously-mentioned restriction might seem like a rather strict requirement to impose on our system's many (in the limit $N \to \infty$) particles. Yet, as our experience of Result 1 tells us, this condition appears to be met in a large swath of parameter space. With Result 1 in hand, we expect this approximation to be extremely accurate for relatively high probabilities of connection *between* communities – that is, for $(p_{\text{in}}, p_{\text{out}})$ pairs satisfying

$$p_{\text{out}} > a p_{\text{in}} + b$$

for some $a, b < 1$. Intuitively, this requirement is necessary for the dynamics of (2.7) to preserve initial separations of particles (with different community belonging) in space.

In Figure 2.18, we offer a representative glance at observed center-of-mass data versus the predictions of our approximation scheme. We look at two initializations from probability parameters $(p_{\text{in}}, p_{\text{out}})$, one with $p_{\text{out}} > p_c$ and one with $p_{\text{out}} < p_c$. The former occurs in the "unmixed regime," while the latter occurs in the "mixed"

regime.

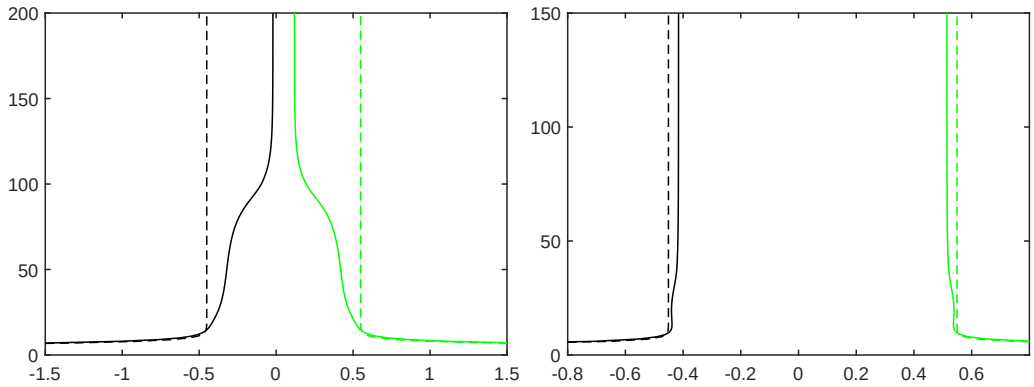

Figure 2.18: x-axis position, y-axis time. Solid lines represent trajectories of each community's center of mass; dashed lines represent our first-order approximation to the communities' centers of mass. Left to right: outer connectivity (p_{out}) of $.5, .65$, respectively. Parameters are as in Figure 2.6.

The equations (2.41)–(2.42) relate the system (2.7) to a simpler system of only two agents: one located at the mean of those particles from the first community, the other at the mean of those particles from the second community. The equations (2.41)–(2.42) are well-understood. Predictably, if $m_1(0) \neq m_2(0)$, the two masses tend to a separation of $|m_1 - m_2| = 1$, with

$$\frac{\mathrm{d}}{\mathrm{d}t}(m_1 - m_2) = Kp\,(m_1 - m_2)$$

for some constant K.

Result 5. *Let* $\mathbf{m} = (m_1, m_2)$ *and* $\tilde{\mathbf{m}} = (\tilde{m}_1, \tilde{m}_2)$ *be trajectories of our center-of-mass equations and approximate center-of-mass equations, respectively, defined by* (2.19) *(for system* (2.7)*) and* (2.41)–(2.42)*. Additionally, let* $p_c = p_{\text{in}}$ *be the threshold value defined in Result 1.*

Then, for $(p_{\text{in}}, p_{\text{out}})$ *with* $p_{\text{out}} > p_c$*, we find* $\tilde{\mathbf{m}}$ *to be an accurate approximation*

to $\mathbf{m}$ *with high probability, meaning*

$$|m_i(t) - \tilde{m}_i(t)| < \delta, \quad i = 1, 2$$

for some $\delta \ll 1$ *and for all* t*.*

That this is the case for large t is clear; the approximate equations (2.41)–(2.42) yield a center-of-mass separation, invariably, of 1. Result 1 suggests $|m_1 - m_2| \to 1$ with high probability for $p_{\text{out}} > p_c$. Hence, for sufficiently large t, we have $|m_i - \tilde{m}_i| \to 0$ (though we have included a small error, likely the result of our first-order integration scheme, in the above). We see Result 5, straightforwardly, in the right panel of Figure 2.18.

For $p_{\text{out}} < p_c$ (outer connection probabilities less than the critical threshold value), we find ourselves in the mixed regime described in Result 1. Accordingly, the small-r interactions we have discarded in our approximation are no longer negligible; as $|m_1 - m_2|$ does not tend to 1, there must be a non-vanishing subset of C_1, C_2 for which particles from the first tend to the same location as some particle from the second over time. Clearly, if $|m_1 - m_2| \not\to 1$, the approximate masses, $\tilde{m}_1$ and $\tilde{m}_2$ will prove to be rather inaccurate as $t \to \infty$.

We turn our attention to the left panel of Figure 2.18. Interestingly, we observe the following.

Result 6. *Let* $\mathbf{m} = (m_1, m_2)$ *and* $\tilde{\mathbf{m}} = (\tilde{m}_1, \tilde{m}_2$ *be trajectories of our center-of-mass equations and approximate center-of-mass equations, respectively, defined by* (2.19) *(for system* (2.7)*) and* (2.41)–(2.42)*. Additionally, let* $p_c = p_{\text{in}}$ *be the threshold value defined in Result 1.*

Then, for $(p_{\text{in}}, p_{\text{out}})$ *with* $p_{\text{out}} < p_c$*, we find* $\tilde{\mathbf{m}}$ *to be an accurate approximation*

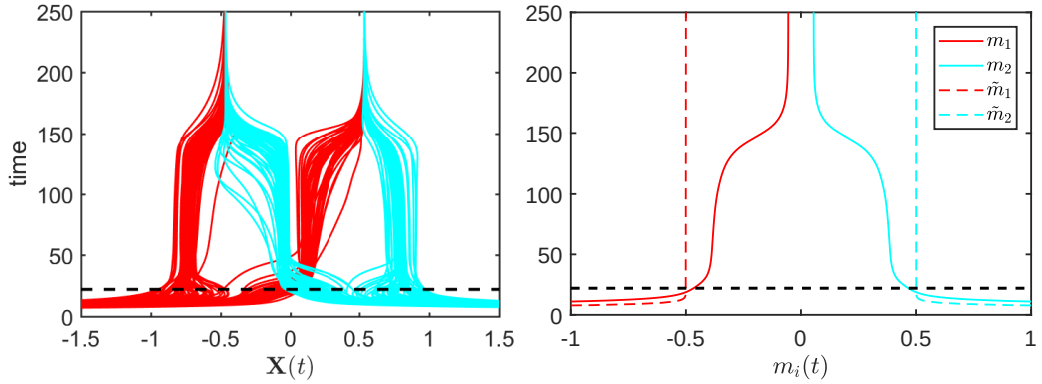

Figure 2.19: Left panel: full particle model; right panel: centers of mass (solid line) with approximation (colored, dashed line). Same colors denote same community membership. Horizontal dashed line is t value at which centers-of-mass separation of 1 is attained. Parameters: $(p_{\text{in}}, p_{\text{out}}, \kappa) = (0.8, 0.5, 0.5)$.

to $\mathbf{m}$ *with high probability for small* t*, meaning there exists a* T *such that*

$$|m_i(t) - \tilde{m}_i(t)| < \delta, \quad i = 1, 2$$

for some $\delta \ll 1$ *and for all* $t < T$*.*

In this sense, Result 6 indicates the center-of-mass approximation accurately captures the initial, convergence-of-communities timescale, even in the regime with small p_{out} relative to p_{in}. We illustrate this point by examining a representative plot of the full particle model (2.7) in Figure 2.19. To generate this figure, we initialize (2.7) with well-separated initial conditions, and probability parameters such that $p_{\text{out}} < p_c(p_{\text{in}})$; that is, generally $(p_{\text{in}}, p_{\text{out}})$ pairs for which we expect to not see trajectories tending to an unmixed state with high probability. In the left panel, we plot the state of each particle, x_i, over time. In the right panel, we plot centers of mass analogous to Figure 2.18.

As we can see, each community initially appears to partition itself into two halves, such that those particles belonging in the left half tend to the smaller of the

two cluster locations as $t \to \infty$. Conversely, those particles belonging in the right half tend to the larger of the two cluster locations as $t \to \infty$, at a distance of 1 from the smaller cluster. In the center-of-mass plot, we see this an interval $(0, T)$ on which $m_i'(t)$ is generally large relative to $m_i'(t)$ on (T, ∞). That is, the centers of mass rapidly converge to a certain separation, at which point mixing behavior begins in earnest.

If we consider individual particle behavior as the result of two competing forces, repulsion from nearby particles and attraction to far-away particles, then the latter point is easy to deduce. Initializing both communities at a large separation with a small deviation from the community's center of mass, the dominant interactions are determined by the kernel function, $F(r)$; it is those interactions of a given x_i with other x_j such that $|x_i - x_j| \gg 1$. For sufficiently small t, more pointedly, *between*-community interactions are all of this type; this is due to the fact that $|x_i(0) - x_j(0)| \gg 0$ if i, j belong to different communities.

The attractive force being the dominant one, again, holds for large separations. Let $F(r)$ be as given previously in (2.5),

$$F(r) = \min(r, 1 - r), \quad r \geq 0.$$

Note that F is bounded above (by 1), with this value being attained at $r = r_c$; additionally, F is unbounded below. Hence, given (2.7) can be additively decomposed over each pairwise interaction, a sufficiently large initial separation must lead to (with high probability) a dominant outer-community force relative to the inner-community force. This is due to

$$\frac{\mathrm{d}m_i}{\mathrm{d}t} = \frac{1}{Nn_i}(S_1 + S_2),$$

where

$$S_1 = \sum_{j \in C_i} \sum_{k \in C_i} a_{jk} F(|x_j - x_k|) \frac{x_j - x_k}{|x_j - x_k|}, \tag{2.43}$$

$$S_2 = \sum_{j \in C_i} \sum_{k \notin C_i} a_{jk} F(|x_j - x_k|) \frac{x_j - x_k}{|x_j - x_k|}. \tag{2.44}$$

That is, S_1 is the force component exerted upon the community's center of mass by its own particles, while S_2 is the force component exerted upon the community's center of mass by other communities' particles. As $|x_j - x_k|$ for $j, k \in C_i$ can be made as small as desired at $t = 0$, and $|x_j - x_k|$ for $j \in C_i, k \notin C_i$ can be made as large as desired, this point is clear.

Of course, as each community's particles creep closer to each other, the community-community separation diminishes, bringing the short-distance repulsive forces more in line with the large-distance attractive forces. The particles find themselves at a lull in the stream's current, as at some point, the repulsion induced by F among particles of the same community is of the same order, and then much larger, than attraction between members of different communities. Hence we eventually expect mixing behavior to prevail. As a loose estimate (motivated by Figure 2.19), we posit this occurs when $|m_1 - m_2| \sim 1$. Note the intersection of the approximate center-of-mass curves with the data; we find

$$|\tilde{m_1}(t) - \tilde{m_2}(t)| = |m_1(t) - m_2(t)| \approx 1$$

at roughly $t \approx 20$ (in this case). Before this point in time, our approximate center of mass curve accurately captures the actual motion of the centers of mass, as particles in each cluster move in tandem towards an average separation of 1. For ease of comparison, this critical time value is included as a dashed horizontal line on the

figure.

It is only *after* this time value that the centers-of-mass data, $\mathbf{m}$ deviate significantly from the estimated centers of mass, $\tilde{\mathbf{m}}$. Hence, despite the inability of the approximate mass solutions to even loosely resemble the actual solution for large t and over probability pairs with $p_{\text{out}} < p_c(p_{\text{in}})$, we still believe it to be useful in assessing the order of the macroscopic, community-wide timescale to then infer when sorting behavior is likely to occur. This feeds into our general interpretation of the system (2.7) as lending itself to a decomposition into large-scale (convergence of centers of mass) and small-scale (mixing) behaviors across certain swaths of $(p_{\text{in}}, p_{\text{out}})$ space.

Estimating System Convergence Times

We now seek to connect our discussion in the previous section – on convergence times – with the approximation presented in this section. To do that, we compare, for various tolerances ϵ, values for the t_{conv} quantities (achieved by numerical integration) – what we call the actual data – with those obtained by the center-of-mass approximation. In the latter case, we denote the quantities as $\tilde{t}_{\text{conv}}$.

To do this, we examine the equations (2.41)–(2.42). As they represent a simple, first-order system, we can solve them precisely for $\tilde{m}_i$, $i = 1, 2$ (see Appendix B). With exact solutions for the $\tilde{m}_i$ in hand, we now set $|\tilde{m}_1(t) - \tilde{m}_2(t)| = 1 + \epsilon$, where again ϵ represents a convergence tolerance – how close we desire our centers of mass to be to a separation of 1. This is necessary to achieve a finite value, as a simple two-particle system initialized at a distance *other than* 1 converges to this distance in the limit $t \to \infty$. By solving this equation for the critical t, we attain the value at which we determine convergence of the two communities up to a certain tolerance; necessarily, this quantity will be a function of the tolerance ϵ.

Remark 2.0.36. *We approximate the quantity* $t_{\text{conv},2}$ *of* (2.39) *with the following:*

$$\tilde{t}_{\text{conv},2}(p;\epsilon,s) = -\ln\left(\frac{\epsilon}{S-1}\right)/p$$

where ϵ *is a separation tolerance,* S *is the colonies' initial separation, and* p *is the communities' outer probability of connection.*

We initialize our system with a fixed inner connection probability p_{in}, letting p_{out} vary between a small value (here, $p_{\text{out}} = 0.2$) and all-to-all connectivity, $p_{\text{out}} = 1$. We take the separation value $\epsilon \in \{0.1, 0.05, 0.01\}$, and assume very well-separated initial conditions like $S = 200$. The two components of each panel of Figure 2.20 are then the following:

1. At each ϵ and for fixed S, a plot of $\tilde{t}_{\text{conv},2}(p)$, where this quantity is defined as in (2.0.36).

2. A plot of $t_{\text{conv},2}$, defined as in (2.39), through evolution of the equations (2.7) until a recorded m_1, m_2 separation of 1 (within given ϵ tolerance).

At each tolerance, there appears to be modest error in our approximation throughout the chosen outer connection probabilities $p_{\text{out}} \in [0.2, 1]$. Despite this, the approximation generally appears to qualitatively represent the data accurately. According to (2.0.36), for fixed ϵ and initial separation s,

$$t_{\text{conv},2} = O(1/p),$$

which is borne out by the data and qualitatively resembles the relationship down to excessively small ϵ.

Interestingly, the relationship holds for outer connection probabilities throughout $0 \ll p < 1$. We stress this point: even for $(p_{\text{in}}, p_{\text{out}})$ pairs in the mixed regime

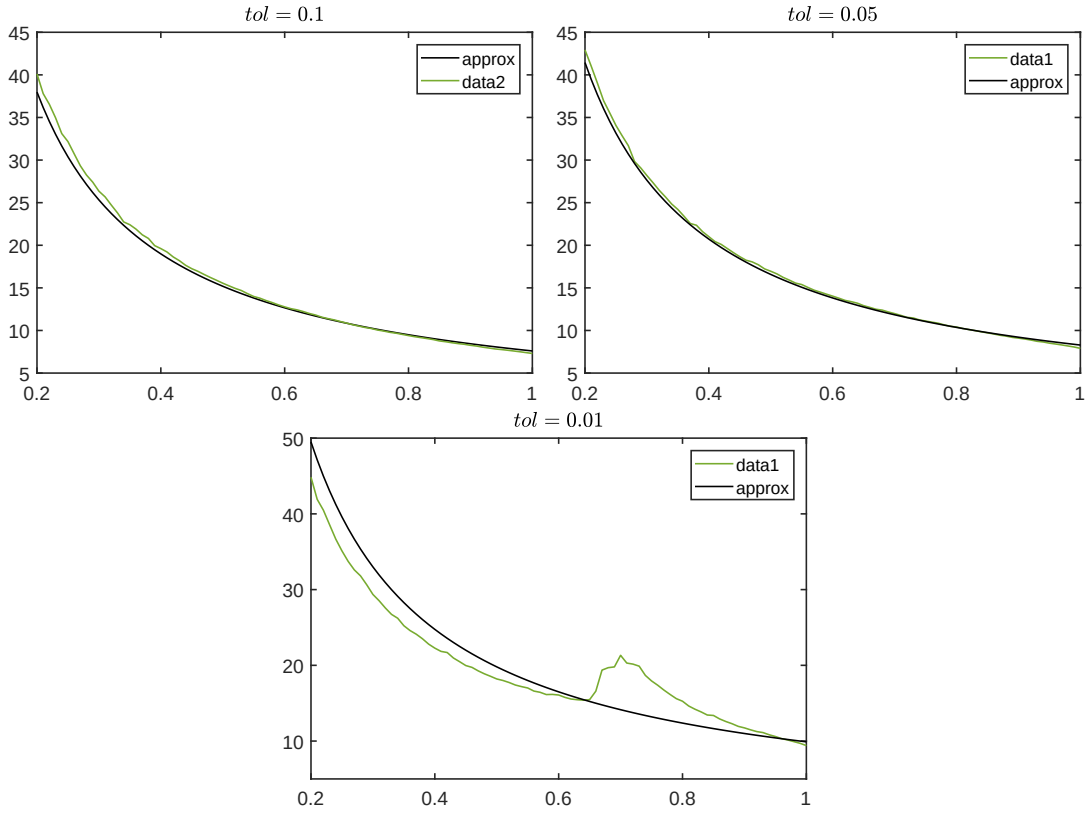

Figure 2.20: x-axis p_{out}, y-axis approximate time to converge (within specified tolerance). Inner-connection probability is 0.8 throughout.

described in Result 1, the time taken for the colonies to converge is adequately described by this $O(1/p)$ quantity. To some extent, this is a restating (and numerical validation) of our prior heuristic assumption; for $t < \hat{t} \approx t_{\text{conv},2}$, the behavior of the system is dominated by the two-colony, macroscopic dynamics. For $t > \hat{t}$, the two-colony dynamics are overwhelmed by the "mixing" dynamics of inner-colony connections.

Naturally, one might want to know how tightly $t_{\text{conv},2}$ clusters around $\tilde{t}_{\text{conv},2}$ as our inner connectivity varies; each panel of the three-panel figure we provided had $p_{\text{in}} = 0.8$ fixed. Accordingly, we attempt to compute the difference between approximate and actual $t_{\text{conv},2}$ over a wide range of $(p_{\text{in}}, p_{\text{out}})$ values.

Definition 2.0.37. *We define the error in replacing* $t_{\text{conv},2}$ *with* $\tilde{t}_{\text{conv},2}$*,* ν*, by*

$$\nu(p_{\text{in}}, p_{\text{out}}, \epsilon) = \left| \mathbb{E}_{\mathcal{G}} \left[t_{\text{conv},2}(\epsilon) \right] - \tilde{t}_{\text{conv},2}(p_{\text{out}}, \epsilon) \right|, \tag{2.45}$$

where the expected value is over all such $\mathcal{G} \sim SBM(N, C, P)$ *for a given probability pair* $(p_{\text{in}}, p_{\text{out}})$ *and number of particles,* N*.*

We estimate the expected value in Definition 2.0.37 by averaging $t_{\text{conv},2}$ over a large number of network initializations. We depict our results in Figure 2.21. As our experience indicates,

1. ν generally remains small even as p_{in} varies, provided p_{out} is not near zero.

2. For $p_{\text{in}} \approx 1$ or $p_{\text{out}} \approx 1$, we find $\nu \approx 0$.

Referencing 2.20, the errors we see here in Figure 2.21 tend to be small relative to $\tilde{t}_{\text{conv},2}$, less than 10%. However, in our sample run, ν begins to experience more pronounced variation as $p_{\text{out}} \to 0.2^{+}$, particularly with higher values as $p_{\text{in}} \to 0$, as well. As the approximate $\tilde{t}_{\text{conv},2}$ is fixed with respect to the inner probability of connection, we infer that the larger errors are indeed the result of greater variation in the actual convergence time quantity, $t_{\text{conv},2}$.

What is the source of such variation? For most starting points on the plot in Figure 2.21, it is difficult to say. However, the sector of large errors for *both* p_{in} and p_{out} small is suggestive of a different threshold than the usual one we have given. Here, we believe the large errors come from the general loss of attraction of even a mixed variant of state (2.18). As seen in Figure 2.3, a decrease in the size of our system's probability parameters leads to variants of the two-cluster states that only converge nearby; these exhibit a broad elongation in our system's community-to-community and sorting convergence timescales. The former timescale is perhaps not represented

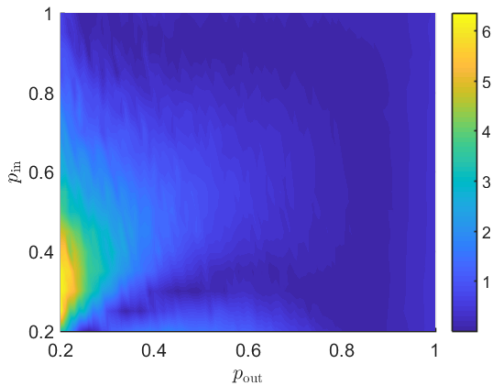

Figure 2.21: A plot of the absolute error in replacing the exact value of $t_{\text{conv},2}$ with the approximation $\tilde{t}_{\text{conv},2}$ over a wide range of inner and outer connectivities. Here, we used a convergence tolerance of $\epsilon = 0.05$.

properly as $(p_{\text{in}}, p_{\text{out}}) \to \mathbf{0}$ and $p_{\text{in}} \sim p_{\text{out}}$, as provided κ is not close to zero, the short- and long-distance forces are, indeed, comparable. This stands in contrast to the implicit assumption made in estimating $\tilde{t}_{\text{conv},2}$ – that the short-distance forces could be neglected.

However, as we first observe in the $\epsilon = 0.01$ panel of Figure 2.20 the approximate quantity $\tilde{t}_{\text{conv},2}$ begins to poorly capture the data throughout the interval $p_{\text{out}} \in [p_{\min}, 1]$ as $\epsilon \to 0^+$. We explore why this is the case.

Remark 2.0.38. *Note that, for* any *fixed outer connection probability p, and initial separation S*

$$\lim_{\epsilon \to 0^+} \tilde{t}_{\text{conv},2} = \lim_{\epsilon \to 0^+} -\ln\left(\frac{\epsilon}{S-1}\right) = \infty,$$

Of course, Remark 2.0.38 is essentially just a restatement of the fact that any two-particle system, initially seeded at a separation other than that prescribed by the kernel $F(r)$, only tends to the prescribed separation in the infinite-t limit. Yet, in terms of actual data, Figure 2.20 suggests, for outer connection probabilities satisfying $0 < p_{\min} < p_{\text{out}} < p_{\max} < 1$ for some particular $p_{\min}$ and $p_{\max}$ (as in the threshold of

Result 1), that

$$\lim_{\epsilon \to 0^+} t_{\text{conv},2} = L < \infty,$$

where L potentially depends on p_{out}. This is because, assuming p_{out} is chosen sufficiently small for the pair $(p_{\text{in}}, p_{\text{out}})$ to yield mixed states with high probability, like suggested in Conjecture 1, we must tend to a community-to-community separation of less-than-one in finite time. The mixed variant of (2.18) from Conjecture 1 attracting such initializations leads to

$$\lim_{t \to \infty} |m_1(t) - m_2(t)| = L < 1.$$

By the definition of the limit, there exists a point in time, say $t = \hat{T}$ (as a function of p_{out}), where $||m_1 - m_2| - L| < (1 - L)/2$ for all $t > \hat{T}$. In particular, this implies $|m_1 - m_2| < 1$ for all $t > \hat{T}$. Hence

$$t_{\text{conv},2}(\epsilon) \leq \hat{T},$$

as $|m_1 - m_2| < 1 < 1 + \epsilon$ for any $\epsilon > 0$.

Accordingly, this result shows that the estimated quantity will begin to deviate significantly from actual $t_{\text{conv},2}$ as tolerances ϵ limit to zero. Hence the quantity is only useful as a close approximation and cannot be interpreted as a function with eventual limit (as $\epsilon \to 0^+$) of $t_{\text{conv},2}$. As such, we should set ϵ small (so that the approximation is useful) but not very near zero.

Perhaps surprisingly, for similarly small ϵ we observe a more egregious error in our approximation; in the supplied figure for $\epsilon = 0.01$, around $p_{\text{out}} \approx 0.65$, we observe a "blip" in our data that is not at all captured by the approximation. The quantity $\tilde{t}_{\text{conv},2}$, of course, is monotone decreasing on $p \in (0, 1)$. What is the source

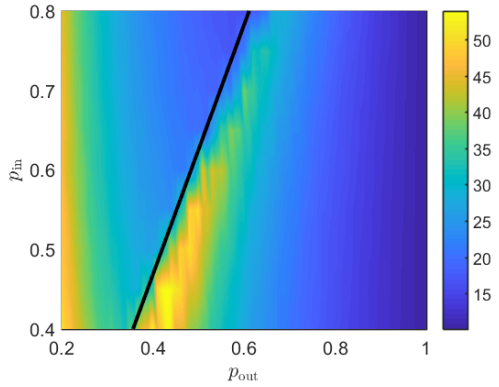

Figure 2.22: Plot of $t_{\text{conv},2}$ over a mesh of inner/outer connection probabilities and $\kappa = 1/2$. The solid line denotes the curve fitted to the "transition point" data in Figure 2.12. Results averaged over 10 runs with point-source initial conditions for each community at $x = -100$ and $x = 100$, respectively. Separation tolerance of $\epsilon = 0.005$.

of this artifact? While it is possible it originates from small errors in our first-order ODE integration scheme, the location of its starting point is strongly suggestive of another dynamic; it appears to come from the p_{out} threshold at which we cross into highly-*unmixed* communities. We explore this below.

In Figure 2.22, we see a surface plot of $t_{\text{conv},2}$ for many $(p_{\text{in}}, p_{\text{out}})$ pairs. Throughout most of the region, we observe a clear trend; for fixed p_{in}, as we decrease p_{out}, $t_{\text{conv},2}$ decreases steadily with it. However, as we observed in our discussion of the previous figure, such a low tolerance creates a unique phenomenon between the two extremes of $p_{\text{out}} \in [0.2, 1]$. We see a band of *large* $t_{\text{conv},2}$ values that, for fixed p_{in}, exceed the values observed for nearby lesser values of p_{out}. Hence, for such a small tolerance, $t_{\text{conv},2}$ is not monotone decreasing, as it appeared to be when ϵ was larger.

Of particular interest to us is where this perhaps unexpected behavior begins. In our $p_{\text{in}} = 0.8$ slice presented previously for $\epsilon = 0.01$, we saw the "blip" occur at $p_{\text{out}} \approx 0.63$, thus we posit it is related to the nearby threshold between mixed/unmixed

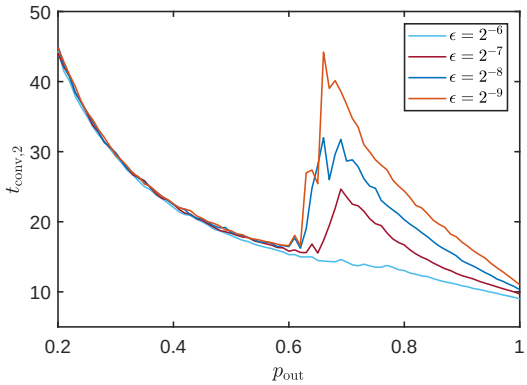

Figure 2.23: Plot of $t_{\mathrm{conv}}, 2$, emphasizing the "blip" properties near the transition point. Here $p_{\mathrm{in}} = 0.8$ and $\kappa = 1/2$, with initial conditions point-source at $x = -100$ and $x = 100$ for the two communities, respectively. Results averaged over 10 runs.

regimes. As such, we take the curve previously fitted for our transition point data,

$$p_c = .637 p_{\mathrm{in}} + .1019,$$

and plot it alongside the surface. Here, we see the fitted curve – which tightly fit the data for the location of the transition point between mixed and unmixed regimes for various p_{in} – accurately captures the onset of the "blip". That is, for fixed p_{in}, the function value $p_c(p_{\mathrm{in}})$ appears to be near the smallest value of p_{out} for which $t_{\mathrm{conv},2}$ is increasing (as a function of p_{out} and for small ϵ).

Another question that arises in our analysis of Figure 2.20 is how the "blip" changes as ϵ changes; we are especially interested in changes in its amplitude and location as $\epsilon \to 0^+$. To establish an acceptable initial answer to this question, we fix $p_{\mathrm{in}} = 0.8$ and generate curves like those in Figure 2.20 for many different, small ϵ where the existence of the "blip" has been already established. We superimpose these plots in a single figure to see their similarities and unique differences.

The two key pieces of information we infer are the following (offered without rigorous proof).

Conjecture 2. *Let $p_c = p_c(p_{\text{in}})$ be the threshold value of Result 1. At each $(p_{\text{in}}, p_{\text{out}})$ pair, suppose $\mathcal{G} \sim SBM(N, C, P)$ is fixed.*

1. *For $p_{\text{out}} < p_c$,*

$$\lim_{\epsilon \to 0^+} t_{\text{conv},2} = L$$

for some L (depending on the probability parameters).

2. *For values of $p_{\text{out}} > p_c$, however, $t_{\text{conv},2} \to \infty$ as $\epsilon \to 0^+$.*

Remark 2.0.39. *The conclusions of Conjecture 2 show the error in approximating $t_{\text{conv},2}$ with $\tilde{t}_{\text{conv},2}$, as in Definition 2.0.37, grows without bound if $p_{\text{out}} > p_c$ (with high probability) and remains bounded if $p_{\text{out}} < p_c$.*

This is something we argued before; in the unmixed regime, communities only tend to a separation of 1 in the infinite limit as $t \to \infty$, hence the aforementioned quantity *must* grow to infinity, as well. What is notable here is the magnitude of the curve's maximum at each ϵ; we observed a rough doubling upon multiplying ϵ by $1/4$. Conversely, the prediction of our approximation ($\tilde{t}_{\text{conv},2}$) suggests the quantity grows approximately like $\ln((S-1)/\epsilon)/p$ as $\epsilon \to 0^+$ – much more slowly.

Alternate Avenues of Analysis

To compensate for the system (2.7)'s challenging randomness – in the sense that every initialization yields not only different initial conditions but a different *system*, with a different network structure – we are aware of two avenues of attack. The first, as we mentioned toward the start of this chapter and as utilized in [35], is to leverage the theory of spectra of random matrices to establish areas in our parameter space for which the remaining eigenvalues (non $\lambda = 0$, recall the system is translation-invariant in continuous time) of the linearized system tend to values less than one

in magnitude, with probability approaching 1 in the limit as $N \to \infty$. This is the notion of "almost surely asymptotically stability," and in a sort of nod to the Law of Large Numbers, the variance in matrix structure is evened out as we take further samples ($N \to \infty$). In our case, we suspect successive linear transformations of E might isolate the components of its block structure, leading to several independent, individual problems that are on the level of the complexity of those seen in [35], [36]. Of course, each block of our model has homogeneous connection structure, being generated from a single probability parameter $P(i, j)$ (for some i, j); thus each can be thought of as representing an Erdős–Rényi graph itself.

An alternate approach has been suggested and developed in [22]. Here, again we consider our system in the asymptotic $N \to \infty$ limit, but instead of analyzing the tendency towards or away from stability of each ordinary system in the sequence, we relate this sequence of systems to a single partial differential equation. That partial differential equation can then be examined and linearized around the relevant solution for *its* behavior, and that behavior can be related back to our solution of interest to the ordinary differential system.

Specifically, we formally interpret (2.7) as a Riemann sum and let $N \to \infty$. To see this, for labeling purposes we imagine infinitely many particles in one-to-one correspondence with the entire unit interval $[0, 1]$. Then $\phi(x, t) : \mathbb{I} \times \mathbb{R} \to \mathbb{R}$ represents the spatial coordinates of the particle corresponding to $x \in [0, 1]$ at time t. The inner terms (excluding e_{nij}) of (2.7) of the form

$$\frac{\mathrm{d}x_i}{\mathrm{d}t} = \frac{1}{N} \sum_{j=1}^{N} e_{nij} F(|x_i - x_j|) \frac{x_i - x_j}{|x_i - x_j|},$$

then resemble function evaluations of $\phi(x, t)$. The coefficient in front of the sum reveals these as evaluations over a uniform partition – sub-intervals of $[0, 1]$ of length

$1/N$. Hence, in the limit, we have the following equivalence:

$$\lim_{N\to\infty} \frac{1}{N} \sum_{j=1}^{N} F(|x_i - x_j|) \frac{x_i - x_j}{|x_i - x_j|} = \int_0^1 F(|\phi(x,t) - \phi(y,t)|) \frac{\phi(x,t) - \phi(y,t)}{|\phi(x,t) - \phi(y,t)|} \, \mathrm{d}y$$

for ϕ as given before.

What do we do about the network term, e_{nij}? Graph limits offer a possible answer. To motivate this, we examine the pixel pictures of a succession of stochastic block graphs.

Definition 2.0.40. *The pixel picture of an undirected and unweighted graph on N nodes, $\Gamma_N(x,y)$, is a symmetric, $\{0,1\}$-valued function on $\mathbb{I} \times \mathbb{I}$ defined by*

$$\Gamma_N(x,y) = e_{Nij} \quad \text{on} \quad \left[\frac{j-1}{N}, \frac{j}{N}\right) \times \left[1 - \frac{i}{N}, 1 - \frac{i-1}{N}\right)$$

for all i, j.

We plot a few of these in Figure 2.24 for our stochastic block model; inner/outer probabilities are fixed, total connections vary (as specified), and graphs are randomly generated for each picture.

Clearly, the limit of Γ_N does not exist in a pointwise sense, provided the various probabilities that define the stochastic graph are neither 0 or 1, we expect to attain both 0 *and* 1 at any (x,y) infinitely many times in the limit as $N \to \infty$; that is, the e_{Nij} are not definite values, but rather they define the probability of seeing a 0 or 1 at a given set of coordinates (x,y). However, the limit of Γ_N exists as a density; for small enough $\epsilon > 0$ and $(x_0, y_0) \in (0,1) \times (0,1)$, we have

$$\lim_{N\to\infty} \int_{x_0}^{x_0+\epsilon} \int_{y_0}^{y_0+\epsilon} \Gamma_N \, \mathrm{d}x \, \mathrm{d}y = \epsilon^2 P(i,j),$$

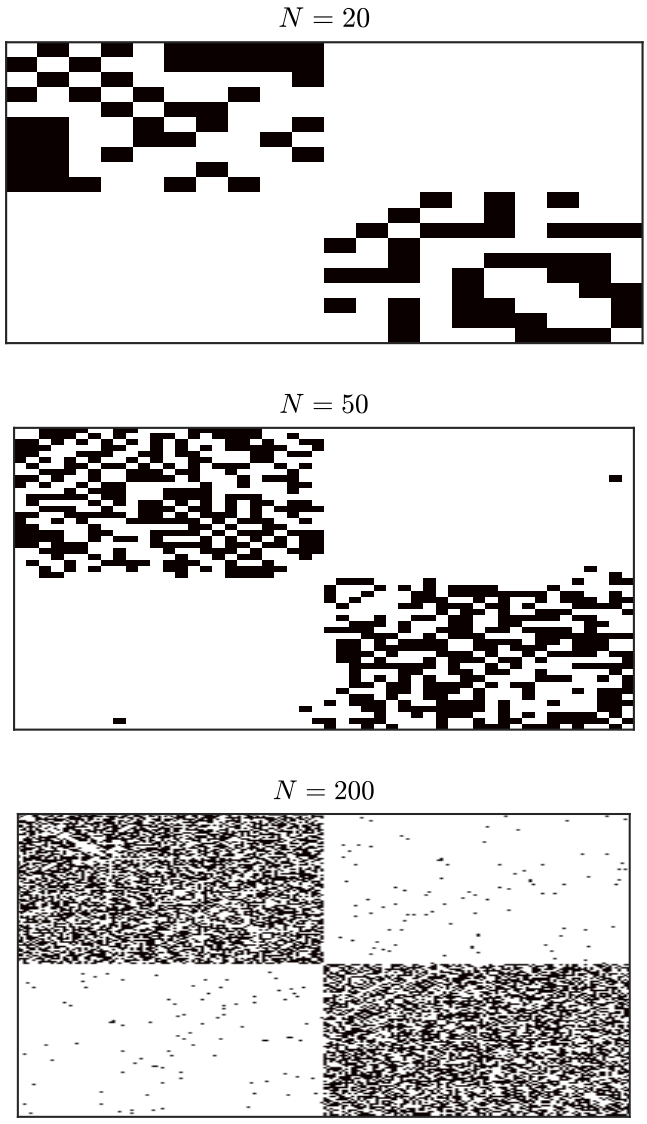

Figure 2.24: Pixel pictures of random networks with the specified number of total particles and two evenly-sized communities. Generated with an inner connection probability of 0.5 and an outer connection probability of 0.01. Note these appear to be converging to a block structure with uniform density in each block.

where P is the square matrix of connection probabilities, m denotes its number of rows/columns, and (i, j) are such that $(x_0, y_0) \in [\frac{i-1}{m}, \frac{i}{m}) \times [1 - \frac{j}{m}, 1 - \frac{j-1}{m}]$. This last line defines the graph limit, $W(x, y)$ – a symmetric, piecewise constant (in the case of the stochastic block model) function on $\mathbb{I} \times \mathbb{I}$. Appropriately, we note the following.

Remark 2.0.41. *Let $\mathcal{G} \sim SBM(N, C, P)$ be a graph generated from the stochastic block model, with $C = (C_1, C_2)$ and $|C_1| = |C_2|$. Then, define the graph limit $W(x, y)$ by*

$$W(x,y) = \begin{cases} P(1,1) & : \quad (x,y) \in [0,1/2) \times (1/2,1] \\ P(1,2) & : \quad (x,y) \in (1/2,1] \times (1/2,1] \\ P(2,1) & : \quad (x,y) \in [0,1/2) \times (0,1/2] \\ P(2,2) & : \quad (x,y) \in (1/2,1] \times (0,1/2] \end{cases}$$

Of course, we take $P(1, 2) = P(2, 1)$ in Remark 2.0.41, as the underlying graphs in the sequence are undirected. We note we have no coherent way of defining $W(x, y)$ along the boundaries of these pieces in the interior of the unit square. However, $W(x, y)$ is used as a density – integrated over measurable subsets of $\mathbb{I} \times \mathbb{I}$. As a subset of $\mathbb{I} \times \mathbb{I}$, these boundaries (the union of a finite number of line segments) have zero measure, hence it does not matter *what* we define $W(x, y)$ to be here. For convenience, we can set $W(x, y) = 0$ along these segments.

Thus, in the limit $N \to \infty$, we arrive at the PDE

$$\frac{\partial \phi(x,t)}{\partial t} = \int_0^1 W(x,y) F(|\phi(x,t) - \phi(y,t)|) \frac{\phi(x,t) - \phi(y,t)}{|\phi(x,t) - \phi(y,t)|} \, \mathrm{d}y, \tag{2.46}$$

where again $\phi : \mathbb{I} \times \mathbb{R} \to \mathbb{R}$, $W(x, y)$ is as given previously, and $F(r) = \min(\kappa r, 1 - r)$ for $0 < \kappa < 1$. To what extent this represents a limit, i.e. in ordinary differential systems tending to this partial differential equation, is beyond the scope of the chapter and is explored in depth in [22].

At this point, we may now seek to explore the linear stability, in (2.46), of the two-cluster steady state analog to the ordinary system (2.7) as $N \to \infty$. We choose the piecewise constant $\phi_s(x,t)$ as follows:

$$\phi_s(x,t) = \begin{cases} -1/2 & : \quad 0 \leq x < 1/2 \\ 1/2 & : \quad 1/2 \leq x \leq 1, \end{cases} \tag{2.47}$$

We may think of this solution as half of the particles (the first piece) are valued at $\phi = -1/2$ and half of the particles (the second piece) are valued at $\phi = 1/2$. We surmise that (2.47) satisfies (2.46), as $\partial\phi_s/\partial t = 0$ for any (x,t) (the supplied solution is fixed in time). On the right-hand side, and for any x, y, t, we have $|\phi(x,t) - \phi(y,t)|$ as an element of $\{0,1\}$. Hence

$$F(|\phi_s(x,t) - \phi_s(y,t)|) = 0$$

uniformly on $\mathbb{I} \times \mathbb{I} \times \mathbb{R}$. Accordingly, the integral on the right-hand side of (2.46) is zero.

Our natural question concerns how a small perturbation of (2.47) evolves in time. For this, we suppose $\phi(x,t) = \phi_s(x,t) + \zeta(x,t)$ for ζ small. Upon substitution into (2.46), we have

$$\frac{\partial \phi_s(x,t)}{\partial t} + \frac{\partial \zeta(x,t)}{\partial t} = \int_0^1 W(x,y) \left(F(|r(x,y,t)|) \frac{r(x,y,t)}{|r(x,y,t)|} \right) \mathrm{d}y. \tag{2.48}$$

for $r(x,y,t) = \phi_s(x,t) - \phi_s(y,t) + \zeta(x,t) - \zeta(y,t)$. We first consider $0 < x < 1/2$. For $0 < y < 1/2$, the terms in the parentheses (2.48) evaluate to $\kappa(\zeta(x,t) - \zeta(y,t))$. For $1/2 < y < 1$, they evaluate to $-(\zeta(x,t) - \zeta(y,t))$. Next, we consider $1/2 < x < 1$. For $0 < y < 1/2$, the terms in the parentheses (2.48) evaluate to $-(\zeta(x,t) - \zeta(y,t))$.

For $1/2 < y < 1$, they evaluate to $\kappa(\zeta(x,t) - \zeta(y,t))$. Splitting the integral in half and using this information, we arrive at, for $0 \leq x < 1/2$,

$$\frac{\partial \zeta(x,t)}{\partial t} = \int_0^{1/2} p_{1,1}\kappa(\zeta(x,t) - \zeta(y,t))\,\mathrm{d}y - \int_{1/2}^{1} p_{1,2}(\zeta(x,t) - \zeta(y,t))\,\mathrm{d}y \tag{2.49}$$

For $1/2 \leq x \leq 1$, we have

$$\frac{\partial \zeta(x,t)}{\partial t} = -\int_0^{1/2} p_{2,1}(\zeta(x,t) - \zeta(y,t))\,\mathrm{d}y + \int_{1/2}^{1} p_{2,2}\kappa(\zeta(x,t) - \zeta(y,t))\,\mathrm{d}y \tag{2.50}$$

At this point, it would be necessary to attempt to assess how the perturbations ζ evolve in time. Typically, we would seek solutions ζ to (2.49)–(2.50) that are proportional to $e^{\lambda t}e^{\imath kx}$; that is, such solutions are exponentially growing (or decaying) modes of certain waves in the spatial dimension. Of course, for linear stability we are interested in whether or not the suitable eigenvalues, λ, are all negative, decaying modes, as this would signify such perturbations vanish in time.

Though we did not pursue this analysis further, additional research may be focused on continuing along these lines to leverage continuum limits of ordinary differential systems on networks to make broad statements about their regions of linear stability/instability (cf. also mean field approaches like [5]). Our concerns with such an approach here were as follows: the dynamics of (2.7) lead to the two-cluster steady state, in which half of our system particles are grouped around, say, $x = 0$ and half of our system particles are grouped around $x = 1$. If we label the particles, in order, with the first half being those at $x = 0$ and the second half being those at $x = 1$, then in passing the system to the continuum limit, it seems as though we cannot avoid representing the two-cluster steady state (finite N) as a discontinuous function, as seen. This causes our linearization to be thought of in a piecewise sense (see after (2.48)), and the applicability of the methods presented in [22] is unclear in

such a case. We can perhaps view (2.47) as a limit of sigmoid-like curves, but again it is unclear as to how that can be related back to the finite-N equations from the presented framework.

More crucially, our plots of solutions to (2.7) depict complex, highly-nonlinear, and often seemingly chaotic (see: small p) behavior. Accordingly, we feel it is rather likely the continuum limit (2.46), should we complete the analysis, would point to a perhaps unconditionally-stable steady state. In this case the complicated behavior we see, from the threshold into mixing of the two-cluster state, the greater degree of sorting behavior as $p_{\text{out}}/p_{\text{in}}$ falls, and the low-p degeneracy of the four- (and possibly more) cluster states, all results from introduced nonlinearities. In a word, the continuum linearization would tell us very little about the system as a whole, and it would tell us nothing about the network structure-dependent phenomena (described in Result 1) endemic to every level of the system (2.7) away from the steady state trajectories.

Finally, we note that our general concern in this chapter of the thesis is not with stability of the cluster states *per se*. Rather, we are interested in a sort of *meta*stability of such states over large initial separations. We have expressed this in the single question, "to what extent do the dynamics of (2.7) preserve large initial separations between communities?" Accordingly, though we have referred to the more classic stability of these states at times, our numerics tend to be cast within the framework of this metastability. Communities are seeded from large separations rather than thin random profiles on, for instance, $[0, 1]$ or small perturbations of the two-cluster state. While the more classical PDE methods of [5, 22] or assessing eigenvalues of the linearized system as a function of the probability parameters would be useful in determining how the latter solutions evolve in time, they are considerably less useful toward achieving the goal we expressed in Question 3. For these reasons,

we decided against such analyses, but future examination along these lines could help paint a fuller picture and would be a more direct extension of [35].

Application: Community Detection

In this section, we seek to answer the question

Question 5. *Can we leverage the dynamics of the system* (2.7) *to detect communities among a stochastic block network?*

We first review the necessary preliminaries.

The development of the theory of networks has granted us much insight into many natural and social systems. One of the most recognizable features of real-world networks is community structure; this term generally refers to the self-arrangement of a network's nodes into homogeneous units. Within each unit, edges between pairs of vertices are dense, while they are relatively sparse *between* communities. The homogeneous nature of such units often allows their behavior to be considered, one at a time, separate from other units. Accordingly, there is appreciable value in understanding complex systems via first identifying their key components – communities.

Henceforth, we refer to *community detection* as the problem of determining a network's community structure given various other pieces of information. On an N-node graph, we typically think of such a problem in the following context: we accept an adjacency matrix E as input, and generate a partition $\mathcal{C}$ of $\{1, 2, 3, \ldots, N\}$ in return. Each component of the partition then represents a distinct "community," insofar as there is a significantly greater edge density between in-member interactions versus out-member interactions.

Disappointingly, as noted in [11], such a problem is often not well-defined despite its broad, accessible appeal. Even the most fundamental building blocks we have referred to here – a *partition* of nodes into homogeneous *communities* – have definitions that shift from application to application and algorithm to algorithm. This imprecision creates clear problems of inconsistency, and there are often many perfectly valid ways of remedying such concerns. While we attempt to define such vital components of an algorithm in a clear way, there is always a certain degree of freedom that potentially affects the algorithm's end result.

We note it is absolutely central for any algorithm suitably efficient for the data at hand; that is, it should use an amount of computer resources not in excess of those available for the task itself. In modern computing structures, the two main bottlenecks for completing the reading and transformation of a large data set are the computer bank's processing power and its available memory. The former determines how quickly an algorithm's sub-tasks can individually be completed, while the latter determines the proportion of the data set the computer can have readily available to work on at any point in time. For large real-world networks, e.g. the entire Internet's collection of nodes (web pages) and edges (hyperlinks), the latter cost can be prohibitive due to repetitive reading and writing of small proportions of the network into memory.

Typically, the *computational complexity* (net computing time) of an algorithm is expressed in terms of a network's vertices, N. For most algorithms it is not possible to do this precisely, thus estimated bounds for "worst" or "best-case compute time" growth are established instead. These tend to be expressed in big-O notation, defined as follows.

Definition 2.0.42. *Let* $f, g : \mathbb{N} \to \mathbb{R}^+$. *Then,* $f = O(g)$ *as* $N \to \infty$ *if and only if*

there exists an $N_0 \in \mathbb{N}$ *and* $C \in \mathbb{R}^+$ *satisfying*

$$f(N) \leq Cg(N) \quad \textit{if } N \geq N_0. \tag{2.51}$$

Hence, in the context of Definition 2.0.42, a statement like $t_{\text{com}} = O(N^k)$ indicates the scalability of an algorithm to large networks. An $O(N^3)$ algorithm may suffice for a given purpose on a small network of $N = 100$ nodes, but our computing load would grow like a factor of 1000 even upon extension to a modestly large network of $N = 1000$ nodes!

Upon addressing some of the inherent inconsistencies of community detection, we try to proceed in a coherent way. Our first goal is a suitable definition of *community*. Glancing at Figure 2.25, there is an undeniable difference in structure between inner- and outer-community nodes and edges. To wit, one might suggest (as in [11]) that if $\mathcal{C}$ is a subgraph of our graph $\mathcal{G}$, with N_c and N as their respective cardinalities, then the difference lies in each block's *inner and outer cluster densities*, defined by

$$\delta_{\text{int}}(\mathcal{C}) = \frac{\text{inner edges in } \mathcal{C}}{N_c(N_c - 1)/2} \tag{2.52}$$

$$\delta_{\text{ext}}(\mathcal{C}) = \frac{\text{outer edges from } \mathcal{C}}{N_c(N - N_c)} \tag{2.53}$$

In (2.52), the denominator represents the number of possible edges between nodes $x, y \in \mathcal{C}$, whereas in (2.53) the denominator represents the number of possible edges between nodes $x \in \mathcal{C}$ and $y \notin \mathcal{C}$. For $\mathcal{C}$ to be a suitable community, we expect δ_{in} to be sufficiently large relative to δ_{ext}.

Of course, if our network is generated via the stochastic block model method, where communities are explicitly placed into the network, then the problem of community detection is to simply accept the network's adjacency matrix E as input

and then determine the communities originally specified for the generating algorithm to build the network. As such, recall our definition of a stochastic block network:

Definition 2.0.43. *(Stochastic block model). Let N and k be positive integers representing the number of vertices and specified communities, respectively. Let P be a k-by-k symmetric matrix with entries valued in $[0,1]$ (the probabilities of connection). Let the $C_1, C_2, \ldots, C_k$ denote the community set partitions of $[N]$. The community labeling vector of length N, X, is determined as follows: for $v \in C_j$ (for some j)*

$$X_v = j.$$

Then the graph $\mathcal{G}$ is drawn from SBM(N, C, P) if, independent of other vertex pairs,

$$e_{Nij} = \begin{cases} 1 & \textit{with probability} \quad P(X_i, X_j), \\ 0 & \textit{with probability} \quad 1 - P(X_i, X_j). \end{cases}$$

We write $\mathcal{G} \sim$ SBM(N, C, P) for short.

Accordingly, in this we are aware of which nodes are connected to which other nodes, but we seek to group these nodes in a way that is consistent with the assumption that there is a potentially different probability of an edge existing if both endpoints belong to the same community as opposed to different communities.

Despite our consistent definition of "community," our variant of this problem, as we have framed it up to this point, can often not be traced back to a single solution. That is, it may be impossible to determine the original partition of nodes into communities, or it may only be possible to partially recover this partition without further information. It is clear our level of certainty depends heavily on the number of sampled, possible connections – rising steadily as N rises – and on the in- and out-degree disparities between elements of each community. As a simple example, consider

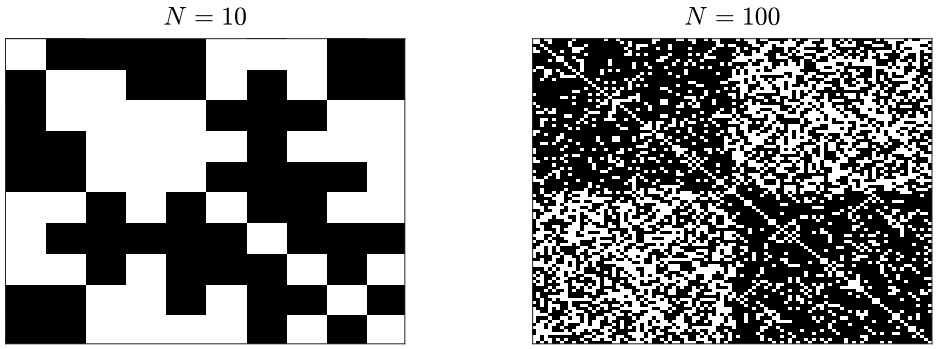

Figure 2.25: Pixel pictures of networks generated from probability parameters $p_{\text{in}} = 0.8$ and $p_{\text{out}} = 0.5$. Note the clearly discernible difference in inner/outer connections in the right panel (large N), unlike the left panel (small N).

the networks of Figure 2.25 (pixel pictures shown). Both networks were generated from the same probability parameters and have two equivalently-sized communities. In the left panel, the total number of nodes (N) was taken to be 10; in the right panel, this number was taken to be 100.

Figure 2.25 makes a strong case that our certainty in community detection depends greatly on (among other factors) the total number of sampled inner/outer connections. It is a hopeless task to try to determine the original partition of nodes that led to the pixel picture in the left panel; indeed, we could interchange any number of the $N = 10$ particles and result in a figure with no discernible difference in community structure, as with $N = 10$ particles we would require a large disparity in inner and outer connection densities. The main mechanism at work here stems from the fact

$$C_{i,\text{in}} = \mathcal{B}(N-1, p_{\text{in}})$$

$$C_{i,\text{out}} = \mathcal{B}(N, p_{\text{out}})$$

where the first line refers to the random variable representing particle x_{i}'s inner degree and the second line its outer degree, and $\mathcal{B}(n,p)$ is the binomial distribution on n trials with probability parameter p. Recalling such a variable has mean np and standard deviation $\sqrt{npq}$ (here $q = 1-p$), we have

$$\begin{aligned}\frac{\sigma_{\mathrm{in}}}{\mu_{\mathrm{in}}} &\sim \frac{\sqrt{Np_{\mathrm{in}}(1-p_{\mathrm{in}})}}{Np_{\mathrm{in}}}\\ \frac{\sigma_{\mathrm{out}}}{\mu_{\mathrm{out}}} &= \frac{\sqrt{Np_{\mathrm{out}}(1-p_{\mathrm{out}})}}{Np_{\mathrm{out}}}\end{aligned}$$

where the $\sim$ above refers to an *asymptotic* equivalence – that is, tending to the same limit as $N \to \infty$. In this sense, how tightly the average particle's in- and out-degree clusters around its mean scales like $1/\sqrt{N}$ as $N \to \infty$ (here small values of N, of course, indicate tighter clustering). For $N = 10$, this "clustering coefficient" is roughly 17% and 31% (of the mean) for a particle's in- and out-degree; compare this to 5% and 10% for $N = 100$.

This is evidenced in Figure 2.25. There is no clear difference between the top-left (inner) quadrant of the graph and the top-right (outer) quadrant of the graph despite the large disparity between p_{in} and p_{out}; in fact, we calculated a $\approx 25\%$ chance of a given particle having the *same* in-degree (out of 4) as out-degree (out of 5)! This probability for $N = 100$, on the other hand, is nearly indistinguishable from 0. While it is certainly *possible* to generate a graph like the right panel of Figure 2.25 with, say, $p_{\mathrm{in}} \leq p_{\mathrm{out}}$, it is exceedingly unlikely, hence we can be reasonably certain our partition is sound and $p_{\mathrm{in}} > p_{\mathrm{out}}$.

We continue along towards answering Question 5 here. We recall system (2.7) has the potential to sort groups of particles with sufficiently large differences in inner/outer edge density, as depicted in, for instance, Figure 2.6 and argued in Result

1. Thus, we would like to leverage the dynamics of this system to detect communities among a stochastic block network.

Definition 2.0.44. *Take $\mathcal{G} \sim SBM(N, C, P)$ as a graph generated from the stochastic block process. Additionally, assume*

$$1 > P(i,i) \gg P(i,j) > 0$$

for each $i, j = 1, 2, \ldots, k$ and $i \neq j$. Then, ***community detection*** *refers to the problem of recovering the community labeling vector of Definition 2.0.12, which assigns a positive integer corresponding to a node's community belonging to each node $i = 1, 2, \ldots, N$.*

Again, while group identity in some practical contexts is not binary (an individual can be a member of two or more friend groups, for instance), we only look for a disjoint partition of nodes into communities. This is also a restriction of the generating algorithm of our model.

A dynamics-based algorithmic approach confers a number of immediate benefits. First, as the method leverages the dynamics of a system of ODEs to obtain more broad, categorical information than precise quantitative data, a simple first-order method (like Euler with a large forward time step) should be generally sufficient. Second, in using a simple numerical scheme to evolve a system of ordinary differential equations, our algorithm is elementary to code, implement, and understand.

An Aggregation Dynamics-Based Algorithm

To illustrate a sample method, we first generate a stochastic block graph, at random, given specified inner and outer community connectivities (below: 0.8 and 0.55, respectively) and evenly-sized communities from a system size of $N = 500$.

Given such a network, we restate our objective: to arrive at a reasonable partition of nodes into communities. We follow Algorithm 2.1 to do this.

Algorithm 2.1: Aggregation Dynamics-Based Algorithm

Parameters: $n_{\text{runs}}, t_{\text{final}}, S, \Delta t, N$

Input: $E = (e_{ij})$

Output: $\hat{C}_1, \hat{C}_2$

Initialization $j = 1, x_{i,0}^0 = \mathcal{U}(-S/2, S/2), \quad i = 1, \ldots, N$

while $j \leq n_{\text{runs}}$ **do**

$\hat{C}_1, \hat{C}_2 = \emptyset$

$\mathbf{x}_j = \text{agg}(\mathbf{x}_{j-1})$ {Run (2.7) with $\kappa = 0$ until t_{final}}

for $1 \leq i \leq N$ **do**

if $x_{i,j} \leq \text{median}_i(\mathbf{x}_j)$ **then**

$\hat{C}_1 = \hat{C}_1 \cup \{i\}$

$x_{i,j} = -S/2$

else

$\hat{C}_2 = \hat{C}_2 \cup \{i\}$

$x_{i,j} = S/2$

end if

end for

$j = j + 1$

end while

That is, we initially seed all particles randomly, run the system (with $\kappa = 0$) until a small time value, at which we split the data into two halves about the median. These are our estimates for the community partitions C_1 and C_2. Then, we re-seed these groups of particles at a large separation, and repeat the process.

Typically, we choose $S \gg 0$ in Algorithm 2.1. The intuition behind this is as follows: as there is no repulsion over short distances, the only force exerted on each particle is what it feels over large distances ($r > 1$). To ensure that each particle is initially guided by the forces exhibited by a large subset of the system's particles, we must pick S to be large. As a particularly degenerate example, if we take S to be 1, any initialization is stable by picking the repulsion parameter $\kappa = 0$. For T, with no repulsive force running counter to the attraction over large distances, the system tends towards steady state rapidly. Under our myriad choices of parameters and initial conditions, we invariably found $T \approx 10$ to be sufficient.

What is the computational complexity of such an algorithm? Under a simple forward Euler timestep and even for N rather large, this is somewhat cheap to compute. The heavy lifting above comes from repeated evaluations of the system (2.7), where

$$U_i^{j+1} = U_i^j + \frac{\mathrm{d}\mathbf{f}}{\mathrm{d}t}\left(U_1^j, U_2^j, \ldots, U_N^j\right)\Delta t \tag{2.54}$$

(here U_i^j refers to the approximate solution to x_i at timestep j and $\mathbf{f}$ represents the right hand side of (2.7)). Each component of $\mathbf{f}'$ consists of a sum over N terms, where each term of the sum includes (for dimension $d = 1$):

1. Computation of $|x_i - x_j| \approx 1\,\mathrm{FLOP}$
2. Computation of $F(r) \approx 1\,\mathrm{FLOP}$
3. Computation of $(x_i - x_j)(|x_i - x_j|)^{-1} \approx 1\,\mathrm{FLOP}$.

Hence, the total computational cost of one such evaluation (2.54) is approximately $3N^2$. Multiplying this figure by the total number of algorithmic evaluations necessary, we conclude our total cost is approximately $3(t_{\mathrm{final}}/\Delta t)n_{\mathrm{iter}}N^2$ operations, or rather it grows like an $O(N^2)$ quantity, for short. We do note that if the existence of many

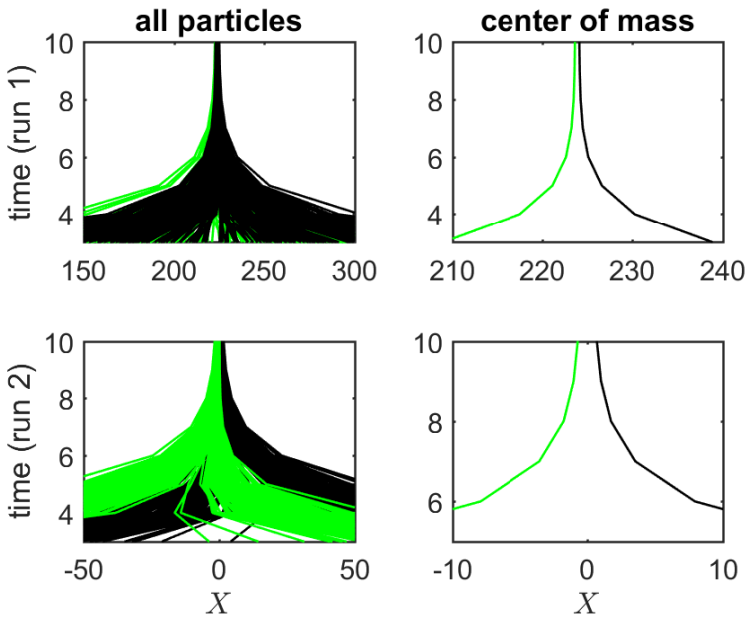

Figure 2.26: The first two iterations of our algorithm on a network generated from $(p_{\text{in}}, p_{\text{out}}, N) = (0.8, 0.6, 500)$. Note the rapid, near-complete recovery of community structure.

zeroes in (2.7) can be assumed, it is perhaps more accurate to phrase this as an $O(M)$ (where M is the total number of edges of $\mathcal{G}$); however, if we make the standard assumption that inner-community edge structure is dense, then the total number of edges of $\mathcal{G}$ will grow like N^2.

We present the results seen in the first two iterations of a sample run in Figure 2.26. After the first iteration, we correctly identified $\approx 66\%$ of our system's particles and the remaining 34% were misidentified. Per the algorithm, we reseed these estimated groups into two clusters and follow by running the code again. Interestingly, in the second run (after the good first approximation), we then correctly grouped 98% of the system's 500 and only misidentified 2%. We surmise this rapid, accurate convergence of the method should occur where the difference in *mean connections* of a particle with other particles from community 1 relative to those from community

2 is not likely to be near zero. This is in contrast to tighter cases like $p_{\text{in}} = 0.8$ and $p_{\text{out}} = 0.65$ that would likely lead to results little better than 50%, even after many runs.

We also include graphs of the communities' centers of mass. In the corresponding graph in the top panels, communities converge to a separation of nearly zero (indicating much mixing has occurred between particles of the two communities); there is still, however, a small separation that allows us to collect more of one group than the other upon splitting the cluster in half. In the bottom panel, the two reseeded clusters rapidly converge to a separation of 1, provided particles have been grouped accurately. This is precisely the prediction of our centers-of-mass approximation, and this offers a useful litmus test for "convergence" of the algorithm.

Where possible, we attempt to frame our discussion of community recovery as in the literature (cf. [1], pp. 9-10). We present the authors' definition of a partition's agreement here verbatim:

Definition 2.0.45. *(Agreement). The agreement between two community vectors $x, y \in [k]^n$ is obtained by maximizing the common components between x and any relabeling of y, i.e.,*

$$A(x, y) = \max_{\pi \in S_k} \frac{1}{N} \sum_{i=1}^{N} \mathbb{1}(x_i = \pi(y_i)), \tag{2.55}$$

where S_k is the group of permutations on $[k]$.

Accordingly, in the asymptotic limit (letting $N \to \infty$), this allows us to define recovery strengths for an algorithm $\tilde{X} = \tilde{X}(\mathcal{G})$. We borrow from [1], providing two for our purposes:

Definition 2.0.46. *Suppose $\mathcal{G}$ is a graph generated from the symmetric stochastic block model with number of nodes N, connection probabilities P, and community*

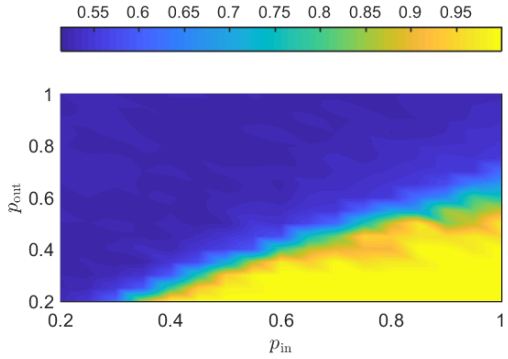

Figure 2.27: A surface plot of accuracy of the community detection algorithm over $(p_{\text{in}}, p_{\text{out}})$ space. Note the sharp transition between near-complete resolvability and mere chance.

labeling vector X. Suppose $\tilde{X}$ represents an algorithm's output (an estimated community partition) from the given input, $\mathcal{G}$. Then

- ***Strong recovery***: $\mathbb{P}\left\{A(X,\tilde{X}) = 1 - o(1)\right\} = 1 - o(1)$,
- ***Weak recovery***: $\mathbb{P}\left\{A(X,\tilde{X}) \geq \alpha\right\} = 1 - o(1)$, $\alpha \in (0,1)$.

Strong recovery implies the size of the set of misidentified particles tends to 0 as $N \to \infty$, while weak recovery implies the actual versus estimated partition agreement tends to the constant proportion of α.

In Figure 2.27, we present data on the accuracy (*agreement*) of our method over a large range of inner and outer connection probabilities. Throughout the figure, we used the following parameters: $S = 1000, t_{\text{final}} = 25, \Delta t = 0.1$ (i.e. 250 timesteps per iteration). As the system (2.7) has no explicit time dependence outside that through the x_i, only the number and size of the timesteps is relevant, not, *per se*, nominal starting or ending time t. For each initialization, we considered the algorithm complete after 5 iterations; at each $(p_{\text{in}}, p_{\text{out}})$ pair, we ran the code 20 times and averaged our accuracy results over these runs. To determine agreement of

the generated partition $\tilde{\mathcal{C}}$ with the actual partition $\mathcal{C}$, we apply the formula (2.55) after the final iteration. Here, the single vertical bars denote standard set cardinality. We observe that the definition of A includes a maximum over all permutations in S_k because it is not possible for us to determine the actual, original labeling that was supplied to generate $\mathcal{G}$; we must be satisfied with a correct partitioning, in the sense that

$$i \neq j, v \in C_i, v' \in C_j \text{ implies } \tilde{X}_v \neq \tilde{X}_{v'}.$$

We may still have $X_v \neq \tilde{X}_v$ despite this, and as such we allow for an interchanging of community labels across all N vertices.

Result 7. *Let $\tilde{X}_r = \mathbb{T}(\mathcal{G}_r)$ denote the output of the previously established algorithm for a given initialization of $\mathcal{G}$ (corresponding to the unknown X) and fixed N. Further, denote by $\bar{A}$ the agreement between the given two vectors averaged across the $r = 1, 2, \ldots, n_{\text{runs}}$ initializations. Experimentally, we find there exist c, d so that*

1. *$p_{\text{in}} > cp_{\text{out}} + d$ implies*

$$\bar{A}_r(X, \tilde{X}) \approx 1,$$

suggesting $A(X_r, \tilde{X}_r) \approx 1$ with high probability ≈ 1.

2. *$p_{\text{in}} < cp_{\text{out}} + d$ implies*

$$\bar{A}_r(X, \tilde{X}) \not\approx 1,$$

suggesting $A(X_r, \tilde{X}_r) \approx 1$ with probability $\not\approx 1$.

Result 7 should remind us of Result 1, though the particular thresholds $(c, d$ values) are distinct. Again, we have an approximately linear relationship between inner and outer connection probabilities; $(p_{\text{in}}, p_{\text{out}})$ on the side with $p_{\text{in}} > p_{\text{out}}$ lead to agreement values near 1, indicating a successful run of the algorithm. On the other

side, agreement values are not near 1; in fact, they appear to approach 0.5 as we take pairs further from the given threshold. This indicates the algorithm is little better at recovering our community partitions than blind guessing. We believe it may be possible to obtain better results (particularly very near the threshold) by adjusting the algorithm parameters $S, t_{\text{final}}, \Delta t$, and the number of iterations – particularly the last three items in this list to take more iterations and more timesteps per iteration – but we generally expect the threshold to remain in place. On the same token, it is also possible the algorithm could be made more efficient, either by taking larger and fewer timesteps or fewer iterations without sacrificing accuracy. As this is an algorithm intended to illustrate a point rather than be used practically, we do not explore the preceding points in detail.

Additionally, we believe the threshold of Figure 2.27 (of course suggestive of the transition between metastability and mixing in the two-cluster steady state of earlier sections) depends heavily on N. As particles are seeded randomly (at a large separation, S) and we ignore repulsion over short distances, these particles tend to converge to the cluster they are most attracted to. Hence, the answer to the problem of strong recovery (as $N \to \infty$) via the algorithm is the same as the answer to the question "for what N is the in- to out-degree ratio large for the average particle, with high probability?" Provided p_{in} is large relative to p_{out}, the number χ grows with increasing probability as N does (see the start of this section). We show this point in Figure 2.28, leaving the algorithmic parameters the same, though fixing $p_{\text{in}} = 0.8$ and examining the algorithm's agreement as N varies (depicted for $N \in \{50, 100, 250\}$). The character of the threshold remains intact, though for this much larger N we see a considerably less stringent threshold for resolvability. This is consistent with the spread coefficient $\frac{\sigma}{\mu}$ decreasing like $1/\sqrt{N}$ as $N \to \infty$, as less variation around a particle's mean in- and out-degree implies the *ratio* of these degrees is more likely

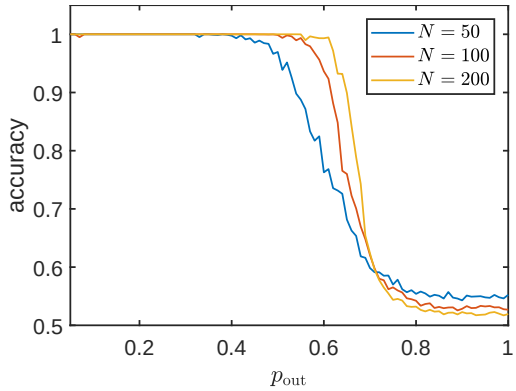

Figure 2.28: A plot of algorithmic accuracy as a function of p_{out} with $p_{\text{in}} = 0.8$ and $N \in \{50, 100, 250\}$. Note the location of the threshold at which near-complete resolvability becomes impossible as N varies.

to be nearer to $p_{\text{in}}/p_{\text{out}}$. Again, we stress that for probability values not satisfying the above restrictions, we suspect rather weak recovery – of agreement $\alpha \approx 0.50$ – as $N \to \infty$.

The previous numerical results and some additional work in Appendix D lead us to the following conjecture, offered without rigorous proof:

Conjecture 3. *Let $\chi = p_{\text{in}}/p_{\text{out}}$ be fixed, and let $\mathcal{G} \sim SBM(N, C, P)$ be a graph randomly generated via the stochastic block model.*

1. *For $\chi > 1$, our algorithm offers strong recovery of $\mathcal{G}$'s community partition in the limit $N \to \infty$. That is, there exists a set of algorithmic parameters for which strong recovery is attained.*

2. *For $\chi < 1$, our algorithm only offers weak recovery (with $\alpha = 0.5$) in the limit $N \to \infty$.*

The caveat expressed in Conjecture 3–1 is important; indeed, by our calculations, a pair such as $(p_{\text{in}}, p_{\text{out}}) = (0.4, 0.2)$ with $N = 200$ resulted in a network structure where communities could be fully resolved after 500 iterations, though not after 50

iterations. In contrast, Conjecture 3–2 indicates no algorithm parameter values can be used to attain weak recovery with $\alpha > 0.5$ or, of course, strong recovery.

The previous example illustrates the utility of our method for community detection. It is a novel approach, relying only on the dynamics of our system to sort particles appropriately. This confers an obvious advantage: it is easy to program and understand, and we are able to leverage well-established ordinary differential system solvers and theory to obtain results. Additionally, as we have learned from the previous discussion of $t_{\text{conv},2}$, the time for communities' centers to converge to an approximate distance of 1, beginning to "branch off" and mix, scales like a small ϵ, S-dependent multiple of $1/p$. Hence, as long as p is supposed to not be prohibitively near zero, we require only a small amount of timesteps per run of the algorithm. This is commonly the case in many real-world instances of stochastic block model-like graphs, but it may pose a large problem in the method for graphs where between-community connections are rather sparse.

Discussion

In this work, we present an in-depth treatment of the behavior of a familiar aggregation model in one dimension. We have established this model over a particular random network topology – the stochastic block model – which consists of a block structure of preset Erdős–Rényi "communities" with prescribed inner and outer link densities. Like other research, we are interested in the aggregation dynamics of the equations (2.7), though we deviate from this similar literature by focusing on the system's so-called "metastable dynamics." That is, we follow particle trajectories initialized from very well-separated positions, by community. This can be likened to a model of political processes, in which groups of individuals with disparate opinions (at one point in time) coalesce or split on key, contentious topics.

Our results suggest the metastable dynamics of (2.7) follow a discernible and predictable pattern; we point to Figure 2.6 for illustration. In our stochastic block structure, we let the probability of links between particles of different communities (p_{out}) vary from 1 to 0. Accordingly, for high p_{out}, we see a preservation of the communities' initial separation as time passes; a particle that evolves from a position very different from another particle will tend towards a cluster location with the same description as $t \to \infty$. As we decrease the proportion of connections drawn between communities, this eventually becomes untrue. When $\frac{1}{\kappa}\, p_{\text{out}}$ becomes sufficiently small relative to the inner probability of connection, p_{in} – the parameter specifying the density of links between particles from the *same* community – initial separations are not always preserved between pairs of particles. That is, two particles that begin at a great distance apart may tend toward the same position as $t \to \infty$. We refer to this phenomenon as communities "mixing." As we decrease p_{out} further, this mixing behavior deteriorates, as particles are no longer likely to tend to a finite number of positions in $\mathbb{R}$ as $t \to \infty$.

Where appropriate, we have noted the dependence of these results (jointly) on the 1D repulsion parameter, κ, and the number of system particles, N. However, in several instances we have taken the opportunity to vary κ, as well; in these cases, we observe that choosing a different $\kappa \in [0, 1]$ does not change the nature of our qualitative results. We still find similar areas in $(p_{\text{in}}, p_{\text{out}})$ space where mixed and unmixed states prevail, and a rather sharp threshold dividing these behaviors. This, of course, is our expectation, given that we characterized many of the important shifts in system behavior as a simple less-than versus greater-than relationship between $p_{\text{in}}/p_{\text{out}}$ and the reciprocal of the repulsion force, $1/\kappa$. Hence, even where we have not explicitly presented results with various κ, we believe their general nature is reflective of a wide range of κ values. A more systematic numerical approach may be necessary

to assess the precise nature of κ on our variant of system (2.7), though we again note this has been carried out on the extremely similar Erdős–Rényi structure in [35] and [36].

Following our exploration of the full particle model (2.7), we convert the system into center-of-mass coordinates by community. We then show the resulting solution curves accurately relay the extent of mixing occurring. This is due to the center-of-mass coordinate communicating the exact proportion of particles at each cluster location (assuming the multi-cluster state is stable). In Figure 2.7, we explore our parameter space in terms of inner and outer connection probabilities, plotting the center-of-mass difference as an output. This plot reveals a fairly sharp threshold that divides our parameter space into two regions: one in which mixing occurs with very high probability, and one in which mixing occurs with very low probability. Moreover, this threshold is a simple, linear relationship of inner and outer connection probabilities. We offer a similar plot for very low average probabilities of connection, $\bar{p}$, and show the threshold between degenerate, widely unstable behavior and pure mixing behavior follows a similar relationship between p_{in} and p_{out}. It is interesting and revealing that, despite the prohibitive dimensionality and complex behavior of the full N-particle model, the system's dynamics can be described rather simply (at great reduction in dimension) upon changing to a new coordinate system.

In Equations (2.38) and (2.39), we define two quantities to communicate the rate at which Equations (2.7) tend to equilibria as $t \to \infty$ and for various parameters and network structure. We re-frame the behavior of this system in the context of a "competing timescales" problem by decomposing its behavior into two qualitative phenomena. The first behavior is the community-wide motion of particles to a prescribed (by $F(r)$) separation of 1; the second behavior is the microscopic, particle-to-particle interaction of mixing, in which each particle tends towards one of two final

positions as $t \to \infty$. The quantities we define in this section are associated with these behaviors. We surmise the ratio between these two timescales must be drastically different in the region of parameter space near the transition from unmixed behavior to mixed behavior – relative to the point at which the greatest degree of mixing occurs. As we see in Figure 2.17, this ratio changes at a rate nearly four times as large near the former point; also, the two quantities near either point follow a very nearly linear relationship. Appropriately, it should thus be possible to predict where we lie on the bifurcation "slice" of Figure 2.10 (or, rather, whether or not we are near a transition point or a $(p_{\text{in}}, p_{\text{out}})$ pair at which a high degree of mixing occurs) by examining the ratio of these two quantities.

In the section that follows, we develop an approximation to the center-of-mass coordinate equations (2.22) through basic Taylor expansions and the assumption that particles belonging to different communities are seeded with well-separated initial conditions. This allows us to eliminate the strict x_i dependence of the $\mathbf{m}$ equations. We find this approximation is accurate throughout the "unmixed" regime, that is those systems for which p_{out} is sufficiently large relative to p_{in}; see the right panel of Figure 2.18 for a representative plot. Even in the "mixed" regime, for which it poorly approximates the overall qualitative behavior of the system, the approximation closely captures the first timescale (see Figure 2.19), referenced previously – the motion of communities to a fixed separation, *prior* to mixing behavior. Hence, it provides a useful characterization of at least one essential component of our system's dynamics. This suggests for small t, up to a certain $t_2 \approx t_{\text{conv},2}$, the dominant force influencing each particle's behavior originates from the particle's interactions with "outsiders," particles from different communities. In this sense, the relevant component of the adjacency matrix, E, is thus the entries that lie outside the main (block) diagonal. After this point in time, our results suggest the dominant force comes from each

particle's inner-community interactions, and correspondingly, the key components of E are the entries along the block diagonal.

Finally, we close with an application to the field of community detection. Noting that, for various choices of probability parameters p_{in} and p_{out}, our system guides particles to final positions that preserve community-to-community separations, we suppose the equations (2.7) can be leveraged to separate groups of particles with a sufficiently different inner/outer connection density. In Figure 2.26, we show the results of a sample run of our algorithm – using successive runs of these equations (with reseeding of system particles at each step) to iteratively obtain a likely partition of the system's N nodes into appropriate communities. Further, the systematic numerical results shown in Figure 2.27 depict, as long as p_{out} is small relative to p_{in}, we can attain near-complete recovery of the original community structure. The implication of Figure 2.28 is this requirement is increasingly relaxed as $N \to \infty$, to the point where the aforementioned maximum value of p_{out} (for near-complete recovery) *tends to* p_{in}. For outer connection probabilities much larger than this value, however, we can do little better than guessing, attaining about 50% accuracy in community recovery. In future research, it would perhaps be beneficial to explore how such an algorithm compares (in terms of accuracy and computational complexity) to more standard methods of community detection on stochastic block networks; among these are treatments of the subject like [1].

CYCLIC FEEDBACK SYSTEMS WITH QUORUM SENSING COUPLING

Contribution of Authors and Co-Authors

Manuscript in Chapter 3

Author: Tomas Gedeon

Contributions: Writing the manuscript, analytic work throughout

Co-Author: Mark Pernarowski

Contributions: Writing the manuscript, analytic work throughout

Co-Author: Adam Wilander

Contributions: Numerical analysis and simulation, editing the manuscript, some figure design

Manuscript Information

Tomas Gedeon, Mark Pernarowski, and Adam Wilander

Bulletin of Mathematical Biology

Status of Manuscript:

_____ Prepared for submission to a peer-reviewed journal
_____ Officially submitted to a peer-review journal
_____ Accepted by a peer-reviewed journal
__X__ Published in a peer-reviewed journal

Publisher: Springer
Published: June 2016, Volume 78, Issue 6, pp 1291-1317
DOI: 10.1007/s11538-016-0187-8

Introduction

Cellular populations need to communicate to facilitate joint, synchronous responses to outside stimuli or to produce a sustained rhythmical output. There has been strong recent interest in mechanisms by which such populations achieve and maintain synchrony. Typically intracellular proteins promote the production of signaling molecules. These diffuse in the extracellular spaces to provide a communication mechanism for the cellular aggregate. When cells use the signaling molecule to sense density of the cell population and use this information to up-regulate their gene expression, such communication is referred to as quorum sensing, and the signaling molecule is typically referred to as an autoinducer. Many such quorum sensing mechanisms have been discovered and modeled. Of particular interest is the emergence and loss of synchronized behavior when the cell density, or some other relevant parameter that characterizes the size of the population is changed.

De Monte *et. al.* [7] studied glycolitic oscillations in yeast both experimentally and theoretically. They observed the loss of population wide oscillations as the density of the cell decreased. They found that the loss of synchronous oscillations was not the result of de-synchronization of individual oscillators and that below a certain density threshold all cells stopped oscillating and entered a steady state. They called this transition *dynamic quorum sensing.*

Taylor *et. al.* [30] studied transition to synchronization in a large population of chemical oscillators (modeled by Belousov-Zhabotniskii equations) as a function of population density in low stirring rate and high stirring rate regimes. These correspond to low and high transport rates of the signaling species, respectively. They found that the transition to synchrony is different in these two cases. While at a high stirring rate, the transition is gradual and oscillators are recruited to the

synchronized pool gradually. Conversely, at a low stirring rate the emergence of synchrony is sudden at a certain density.

In this paper we study the emergence of oscillations and complex dynamics in variants and generalizations of a synthetic biology model first introduced by Garcia-Ojalvo *et. al.* [12]. Their model consists of a repressilator coupled to a quorum sensing module from *Vibrio fischeri*. Each cell in the aggregate is equipped with a three gene network that admits autonomous oscillations and is connected to a *Vibrio fischeri* module that produces and responds to a diffusible autoinducer AI. The transmembrane transport of the autoinducer is assumed proportional to the difference between the aggregate average and the local concentration. In their model only $TetR$ promotes the autoinducer. This feedback can produce stable steady behavior, and both synchronous and asynchronous oscillations [26]. However, when a different network protein promotes the autoinducer, much more complicated dynamics can occur. Ulner *et. al.* [34] and Koseska *et. al.* [18] examined the dynamics of small cell aggregates when CI promoted the autoinducer. Such systems exhibit complex multistable behavior. Although synchronous steady and oscillatory states are also possible, much of the aggregate behavior is a mixture steady and oscillatory states. All of these behaviors depend greatly on parameter values and the number of cells N.

Here we present a unified approach for categorizing and analyzing all such models. In the aforementioned studies, cells had a $K = 3$ gene network, and one protein Ω promoted the autoinducer S. We illustrate three such networks in Figure 3.1. When $\Omega = A$ the dynamics are simple in the sense that the $N = 1$ system has a unique equilibrium (Figure 3.1(a)). For $N \geq 2$ we show that two Hopf branches emerge, one of which is dependent on the quorum sensing parameter q. Since such systems have a unique equilibria, we can show the aggregate remains

(locally) *monostable* between synchronous equilibria and synchronous periodic orbits. We prove the majority of these results for a much larger class of Nf-Ns (Negative feedback - Negative sensing) models having n genes. Such models are defined in Section 2 and have a unique synchronous equilibria which can destabilize only by a Hopf bifurcation. Lastly, we numerically demonstrate that for one such model only the quorum or q-dependent Hopf branch (HB_1) has emergent stable period orbits (cf. Figure 4,5).

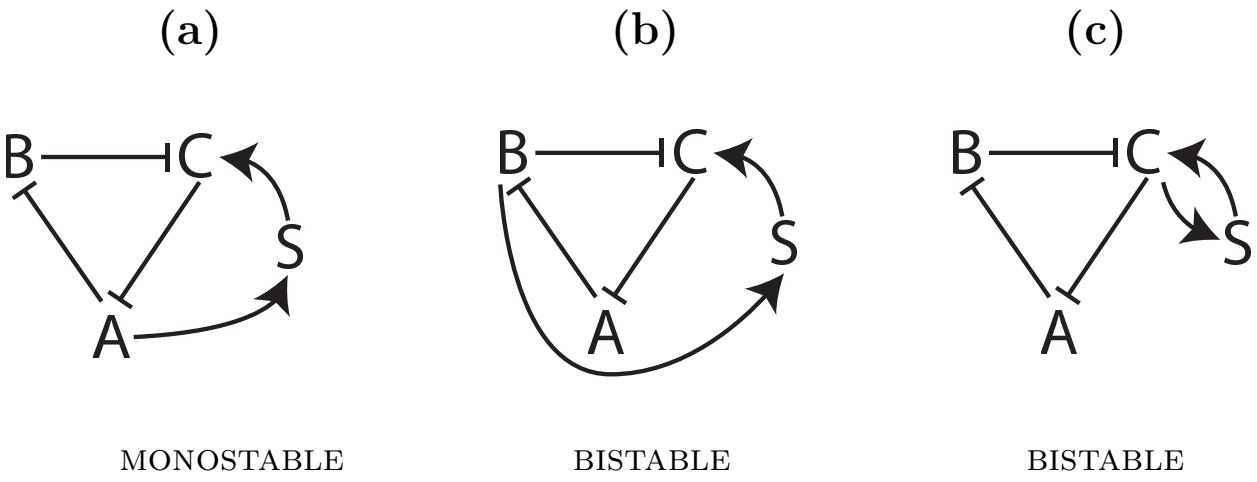

Figure 3.1: Schematics for three different $K = 3$ repressillator circuits. In each circuit $A = TetR, B = CI, C = LacI$ and a different protein $\Omega \in \{A, B, C\}$ upregulates the diffusive signal S. This *autoinducer* S upregulates C in all networks. When $\Omega = A$ the network dynamics are monostable (simple). Otherwise, the network dynamics can be bistable (complex).

Aggregate dynamics are very different when other proteins Ω promote the autoinducer in the repressilator model. We show that, when $\Omega = CI$ or $LacI$ (Figure 3.1(b)-(c) with $\Omega = B, C$) the existence of equilibria in the aggregate depends only on knowing the roots of a single scalar function whose root locus is cubic shaped. Such is the case in many bistable systems. In this case we show the saddle node

bifurcations define parameter sets where the aggregate is either monostable or has a huge numbers of equilibria. Koseska *et. al.* [18] numerically demonstrated ($N = 5$ cells) how these equilibria also lead to numerous new Hopf bifurcations and hence prolific multistability.

In Section 2, we define both the Garcia-Ojalvo *et. al.* [12] and Nf-Ns models. The latter model generalizes the former but can have an arbitrary number of genes n. Both are shown to have a Jacobian with a special block structure. In Section 3, we exploit this block structure to show the stability of synchronous equilibria depends only on one $(2n+1)^{th}$ degree polynomial where n is the number of genes in the model. Noteably, the stability is independent of the number of cells N. In Section 4, we prove the Nf-Ns system has a sole (synchronous) equilibria that can only destabilize via a Hopf bifurcation. Since the Garcia-Ojalvo *et. al.* [12] model is an Nf-Ns system the same results hold. For the former model we additionally show only two Hopf branches exist and only the quorum sensing dependent one is stable. In Section 5 we then show that for the $\Omega = B, C$ [1] feedback cases the system may have multiple equilibria. In this bistable case, a systematic description of all such equilibria is given in terms of a "consistency" condition.

Cyclic Feedback Models with Quorum Sensing

Most recent repressillator models incorporating quorum sensing [7, 18, 26, 33, 34, 37] are variations or simplifications of the model due to Garcia-Ojalvo et al. [12]. In all these studies, either $TetR$ (A) or CI (B) promotes the production of the autoinducer involved the quorum sensing. When $TetR$ promotes the autoinducer, the resulting dynamics are relatively simple (monostable case). However, when CI promotes the

[1] or CI and LacI, respectively

autoinducer, the dynamics can be very complex (bistable case). We cast all models into a general construct more amenable for local analyses and helpful for making simple generalizations regarding network dynamics.

We first define the model of Garcia-Ojalvo, Ellowitz and Strogatz [12] who studied a synthetic gene network which included quorum sensing for synchronization. A subsequent numerical bifurcation study can be found in Potapov et al. [26]. The model network illustrated in Figure 3.2 has two basic parts. One is a sub-network of three genes that repress each other in a cycle. Each gene is modeled by two variables, one representing abundance of mRNA and the other abundance of the corresponding protein. Specifically, the gene lacI expresses its protein LacI, and LacI inhibits transcription of the gene tetR. The protein TetR expressed by the gene tetR inhibits transcription of the gene cI. Lastly, protein CI, expressed by the gene cI, inhibits transcription of the gene lacI, thus completing the cycle. Every protein competes with polymerase for binding sites on a promoter and in this way inhibits the transcription from DNA to the corresponding mRNA. Therefore, as more protein is produced, less mRNA of the subsequent gene is produced. The other part of the network is another gene, luxI, up-regulated by tetR protein, produces protein LuxI which synthesizes a small molecule known as an autoinducer AI. This autoinducer (acylated homoserine lactone) can diffuse freely through the cell membrane and the extracellular medium. The combination of AI and a second protein (LuxR) will activate transcription of the gene lacI. Therefore, the mRNA (lacI) dynamics are different from the other two mRNA. Under these and other assumptions the equations describing the protein and mRNA concentrations in the i^{th} cell in a collection of N cells are:

$$
\begin{aligned}
\dot{a}_i &= -a_i + \Phi(C_i) && (tetR)\\
\dot{A}_i &= -\beta A_i + \beta a_i && (TetR)\\
\dot{b}_i &= -b_i + \Phi(A_i) && (cI)\\
\dot{B}_i &= -\beta B_i + \beta b_i && (CI)\\
\dot{c}_i &= -c_i + \Phi(B_i) + \Gamma(S_i) && (lacI)\\
\dot{C}_i &= -\beta C_i + \beta c_i && (LacI)\\
\dot{S}_i &= -(k_{s0}+\eta)S_i + k_{s1}A_i + \frac{\eta\, q}{N}\sum_{j=1}^{N} S_j && (AI)
\end{aligned}
\tag{3.1}
$$

where

$$
\Phi(z) = \frac{\alpha}{1+z^n}
$$

$$
\Gamma(z) = \frac{\kappa\, z^m}{1+z^m}
$$

are the assumed nonlinearities for transcription feedback by the proteins and autoinducer. The system (3.1) models the network in Figure 3.1(a). Inhibitory feedback within the network occurs through the bounded and decreasing function $\Phi(z)$. Conversely, the positive autoinducer feedback occurs through $\Gamma(z)$ which is bounded and increasing. Below we generalize the model above in several ways. Most notably, some monotonicity properties on $\Phi(z)$ are relaxed resulting in what will later be defined as the Nf-Ns model. But for numerical calculations we use (3.1) with $\Phi(z)$ and $\Gamma(z)$ defined above as are used in preceding studies [12, 18, 26, 33, 34].

A lowercase convention is used to indicate mRNA concentrations whereas uppercase indicates their associated protein. Thus, a_i is the (tetR) mRNA concentration

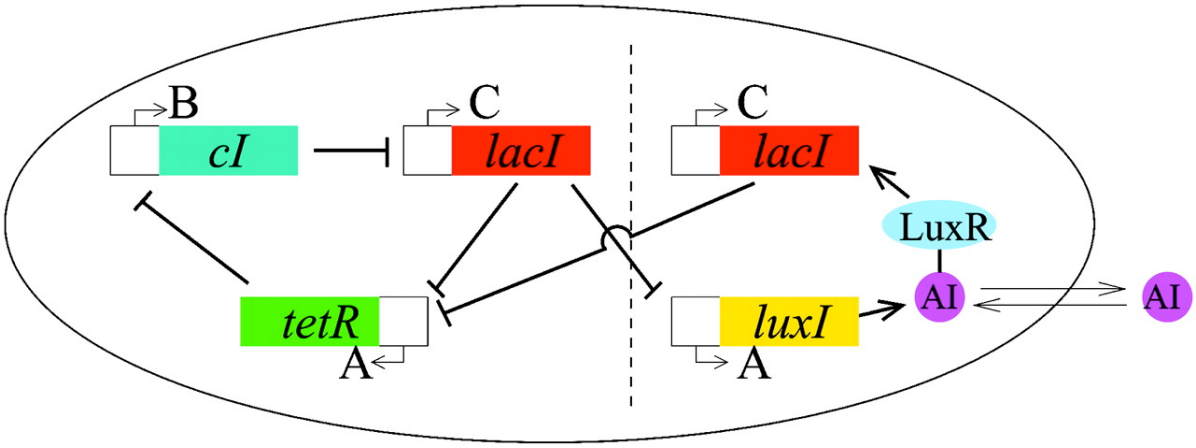

Figure 3.2: A synthetic gene network in *E. Coli* proposed by Garcia-Ojalvo J et al. [12]. The left portion of the network is the standard repressilator model. The right side includes a TetR mechanism for autoinducer (AI) production. The autoinducer passively diffuses into extracellular regions which enables quorum sensing in a cell collective.

in the i-th cell and A_i is the associated (TetR) protein concentration. The (all to all) coupling between cells is evident in the last term of $\dot{S}_i$. In (3.1) the parameter η is the permeability of the cell membrane to the autoinducer S_i. The quorum sensing parameter $q \in (0, 1)$ is derived from a quasi-steady state approximation to the equation for extracellular autoinducer concentration S_e :

$$\frac{dS_e}{dt} = -k_{se} S_e + k_{\text{diff}} \left(\bar{S} - S_e \right) \qquad , \qquad \bar{S} = \frac{1}{N} \sum_{i=1}^{N} S_i \quad .$$

Such an approximation yields

$$q = \frac{k_{\text{diff}}}{k_{se} + k_{\text{diff}}} = \frac{\rho_e}{k_{se} + \rho_e}$$

which is roughly proportional to cell density ρ_e when $\rho_e \ll k_{se}$ [12]. Thus, at low cell densities, q is small while at large densities q is near unity.

To completely define our more general Nf-Ns model, we first generalize the

intracellular network of Garcia-Ojalvo *et. al* [12]. Instead of a network of $K = 3$ genes we consider a general cycle of $K = n$ genes in cell i. We continue to represent each gene j by two variables X_j (representing mRNA concentration) and x_j (representing protein concentration)

$$\begin{aligned} \dot{x}_j &= -c_j x_j + \Phi_j(X_{j-1}) \\ \dot{X}_j &= b_j x_j - a_j X_j \qquad , \qquad j = 1, \ldots, n-1 \end{aligned} \tag{3.2}$$

The indices are considered modulo n and so x_0 is identified with x_n. Without loss of generality we assume that the feedback from the autoinducer affects variable x_n

$$\begin{aligned} \dot{x}_n &= -c_n x_n + \Phi_n(X_{n-1}) + \Gamma(S_i) \qquad , \\ \dot{X}_n &= b_n x_n - a_n X_n. \end{aligned} \tag{3.3}$$

In (3.2)-(3.3), all the constants a_j, b_j, c_j are assumed to be positive and $\Gamma(S_i)$ is any positive, bounded and increasing function of the autoinducer concentration S_i in cell i. The functions $\Phi_j(z)$ need not be the same but must be positive, bounded and monotonic. In particular, $\Phi_j(z)$ may be either increasing or decreasing. This should be contrasted to the model (3.1) where $\Phi_j(z) = \Phi(z)$ for all $j = 1, 2, 3$ and all $\Phi_j(z)$ were decreasing.

We examine the effect of differing autoinducer feedback mechanisms on the global dynamics of the quorum. Specifically, we examine the system above, where the synchronizing signal is placed at a different position in the loop.

$$\dot{S}_i = -(k_{s0} + \eta) S_i + k_{s1} \Omega + \frac{\eta\, q}{N} \sum_{i=1}^{N} S_i \qquad , \qquad \Omega \in \{X_1, X_2, \ldots, X_n\} \tag{3.4}$$

As depicted in Figure 3 there are two feedback loops in the system (3.2)-

(3.4). The first, internal feedback loop consists of $X_1, \ldots, X_n$ and interactions described in (3.2) and (3.3). The second, quorum sensing feedback loop consists of $X_1, X_2, \ldots, X_k = \Omega, S_i, X_n$. The quorum sensing loop couples the cells in the system together. We now associate a sign to each loop.

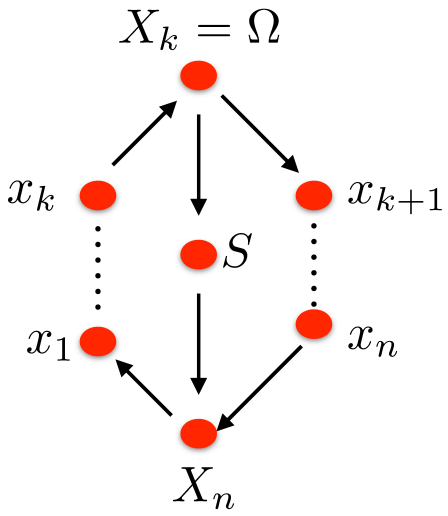

Figure 3.3: A schematic of the Nf-Ns system which generalizes the standard represillator model. The system has n genes and therefore $2n$ nodes along the perimeter cycle, see (2.2)-(2.4). The synchronizing signal $\Omega = X_k$ can occur at different positions in the perimeter cycles. We require that the number of negative feedbacks along the perimeter cycle is odd ($\bar{\beta} = -1$) and also that the number of negative feedbacks along the left loop that includes $\Omega \to S \to x_n$ is odd ($\bar{\alpha} = -1$).

Definition 3.0.1. *Let* $\delta_i = sgn\Phi_i'$. *Let*

$$\bar{\alpha} := \Pi_{i=1}^{n}\delta_i, \quad \bar{\beta} := \Pi_{i=1}^{k}\delta_i, \text{ where } k \text{ is the index such that } X_k = \Omega.$$

We say that the internal loop has a negative (positive) feedback if $\bar{\alpha} = -1$ *(*$\bar{\alpha} = 1$*) respectively. We say that the coupling loop has a negative (positive) feedback if* $\bar{\beta} = -1$

($\bar{\beta} = 1$) respectively.

Note that this definition of negative and positive feedback agrees with the standard definition for cyclic feedback systems [13,14,20]. Theory developed in these papers shows that negative feedback systems with sufficiently high gain [31,32] admit a stable periodic orbit, while positive feedback systems do not. Since we are interested in synchronization of stable oscillations, we will restrict ourselves to $\bar{\alpha} = -1$ i.e. the case when the internal loop is negative. Clearly, the repressilator studied in [12] falls into this category.

Definition 3.0.2. *We say that the system (3.2)-(3.4) is a negative feedback system with negative sensing (Nf-Ns system) if $\bar{\alpha} = -1$ and $\bar{\beta} = -1$.*

Given our preceding definitions, the number of genes n, the monotonicity of each $\Phi_j(z)$ and the index k defining Ω in $\Omega = X_k$ all affect the parity parameters $\bar{\alpha}$ and $\bar{\beta}$ in Definition 2.1. For instance, in the repressilator model (3.1) one can choose $\Omega \in \{X_1, X_2, X_3\} = \{A, B, C\}$ for the feedback to the autoinducer but only for $\Omega = A$ is the system Nf-Ns.

Ultimately, we seek to understand the dynamics of N identical Nf-Ns cells. To be more explicit we let i index each cell. Then, the state of each cell is given by

$$\mathbf{x}_i = (x_1^i, X_1^i, x_2^i, X_2^i, \ldots, x_n^i, X_n^i, S_i).$$

Thus, X_j^i is the dependent variable for the j^{th} mRNA in cell i. As was previously defined, S_i is the autoinducer concentration in cell i. With these definitions we may now state the main result of our paper in the following Theorem.

Theorem 3.0.3. *Let (3.2)-(3.4) be an Nf-Ns system with N identical cells. Then*

1. *There exists a unique equilibrium E that is symmetric i.e., there exist $\bar{X}_j, \bar{x}_j$ and $\bar{S}$ such that $X_j^i = \bar{X}_j, x_j^i = \bar{x}_j, S_i = \bar{S}$ for all $i = 1, \ldots, N$.*

2. *Equilibrium E can loose stability only through a Hopf bifurcation.*

3. *There are exactly two such Hopf bifurcations. One depends on the quorum sensing parameter q. The other does not.*

4. *A branch of synchronous periodic orbits emerge from the q-dependent Hopf bifurcation.*

5. *The q-independent Hopf bifurcation does not have a branch of synchronous periodic orbits.*

Our results explain and significantly generalize numerical observations reported in the literature. The system (3.1) with $\Omega = A$ was studied in [12]. In their study, the quorum sensing index as defined in Definition 3.0.1 is $\bar{\beta} = -1$, and they found only symmetric oscillations in their numerical examinations of the Nf-Ns system.

However, when $\Omega = B$ as in [18, 33, 34], *CI* promotes the autoinducer and the quorum sensing index $\bar{\beta} = 1$. The resulting dynamics are significantly different. The numerical studies demonstrated the existence of synchronous and asynchronous oscillations as well as the coexistence of stable equilibria and periodic orbits. This seems to indicate that the systems with negative feedback ($\bar{\alpha} = -1$) but a positive quorum sensing loop ($\bar{\beta} = 1$) are capable of bistable behavior. Later we shall demonstrate numerically for the repressilator model [12] that when $\Omega = C$, the quorum sensing loop is positive and the system can exhibit bistable behavior.

General Framework

In what follows, we assume cell to cell homogeneity in intracellular dynamics. Such models can be cast in a simple general framework. To do so recall the state of

each cell is given by

$$\mathbf{x}_i(t) = (x_1^i, X_1^i, x_2^i, X_2^i, \ldots, x_n^i, X_n^i, S_i) \in \mathbb{R}^l$$

where $l = 2n + 1$.

In the model (3.1), $l = 7$, while in other repressilator model studies $l = 3$ [37]. But in our general model (3.2)-(3.4) we have $l = 2n + 1$ where n is the number of genes. Then the state of the quorum of N cells is given by

$$\mathbf{x} = (\mathbf{x}_1, \mathbf{x}_2, \ldots, \mathbf{x}_N)^T \in \mathbb{R}^{Nl}$$

When the inter-cell coupling $q = 0$, the intracellular chemical kinetics is represented by

$$\frac{d\mathbf{x}_i}{dt} = f(\mathbf{x}_i; \mu) \tag{3.5}$$

for some function f and parameters μ. Cell to cell homogeneity is reflected in the fact $f(\mathbf{x})$ is the same for each cell i in (3.5).

For quorum models where auto-inducers sense extracellular averages ($q \neq 0$) an additional term needs to be added to (3.5):

$$\frac{d\mathbf{x}_i}{dt} = f(\mathbf{x}_i; \mu) + \mathcal{Q}\mathbf{x} \tag{3.6}$$

where $\mathcal{Q}$ is a constant coupling matrix having the block structure:

$$\mathcal{Q} = \begin{bmatrix} C & C & \ldots & C \\ C & C & \ldots & C \\ \vdots & \vdots & \ldots & \vdots \\ C & C & \ldots & C \end{bmatrix} \tag{3.7}$$

for some $C \in \mathbb{R}^{l\times l}$. Then the N-cell model is

$$\frac{d\mathbf{x}}{dt} = F(\mathbf{x};\mu) = \begin{pmatrix} f(\mathbf{x}_1;\mu) + \mathcal{Q}\mathbf{x} \\ f(\mathbf{x}_2;\mu) + \mathcal{Q}\mathbf{x} \\ \vdots \\ f(\mathbf{x}_N;\mu) + \mathcal{Q}\mathbf{x} \end{pmatrix} \tag{3.8}$$

For appropriately defined $f(\mathbf{x};\mu)$ and $\mathcal{Q}$, the models in [12,18,33,34] and our general model (3.2)-(3.4) can all be written as (3.8). The form of (3.8) also results in linearized systems having a very specialized structure. In general the linearized system about $\bar{\mathbf{x}}(t)$ is

$$\frac{d\mathbf{z}}{dt} = DF(\bar{\mathbf{x}})\mathbf{z} \tag{3.9}$$

where $DF(\bar{\mathbf{x}})$ is the Jacobian of F in (3.8) evaluated at $\bar{\mathbf{x}}$. For equilibria $\bar{\mathbf{x}} = (\bar{\mathbf{x}}_1, \bar{\mathbf{x}}_2, \ldots, \bar{\mathbf{x}}_N)^T$ is constant and $F(\bar{\mathbf{x}}) = 0$. And, for the coupling (3.7), we may represent this Jacobian in the block form

$$DF(\bar{\mathbf{x}}) = \begin{bmatrix} A_1 + C & C & \ldots & C \\ C & A_2 + C & \ldots & C \\ \vdots & \vdots & \ldots & \vdots \\ C & C & \ldots & A_N + C \end{bmatrix} \tag{3.10}$$

where $A_i = Df(\bar{\mathbf{x}}_i)$. Further note that when the equilibrium is synchronous, all the $\bar{\mathbf{x}}_i$ are the same, so that $A_i = A$ for all $i = 1, 2, \ldots N$. All of these observations are true regardless of the chemical kinetics imposed via the function f, the number of cells N, the number of relevant intracellular concentrations and the number of auto-inducers which sense extra-cellular averages.

Stability of Synchronous Equilibria

In this section we derive linear stability criteria for synchronous equilibria $\bar{\mathbf{x}}$. The Jacobian of the linearized system (3.9) has the block structure:

$$DF(\bar{\mathbf{x}}) = \begin{bmatrix} A+C & C & \dots & C \\ C & A+C & \dots & C \\ \vdots & \vdots & \dots & \vdots \\ C & C & \dots & A+C \end{bmatrix} \tag{3.11}$$

where $A, C \in \mathbb{R}^{l\times l}$. Its spectrum is then determined by the following theorem. Our proof is similar to the analysis in Pecora and Caroll [25].

Theorem 3.0.4. *The characteristic equation of $M \equiv DF(\bar{\mathbf{x}})$ is*

$$P(\lambda) = Q(\lambda)R(\lambda)^{N-1} = 0 \tag{3.12}$$

where $Q(\lambda)$ and $R(\lambda)$ are the characteristic polynomials of the matrices $A+NC$ and A, respectively.

Proof. We first note that the block symmetric matrix $M \equiv DF(\bar{\mathbf{x}})$ can be written compactly as the matrix direct product:

$$M = I \otimes A + \mathbf{1} \otimes C \tag{3.13}$$

where $I \in \mathbb{R}^{N\times N}$ is the identity matrix, $\mathbf{1} \in \mathbb{R}^{N\times N}$ is the matrix of ones and $A, C \in \mathbb{R}^{l\times l}$. Since the eigenvalues of $\mathbf{1}$ are N with multiplicity 1, and 0 with multiplicity $N-1$ there exists a diagonalizing matrix S such that $\mathbf{1} = S^{-1}DS$ where $D = diag(N, 0, 0, \dots, 0)$. Next, we define $T = S^{-1} \otimes I_K$ where $I_l \in \mathbb{R}^{l\times l}$ is the

identity matrix. Noting that I is invariant with respect to similarity transformations, it is readily seen in Lemma 3.0.6 that

$$M' \equiv T^{-1}MT = I \otimes A + D \otimes C \ .$$

Given D, the block diagonal matrix M' has one block $A + NC$ and $N - 1$ blocks A. Therefore,

$$det(M) \ = \ det(A + NC)\ det(A)^{N-1}$$

To find the characteristic polynomial $P(\lambda)$ of M one merely replaces A by $A - \lambda I$ to get

$$\begin{aligned} P(\lambda) &= det(M - \lambda I) \\ &= det(A + NC - \lambda I)\ det(A - \lambda I)^{N-1} \\ &= Q(\lambda)\ R(\lambda)^{N-1} \end{aligned}$$

where $Q(\lambda)$ and $R(\lambda)$ are the characteristic polynomials of $A+NC$ and A, respectively. □

Remark 3.0.5. *Our result can be recast as an instance of a Master stability function [25] which is applicable to any type of symmetric coupling. To see this we rewrite (3.6) in the form*

$$\frac{d\mathbf{x}_i}{dt} = g(\mathbf{x}_i; \mu) + \mathcal{R}\mathbf{x} \tag{3.14}$$

where $\mathcal{R}$ is a constant matrix with the block structure

$$\mathcal{R} = \begin{bmatrix} (1-N)C & C & \dots & C \\ C & (1-N)C & \dots & C \\ \vdots & \vdots & \dots & \vdots \\ C & C & \dots & (1-N)C \end{bmatrix} \tag{3.15}$$

and

$$g(\mathbf{x}_i;\mu) = f(\mathbf{x}_i;\mu) + \mathcal{Z}\mathbf{x}$$

with

$$\mathcal{Z} = \begin{bmatrix} NC & 0 & \dots & 0 \\ 0 & NC & \dots & 0 \\ \vdots & \vdots & \dots & \vdots \\ 0 & 0 & \dots & NC \end{bmatrix}.$$

While form (3.14) clearly shows that the diagonal $\mathbf{x_1} = \ldots = \mathbf{x_N}$ is invariant since $\mathcal{R}\mathbf{x} = 0$ on diagonal, the form (3.6) has an advantage that it moves the quorum parameter representing cell density q into the coupling term $\mathcal{Q}$. In particular, we can rewrite the equation (3.4) as

$$\dot{S}_i = -k_{s0}S_i + k_{s1}\Omega_i - \eta(1-q)S_i + \frac{\eta q}{N}\left((1-N)S_i + \sum_{j\neq i} S_j\right)$$

where the first 3 terms are parts of function $g(\mathbf{x_i})$ and the last term is part of the coupling matrix $\mathcal{R}$.

Lemma 3.0.6. *Given the definition of M, S and T in Theorem 3.0.4*

$$T^{-1}MT = I \otimes A + D \otimes C\ .$$

Proof. First note that the diagonalizing matrix S of $\mathbf{1}$ is:

$$S = \begin{bmatrix} 1 & 1 & \dots & \dots & 1 \\ 1 & -1 & 0 & \dots & 0 \\ 1 & 0 & -1 & \dots & 0 \\ \vdots & \vdots & \dots & \vdots & \vdots \\ 1 & 0 & \dots & 0 & -1 \end{bmatrix}$$

We now use the distributive and mixed-product properties of the Kronecker product given $T = S^{-1} \otimes I_K$:

$$\begin{aligned} MT &= (I \otimes A + \mathbf{1} \otimes C)\left(S^{-1} \otimes I_K\right) \\ &= (I \otimes A)\left(S^{-1} \otimes I_K\right) + (\mathbf{1} \otimes C)\left(S^{-1} \otimes I_K\right) \\ &= (IS^{-1}) \otimes (AI_K) + (\mathbf{1}S^{-1}) \otimes (CI_K) \\ &= S^{-1} \otimes A + \mathbf{1}S^{-1} \otimes C \end{aligned}$$

In a similar fashion one uses $T^{-1} = S \otimes I_K$ to expand

$$T^{-1}MT = (S \otimes I_K) \times \left(S^{-1} \otimes A\right) + (S \otimes I_K)\left(\mathbf{1}S^{-1} \otimes C\right) = I \otimes A + D \otimes C$$

□

Lemma 3.0.7. *Let λ_Q (λ_R) be a root of $Q(\lambda)$ ($R(\lambda)$) and let v_Q (v_R) be the corresponding eigenvector of $A + NC$ (A)*

$$(A + NC)v_Q = \lambda_Q v_Q \qquad Av_R = \lambda_R v_R.$$

Then

1. *the vector* $\mathbf{v_Q} := (v_Q, v_Q, \ldots, v_Q)^T$ *where* v *repeats* N *times is an eigenvector of (3.11) with eigenvalue* λ_Q.

2. *the vector* $\mathbf{v_R} := (v_R, v_R, \ldots, v_R)^T$ *where* v *repeats* N *times is NOT an eigenvector of (3.11) with eigenvalue* λ_R.

Proof. Result (1) follows directly by multiplying $DF(\bar{x})\mathbf{v_Q}$ with $DF(\bar{x})$ defined in (3.11).

To show (2) observe first that

$$DF(\bar{x})\mathbf{v_R} = (v, v, \ldots, u)^T \quad \text{where} \quad u = \lambda_R v_R + NCv_R.$$

Note that if we show that $v_R \notin C$, then $\mathbf{v_R}$ is not an eigenvector of $DF(\bar{x})$, which is the statement (2).

We will now show that $v_R \notin C$. Since C has the unique non-zero element in the lower right corner, this is equivalent to show that the last component of v_R is non zero $[v_R]_{2n+1} \neq 0$.

Assume, by contradiction, that $[v_R]_{2n+1} = 0$. We show that if $(A - \lambda_R I)v_R = 0$ and $[v_R]_{2n+1} = 0$, then $v_R \equiv 0$. Since v_R is perpendicular to the last row of A, and this row has only two nonzero elements in column $2K$ and the last column $2n+1$, our assumption $[v_R]_{2n+1} = 0$ implies $[v_R]_{2K} = 0$. Next, consider the $2K$-th row of A which is also perpendicular to v_R and has only two non-zero entries in columns $2K-1$ and $2K$. Then $[v_R]_{2K} = 0$ implies $[v_R]_{2K-1} = 0$. Realizing that each row of A, except the row $2n-1$, has two entries, the same argument sequentially establishes that $[v_R]_i = 0$ for all i. □

Remark 3.0.8. *The first result of Lemma 3.0.7 implies that the eigenspace at the Hopf bifurcation at $\lambda_Q = i\omega$ is invariant under symmetry group S_N generated by relabelling of the oscillators. By the equivariant Hopf bifurcation theory [16, 28], for every isotropy subgroup $\Sigma \subset S_N \times S^1$ with a two dimensional fixed point space, there will be a small amplitude periodic orbit emanating from the equilibrium having Σ as their group of symmetries. Since the two dimensional real eigenspace corresponding to $\lambda_Q = i\omega$ is invariant under $S_N \times \{1\}$, this theory guarantees existence of a branch of synchronous oscillations. Which of these branches of periodic orbits will be stable depends on delicate analysis of higher order terms of the nonlinearities, see [8].*

On the other hand, the second result of Lemma 3.0.7 implies that the loss of stability of synchronous equilibrium through Hopf bifurcations where $\lambda_R = i\omega$ is a root of $R(\lambda)$ will lead to oscillations which will not be synchronous since the eigenspace at the Hopf bifurcation is not not invariant under S_N symmetry. In this case different cells will oscillate with either different amplitudes, or different phases.

At this point we may make one very important observation. The stability of any synchronous equilibria is independent of the number of cells N. If the autoinducer sensing terms contain only average terms such as $\frac{\eta\, q}{N} \sum_{i=1}^{N} S_i$ then it is not hard to see, given how C is defined, that neither $A + NC$ nor A depend on N. Consequently, for models defined by (3.6), the stability of synchronous states and the possible emergence of oscillatory solutions from them have nothing to do with the number of cells.

Nf-Ns Model

We now focus on the Nf-Ns model where $\bar{\alpha} = \bar{\beta} = -1$ in Definition 3.0.1. Again, the state variable for cell i is

$$\mathbf{x}_i = (x_1^i, X_1^i, x_2^i, X_2^i, \ldots, x_n^i, X_n^i, S_i)$$

A superscript is used to index the cell while subscripts index the gene number. These conventions will be retained in subsequent calculations. Also, lowercase x denote the mRNA, uppercase X denote proteins and S the autoinducer. Then, the quorum state $\mathbf{x} = (\mathbf{x}_1, \mathbf{x}_2, \ldots, \mathbf{x}_N)^T \in \mathbb{R}^{(2n+1)N}$, and the model (3.2)-(3.4) can be written in the compact form

$$\frac{d\mathbf{x}}{dt} = F(\mathbf{x}; \mu) \tag{3.16}$$

for an appropriately defined F.

Again, by convention we will let overbars denote equilibria as in $F(\bar{\mathbf{x}}) = 0$ where $\bar{\mathbf{x}} = (\bar{\mathbf{x}}_1, \bar{\mathbf{x}}_2, \ldots, \bar{\mathbf{x}}_N)^T$. Our ultimate goal is to understand how and under what circumstances synchronous oscillations might emerge in the genetic network.

In the next section, we prove the Nf-Ns model has a sole (synchronous) equilibria which can be parametrized explicitly in terms of the equilibrium value of x_n. Afterwards we prove such equilibria can only destabilize via Hopf bifurcations.

Existence and Uniqueness of Synchronized Equilibrium

In this section we show the only positive equilibria of the system (3.2)-(3.4) are synchronous:

$$\bar{\mathbf{x}}_i = (x_1, X_1, x_2, X_2, \ldots, x_n, X_n, S) \qquad , \qquad \forall i = 1, 2, \ldots N \tag{3.17}$$

for some positive $x_1, X_1, x_2, X_2, \ldots, x_n, X_n$ and S.

Theorem 3.0.9. *Suppose $\Phi_j(z)$ are monotonic for $j = 1, 2, \ldots n$ and that $\Gamma(z)$ is monotonically increasing. Further suppose there exists constants a, κ_1 and κ_2 such that*

i) $\Phi_j(z) \geq 0$, $\Phi_j(0) > a > 0$ and $\Phi_j(z) < \kappa_1$ for all $z \geq 0$ for all $j = 1, 2, \ldots n$.

ii) $\Gamma(z) > 0$ for $z > 0$ and $\Gamma(z) < \kappa_2$ for all $z \geq 0$

then (3.2)-(3.4) has a unique positive equilibria $\bar{\mathbf{x}}$ which is synchronous.

Proof. From the form of the equations (3.2)-(3.4) it is evident that

$$X_j^i = \frac{b_j}{a_j} x_j^i$$

and

$$x_j^i = \frac{1}{c_j} \Phi_j(X_{j-1}^i).$$

Let

$$\Psi_j(z) = \frac{b_j}{a_j c_j} \Phi_j(z).$$

Then

$$X_j^i = \Psi_j(X_{j-1}^i).$$

Using this we observe that we can write for all i

$$\begin{aligned} X_k^i &= \Psi_k \circ \Psi_{k-1} \circ \Psi_1(\frac{b_n}{a_n} x_n) =: H(x_n) \\ X_{n-1}^i &= \Psi_{n-1} \circ \Psi_{n-2} \circ \Psi_1(\frac{b_n}{a_n} x_n) =: G(x_n) \end{aligned} \tag{3.18}$$

Next note $\dot{S}_i = 0$ implies

$$-(k_{s0} + \eta)S_i + k_{s1}X_k^i + \eta\ qS = 0 \tag{3.19}$$

where the i-independent average [2] in (3.19) is:

$$S \equiv \frac{1}{N}\sum_{i=1}^{N} S_i$$

Solving for S_i we find

$$S_i = \gamma_1 X_k^i + \gamma_0 S \tag{3.20}$$

where the parameters defining S_i are both positive and do not depend on i:

$$\gamma_1 = \frac{k_{s1}}{\eta + k_{s0}} \qquad , \qquad \gamma_0 = \frac{\eta\ q}{\eta + k_{s0}} \quad .$$

Collectively, using the equation

$$0 = \dot{x}_n^i = -c_n x_n^i + \Phi_n(X_{n-1}^i) + \Gamma(S_i)$$

and plugging in expressions from (3.18) we find that all x_n^i must be roots of the same function:

$$F(x) := \Phi_n(G(x)) + \Gamma(\gamma_1 H(x) + \gamma_0 S) - c_n x.$$

We now show $F(x)$ has a sole root for each $S > 0$ in which case all x_n^i equal the same root x_n and all equilibria of (3.1) are synchronous. First we note that because

[2] When the equilibria $\bar{\mathbf{x}}$ is synchronous, $S_i = S$ for all i

of the assumptions of nonnegativity, for all $S > 0$ we have

$$F(0) = \Phi_n(G(0)) + \Gamma(\gamma_1 H(0) + \gamma_0 S) \geq \Gamma(\gamma_0 S) > 0.$$

Then since

$$\lim_{x\to\infty} (\Phi_n(G(x)) + \Gamma(\gamma_1 H(x) + \gamma_0 S) - c_n x) < \lim_{x\to\infty} \kappa_1 + \kappa_2 - c_n x$$

it is apparent $F(x) < 0$ for x sufficiently large. Thus $F(x)$ has a root. This root is unique since F is a monotonically decreasing function.

To see this we first observe that the sign of the derivative

$$sgn\ \frac{d}{dx}(\Phi_n(G(x)) = \Pi_{i=1}^{n} \Phi_i' = \bar{\alpha}.$$

Similarly, the sign of the derivative of the second term

$$sgn\ \frac{d}{dx}\left(\Gamma(\gamma_1 H(x) + \gamma_0 S)\right) = sgn\ \Gamma' sgn\ \frac{d}{dx} H(x) = \bar{\beta}$$

since $sgn\ \Gamma' = 1$ by assumption. Since in Nf-Ns systems both $\bar{\alpha} = \bar{\beta} = -1$, $F(x)$ is decreasing and has a sole positive root for each $S > 0$. □

Equilibria Destabilization for a General Case

Given Theorem 3.0.4 the stability of $\bar{\mathbf{x}}$ will depend only on the spectra of A and $A + NC$, which differ only in the lower right single element. We define

$$A_\zeta = \begin{bmatrix} -c_1 & 0 & 0 & 0 & 0 & \dots & \Phi_1'(x_n) & 0 \\ b_1 & -a_1 & 0 & 0 & 0 & \dots & 0 & 0 \\ 0 & \Phi_2'(x_1) & -c_2 & 0 & 0 & \dots & 0 & 0 \\ 0 & 0 & b_2 & -a_2 & 0 & \dots & 0 & 0 \\ 0 & 0 & 0 & \Phi_3'(x_2) & -c_3 & \dots & 0 & 0 \\ \vdots & & \vdots & & \vdots & & \vdots & \\ 0 & 0 & 0 & \Phi_n'(x_{n-1}) & -c_n & \dots & 0 & \Gamma'(S) \\ 0 & 0 & 0 & 0 & 0 & \dots & -a_n & 0 \\ 0 & k_{s1} & 0 & 0 & 0 & \dots & 0 & -\zeta \end{bmatrix} \tag{3.21}$$

whose characteristic polynomial is

$$P_\zeta(\lambda) \equiv det(A_\zeta - \lambda I) \qquad , \qquad \zeta > 0 \ .$$

In matrix A_ζ we placed k_{s1} in the second column - this correspond to $k = 1$ where variable X_1 is involved in the quorum sensing feedback loop. For general k the number k_{s1} will be in the column $2k$.

Then if we define

$$\zeta_1 = k_{s0} + (1 - q)\eta \qquad , \qquad \zeta_2 = k_{s0} + \eta$$

the respective characteristic polynomials of $A + NC$ and A in Theorem 3.0.4 are:

$$\begin{aligned} Q(\lambda) &= P_{\zeta_1}(\lambda) \\ R(\lambda) &= P_{\zeta_2}(\lambda) \end{aligned}$$

where $\zeta_1 < \zeta_2$ and only $Q(\lambda)$ depends on the quorum sensing parameter q. It therefore suffices to examine roots of the polynomial $P_\zeta(\lambda)$.

The sparsity of A_ζ helps in the computation of $P_\zeta(\lambda)$. We let $M_{i,j}$ be the submatrix obtained by deleting the i^{th} row and j^{th} column of $A_\lambda \equiv A_\zeta - \lambda I$. Then the Laplace expansion of A_λ about the last row yields:

$$P_\zeta = -(\lambda + \zeta)\ |M_{2l+1,2l+1}| - k_{s1}\,|M_{2l+1,2k}|$$

where k is the index of the variable X_k which is involved in quorum sensing loop.

We first indicate computation of $|M_{2l+1,2l+1}|$. This minor has elements only on the two diagonals of the matrix: the main diagonal, and the lower diagonal, into which we include the element $\Phi_1'(x_n)$ in the upper right corner of $M_{2l+1,2l+1}$. This structure implies that there are exactly two nonzero products in the determinant calculation that multiply elements along these two diagonals. Therefore

$$\begin{aligned} |M_{2l+1,2l+1}| &= \Pi_{i=1}^n(-c_i - \lambda)(-a_i - \lambda) - \Pi_{i=1}^n b_i \Pi_{i=1}^n \Phi_i' \\ &= \Pi_{i=1}^n(c_i + \lambda)(a_i + \lambda) - \bar{\alpha}\Pi_{i=1}^n b_i |\Pi_{i=1}^n \Phi_i'| \end{aligned} \tag{3.22}$$

where in the last equality we used definition of $\bar{\alpha}$.

The calculation of the term $|M_{2l+1,2k}|$ is more involved since we will need to discuss its dependence on k. We perform the calculation on the matrix (3.21) where $k = 1$; we then make few remark on the general case. Note that there is unique nonzero

element in the second row of $M_{2l+1,2}$; so every nonzero term in the determinant must contain the entry b_1. Expanding around pivot b_1 in turn forces selection of $\Phi_1'(x_n)$ as the next pivot in the first row.

For general k, an analogous process forces selection of (in order)

$$b_k,\ \Phi_{k-1}',\ b_{k-1},\ \Phi_{k-1}', \ldots, b_1,\ \Phi_1'.$$

After this backward sweep, we go back to the example (3.21) and expand the matrix forward along the diagonal from column 2. In the row 3 we need to expand around $(-c_2 - \lambda)$, which then forces $(-a_2 - \lambda)$. It follows that in order to get a nonzero product we need to expand along the diagonal elements

$$(-c_2 - \lambda), (-a_2 - \lambda), \ldots (-c_{n-1} - \lambda), (-a_{-1} - \lambda).$$

However, the only nonzero element in the last column of $M_{2l+1,2}$ is $\Gamma'(S)$. Therefore, in order to ensure nonzero product in the determinant we need to pivot on $\Gamma'(S)$ and, finally, include b_n.

Therefore, for general k we have

$$\begin{aligned} |M_{2l+1,2k}| &= \Gamma'(S) b_n \left(\Pi_{i=k}^{n-1}(-c_i - \lambda)(-a_i - \lambda)\right) \Pi_{i=1}^{k} b_i \Pi_{i=1}^{k-1} \Phi_i' \\ &= \Gamma'(S) b_n \left(\Pi_{i=k}^{n-1}(c_i + \lambda)(a_i + \lambda)\right) \Pi_{i=1}^{k} b_i \Pi_{i=1}^{k-1} \Phi_i' \end{aligned} \tag{3.23}$$

Note that since

$$\bar{\alpha} = sgn \Pi_{i=1}^{n} \Phi_i' = sgn(\Pi_{i=1}^{k-1} \Phi_i' \Pi_{i=k}^{n} \Phi_i') = sgn(\Pi_{i=1}^{k-1} \Phi_i') \bar{\beta}$$

and $\bar{\alpha} = \bar{\beta} = -1$ in the Nf-Ns case, we have

$$\Pi_{i=1}^{k-1}\Phi_i' > 1.$$

Using these results we compute $\bar{P}(\lambda) = -P_\zeta(\lambda)$

$$\bar{P}(\lambda) = (\lambda+\zeta)\Pi_{i=1}^{n}(c_i+\lambda)(a_i+\lambda) + \rho_1(\lambda+\zeta) + \rho_2(\Pi_{i=k}^{n-1}(c_i+\lambda)(a_i+\lambda)) \quad (3.24)$$

where

$$\begin{aligned} \rho_1 &= -\bar{\alpha}\Pi_{i=1}^{n} b_i |\Pi_{i=1}^{n}\Phi_i'| > 0 \\ \rho_2 &= \Phi_i' k_{s1}\Gamma'(S) b_n \Pi_{i=1}^{k} b_i \Pi_{i=1}^{k-1}\Phi_i' k_{s1}\Gamma'(S) > 0 \end{aligned}$$

Note we negated P_ζ to remove several minus signs. Again, all parameters are positive. Importantly, this implies

$$\bar{P}(\lambda) > 0 \quad , \quad \forall\lambda > 0$$

for all positive model parameters μ. This means that regardless of parameter values μ, the Jacobian $DF(\bar{\mathbf{x}})$ can not have positive real eigenvalues . Consequently, destabilization of equilibria can occur only as a result of a Hopf bifurcation. In so much as we are interested in the emergence of oscillations we next seek to locate such Hopf points.

We rewrite (3.24) in the following way

$$\bar{P}(\lambda) = (\lambda+\zeta)[p^n(\lambda) + \rho_1] + \rho_2 p^k(\lambda) \quad (3.25)$$

where

$$p^s(\lambda) := \Pi_{i=1}^{s}(c_i+\lambda)(a_i+\lambda).$$

To find Hopf point loci, we exploit the fact that $\bar{P}(\lambda)$ defined in (3.25) depends linearly on ρ_1 and ρ_2. At Hopf points $\lambda = iy, y \in \mathbb{R}$ so the two equations

$$\mathbb{R}e\left(\bar{P}(iy)\right) = \mathcal{P}_1(y, \rho_1, \rho_2) = 0 \tag{3.26}$$

$$\mathbb{I}m\left(\bar{P}(iy)\right) = \mathcal{P}_2(y, \rho_1, \rho_2) = 0 \tag{3.27}$$

represent a solvable linear system whose solution (ρ_1, ρ_2) is parametrized by the local frequency y.

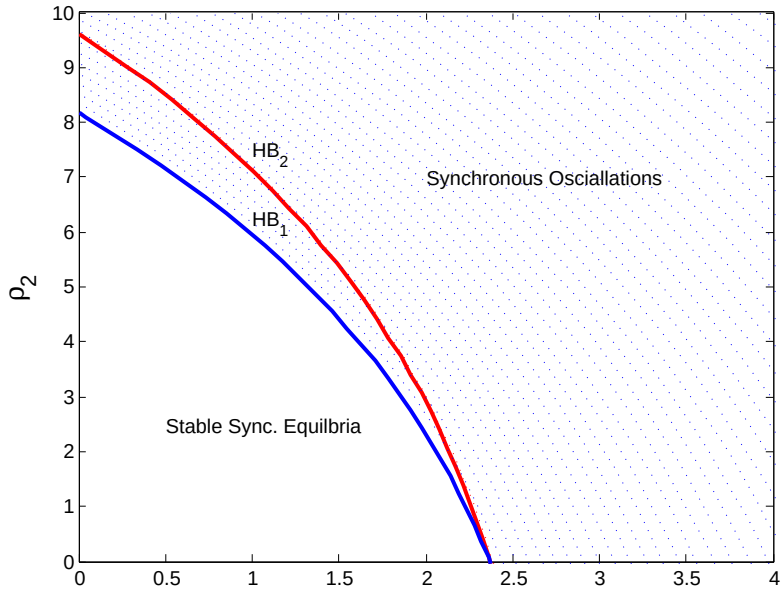

Figure 3.4: Shows the loci of Hopf curves HB_i of the repressilator model [12] derived by solving the system (3.26)-(3.27) for $\zeta = \zeta_i, i = 1, 2$. The blue HB_1 curve is the locus of Hopf points that depend on the quorum sensing parameter q. In contrast, the red HB_2 curve is the locus of Hopf points that do not depend on q. Above HB_1 the sole (synchronous) equilibria is unstable (shaded region). For (ρ_1, ρ_2) below this curve, the sole equilibria is stable. Parameter values needed to compute Hopf curves are $(\beta, k_{s0}, k_{s1}, \eta, q) = (1, 1, 0.01, 2, 0.2)$.

We demonstrate this procedure for finding Hopf loci on the Garcia-Ojalvo *et al.* represillator model [12] which belongs to the Nf-Ns class of models. The results

of these calculations are used in Figure 4 to plot the two Hopf Loci curves defined by $\zeta = \zeta_i, i = 1, 2$. In addition to these two curves (3.26)-(3.27) was solved using $\lambda = x + iy$ for various positive x values. Such curves correspond to locations within the (ρ_1, ρ_2)-plane where the sole equilibria are unstable (shaded region). For the parameters used in Figure 4 we observe:

- Only the Hopf locus HB_1 separates regions of equilibria stability. Moreover, only this curve depends explicitly on q through $\zeta_1 = k_{s0} + (1 - q)\eta$. The destabilization of the equilibria at HB_1 occurs at smaller ρ_k values than those on HB_2 as ρ_k is increased $(k = 1, 2)$. Thus, in this sense and this case, the quorum sensing mechanism causes an *early* onset of system oscillations (HB_1 and HB_2 coincide when $q = 0$).

- The Hopf locus HB_1 corresponds to roots of polynomial $Q(\lambda)$ which by Remark 3.0.8 corresponds to birth of synchronous oscillations i.e oscillations that are identical in each cell.

We conclude this section by noting the emergence of Hopf points in other model parameters can also be found but must be located numerically. One such result is shown in Figure 5. Two analogous curves for HB_1 and HB_2 are shown in the (α, β)-plane. In the inlay, a bifurcation diagram of the A_1 component versus α for $\beta = 1$ and $N = 2$ cells is shown. The emergence of periodic orbits (and their stability) is clearly evident. Lastly, note that for each α the model has at most one (synchronous) attractor. As a reminder it is for this reason we refer to this class of models as monostable.

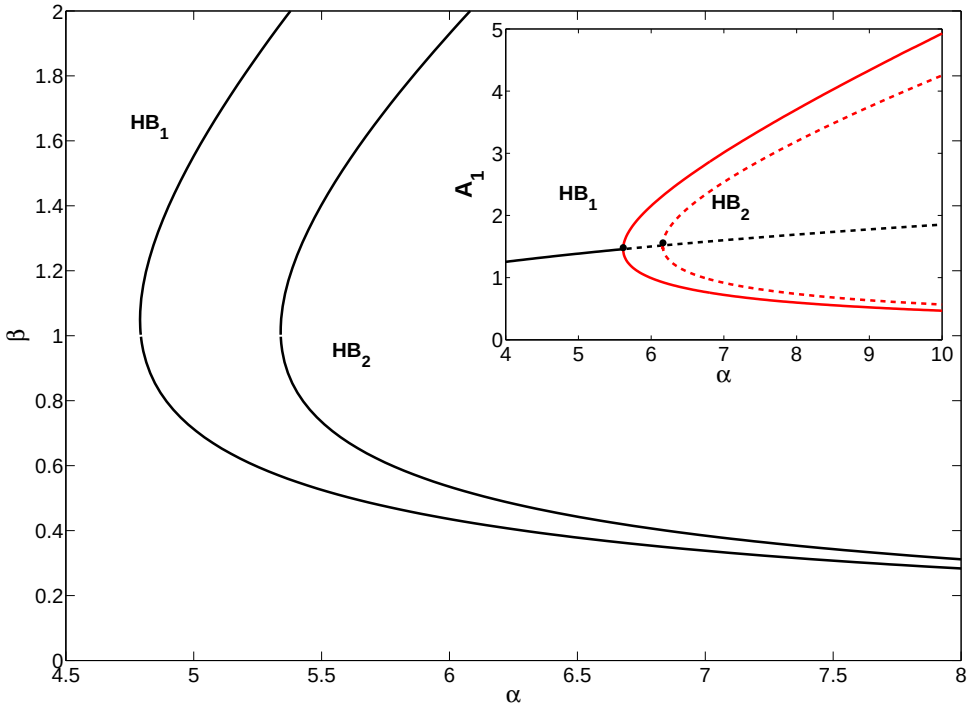

Figure 3.5: Shows Hopf Bifurcation loci in an $N = 2$ cell model. The criticality of the Hopf bifurcations is indicated in the inlay for $\beta = 1$. For all α shown the model is monostable. Parameter values used were $(n, m, \kappa, k_{s0}, \eta, k_{s1}, q) = (2, 1, 25, 1, 2, 0.01, 1)$

Bistable Models

In this section we analyze the effects of different positive feedback mechanisms for the quorum sensing. When the system is not Nf-Ns, multiple equilibria are possible and the dynamics can be much more complicated. We illustrate such possibilities on two simple variants (see Figure 3.1) of the repressilator model (3.1) of Ojalvo [12]. In the original model [12], tetR ($\Omega = A$) provided positive feedback. Alternately, in [18, 33, 34] it was assumed cI provided the feedback ($\Omega = B$). In this case, the sole change to the model was the second term of the auto-inducer equation. For clarity,

these two models are defined by

$$\begin{aligned}
\dot{a}_i &= -a_i + \Phi(C_i) && (tetR)\\
\dot{A}_i &= -\beta A_i + \beta a_i && (TetR)\\
\dot{b}_i &= -b_i + \Phi(A_i) && (cI)\\
\dot{B}_i &= -\beta B_i + \beta b_i && (CI)\\
\dot{c}_i &= -c_i + \Phi(B_i) + \Gamma(S_i) && (lacI)\\
\dot{C}_i &= -\beta C_i + \beta c_i && (LacI)
\end{aligned} \tag{3.28}$$

where, when $\Omega = B$, the autoinducer equation is

$$\dot{S}_i = -(k_{s0} + \eta)S_i + k_{s1}B_i + \frac{\eta\ q}{N}\sum_{i=1}^{N} S_i \tag{3.29}$$

When $\Omega = C$, the autoinducer equation is:

$$\dot{S}_i = -(k_{s0} + \eta)S_i + k_{s1}C_i + \frac{\eta\ q}{N}\sum_{i=1}^{N} S_i \tag{3.30}$$

Note that we use the lower case variable names a_i, b_i, c_i in (3.28) for time dependent protein concentrations. This should not be confused with the use of the same letters as parameter names in the generalized Nf-Ns models.

At least for (3.29), such minor differences were shown to profoundly change the behavior of the network. Here we seek a unified theory to provide a partial explanation of such differences. Firstly we use the same procedure outlined in Section 3 to determine equilibria values. Regardless of whether A, B or C provides positive feedback

$$a_i = \Phi(c_i) \qquad b_i = \Phi^2(c_i)$$

Then, at equilibrium,

$$S_i = \gamma_1 \Phi(c_i) + \gamma_0 S \tag{3.31}$$

$$S_i = \gamma_1 \Phi^2(c_i) + \gamma_0 S \tag{3.32}$$

$$S_i = \gamma_1 c_i + \gamma_0 S \tag{3.33}$$

in which case c_i must be the a root of (respectively)

$$F_a(c) \equiv \Phi^3(c) + \Gamma(\gamma_1 \Phi(c) + \gamma_0 S) - c \tag{3.34}$$

$$F_b(c) \equiv \Phi^3(c) + \Gamma(\gamma_1 \Phi^2(c) + \gamma_0 S) - c \tag{3.35}$$

$$F_c(c) \equiv \Phi^3(c) + \Gamma(\gamma_1 c + \gamma_0 S) - c \tag{3.36}$$

In all three cases $\Phi^3(c) - c$ is an initially (strictly) positive decreasing function which is negative for all c sufficiently large. Thus the monotonicity properties of F_x are relegated to those of the second (middle) term of F_x. In Theorem 3.0.9 we proved $F_a'(c) < 0$ for all c, a fact which depended on the argument of Γ being a decreasing function of c. As a consequence, F_a had a sole root and only synchronous equilibria were possible. Synchronous equilibria are also possible in the other cases. Such equilibria have $S_i = S$ for all i where from (5.4)-(5.9) we deduce

$$S = \gamma \Phi(c)$$

$$S = \gamma \Phi^2(c)$$

$$S = \gamma c$$

where

$$\gamma = \frac{\gamma_1}{1 - \gamma_0}$$

and c is any root of

$$\begin{aligned} F_a(c) &= \Phi^3(c) + \Gamma(\gamma\Phi(c)) - c \\ F_b(c) &= \Phi^3(c) + \Gamma(\gamma\Phi^2(c)) - c \\ F_c(c) &= \Phi^3(c) + \Gamma(\gamma c) - c \end{aligned}$$

respectively. In Figure 6 we show graphs of $F_b(c)$ and $F_c(c)$ for various S values demonstrating bistability is possible for both mechanisms. In both cases, $F_x(c;S) = 0$ for three distinct roots

$$c = \bar{c}_1(S), \bar{c}_2(S), \bar{c}_3(S) \qquad , \qquad S \in (S_-, S_+)$$

The red curves in Figure 6 show the saddle node bifurcations of $F_x(c;S) = 0$, namely $S = S_-$ and $S = S_+$. Only for $S \in (S_-, S_+)$ can $F_x(c;S) = 0$ have three roots. Consequently, the associated systems have three synchronous equilibria $c_i = \bar{c}_k(S)$, $k = 1, 2, 3$.

Additional asynchronous equilibria may exist but they must satisfy a consistency condition. To define this condition we note system equilibrium are uniquely determined by:

$$\mathbf{c} \equiv (\bar{c}_{m_1}(S), \bar{c}_{m_2}(S), \ldots \bar{c}_{m_N}(S)) \qquad , \qquad m_k \in \{1, 2, 3\}$$

For this illustration we consider the case where C provides the positive feedback to the autoinducer so that S_i satisfy (3.30). Then, adding (3.33) in $i = 1, 2, \cdots N$ and

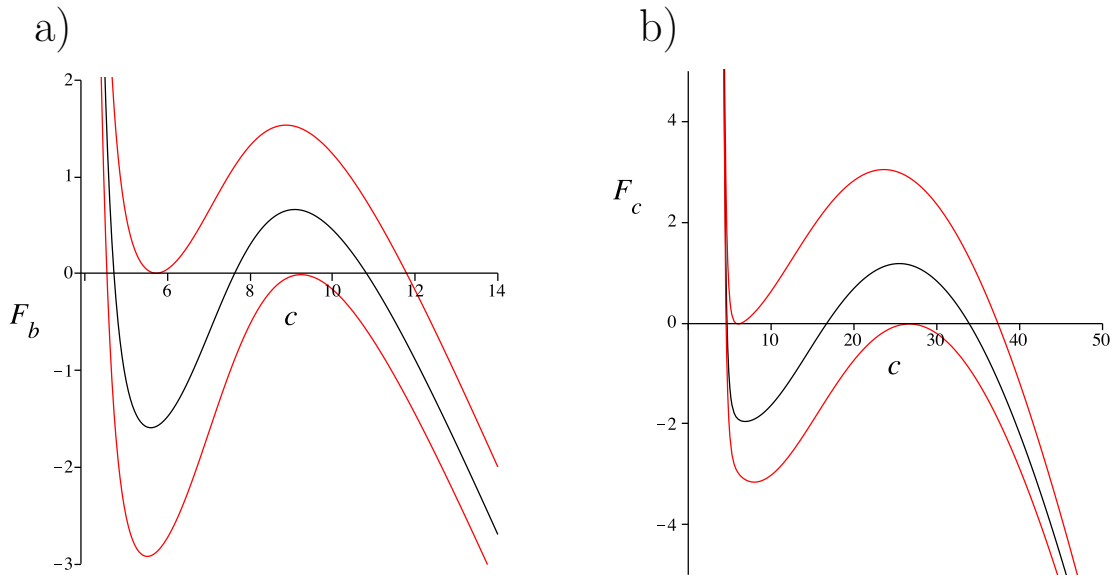

Figure 3.6: Shows plots of $F_b(c;S)$ (left) and $F_c(c;S)$ (right) for various values of autoinducer concentration S. In both cases, saddle-node bifurcations are evident (red). For $S \in (S_-, S_+)$, both functions have three roots. Otherwise, F_b and F_c have single roots. Parameter values the B-feedback in a) were $\mu = (\alpha, \beta, \kappa, n, m, k_{s0}, k_{s1}, \eta, q) = (216, 0.1, 25, 2.6, 1, 1, 0.01, 2, 0.3)$. For C-feedback the parameter values were $\mu = (\alpha, \beta, \kappa, n, m, k_{s0}, k_{s1}, \eta, q) = (216, 1.0, 55, 2.6, 2, 15, 0.6, 2, 0.4)$

dividing by the number of cells N we find S must be equal to the average

$$S = \gamma \left(\frac{N_1}{N} \, \bar{c}_1(S) + \frac{N_2}{N} \, \bar{c}_2(S) + \frac{N_3}{N} \, \bar{c}_3(S) \right) \equiv \Lambda_{(N_1,N_2,N_3)}(S) \tag{3.37}$$

where N_k is the number of components with $\bar{c}_k(S)$. Alternately, if B provides the autoinducer feedback, averaging (3.32) yields the consistency condition

$$S = \gamma \left(\frac{N_1}{N} \, \Phi^2\left(\bar{c}_1(S)\right) + \frac{N_2}{N} \, \Phi^2\left(\bar{c}_2(S)\right) + \frac{N_3}{N} \, \Phi^2\left(\bar{c}_3(S)\right) \right) \equiv \Lambda_{(N_1,N_2,N_3)}(S) \tag{3.38}$$

In Figure 7 we show a plot of $\Lambda(S)$ versus S for $N = 3$ cells and all permutations

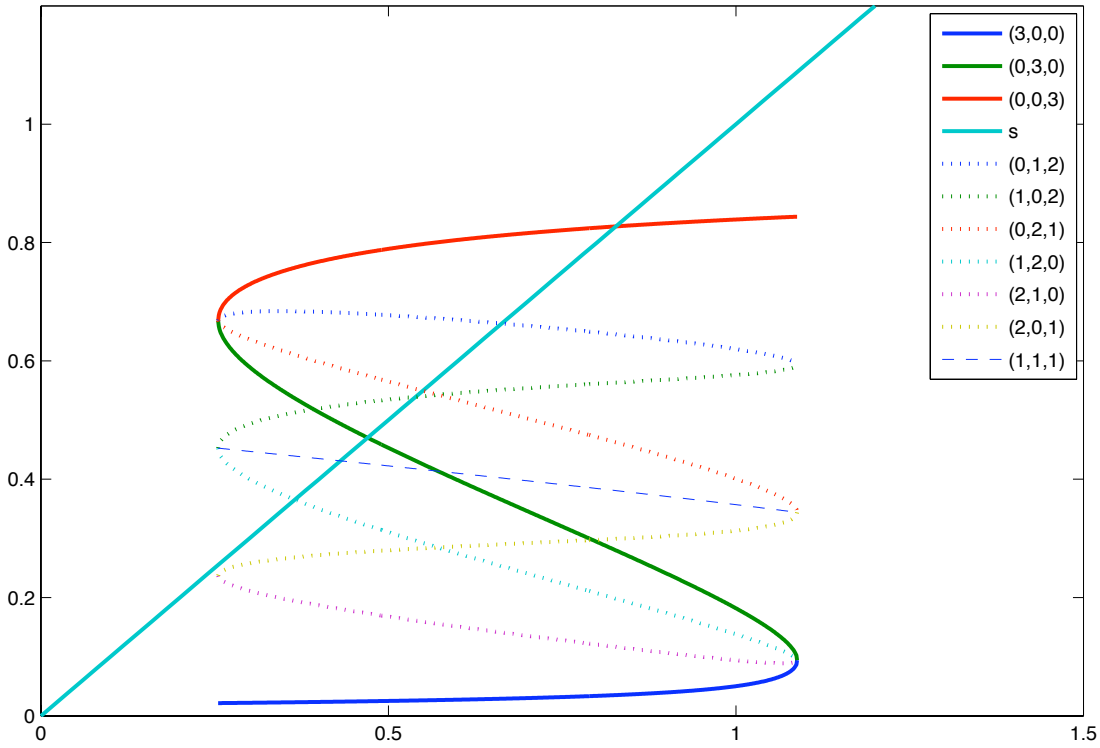

Figure 3.7: Asynchronous equilibria with B feedback. Shows a plot of $\Lambda(S)$ for all different (N_1, N_2, N_3) values versus S (straight line). The S values at intersection points are the only S values possible for (all) equilibria.

of (N_1, N_2, N_3). Since B provides the autoinducer feedback, the consistency condition (3.38) defines $\Lambda(S)$. Then, each intersection point in Figure 6 corresponds to a value of S at which the system has an equilibria. Recalling S is the average autoinducer concentration at equilibria, the individual cell equilibria values S_i are most generally not the same. Intersections above with the bold lines indicate the three possible synchronous equilibria. All others are asynchronous. We see in Figure 7 that many of these (dashed lines) also undergo saddle node bifurcations. Regardless, given (3.38), the S values of all intersection points lie within (S_-, S_+). Additional Hopf bifurcations which emerge from these new equilibria must also occur for S within this

same interval. It is therefore of great interest to understand when such intervals exist and how broad they are.

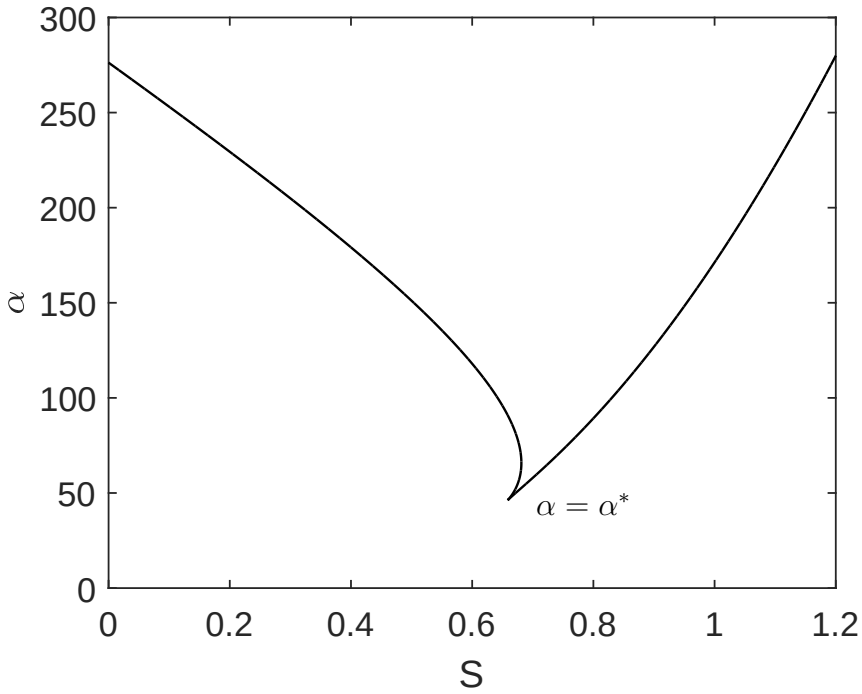

Figure 3.8: Numerical continuation of the interval (S_-, S_+) illustrated in Figure 3.8. As the parameter α is decreased the interval disappears in a cusp bifurcation when $S_- = S_+$. At low α the system is monostable. Parameter values for the computations were $\mu = (\alpha, \beta, \kappa, n, m, k_{s0}, k_{s1}, \eta, q) = (*, 0.1, 25, 2.6, 1, 1, 0.01, 2, 0.3)$.

In Figure 8 we show the numerical continuation of the interval $I = (S_-, S_+)$ as a function of the activation parameter α. The interval width decreases with α and ultimately disappears in a cusp bifurcation at $\alpha = \alpha^*$. Consequently, the system becomes monostable for $\alpha < \alpha^*$. For $\alpha > \alpha^*$ there are a multitude of asynchronous equilibria as predicted in Figure 7. One example showing this is presented in Figure 9 where model parameter values are set to those in Figure 7 while varying the quorum sensing parameter q. Even though the number of cells $N = 3$ is small there are numerous stable and unstable branches of equilibria, as well as saddle node and Hopf bifurcations. Numerical studies show such bifurcation diagrams to be typical of the bistable B feedback variant (Koseska *et. al.* [18]).

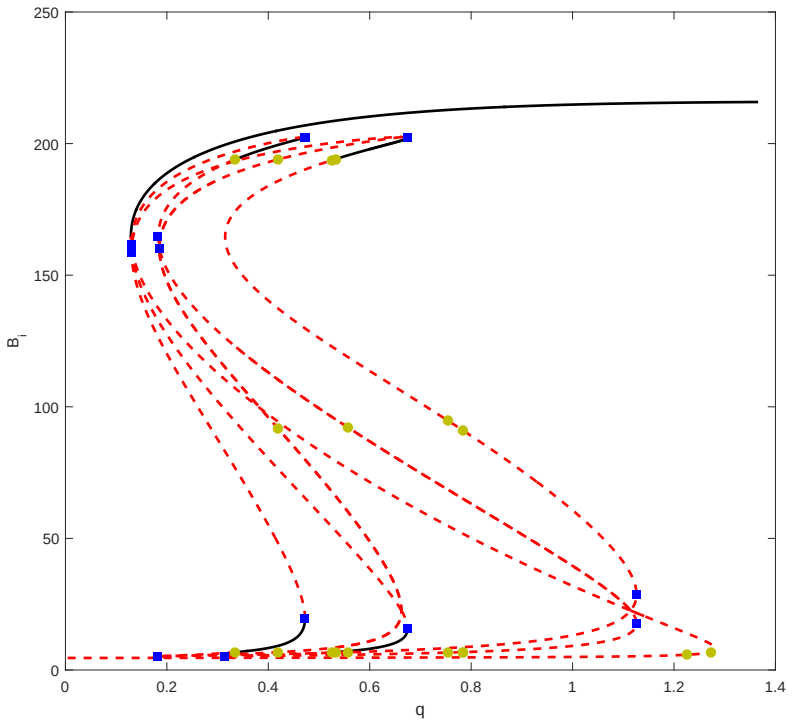

Figure 3.9: B_i versus quorum sensing parameter q for $\alpha > \alpha^*$ value where multistability is possible. Multiple stable (solid) and unstable (dashed) equilibria branches are shown. Saddle node (squares) and Hopf bifurcation (circles) points are numerous even in this $N = 3$ cell computation.

Conclusion

The major contribution of this paper is development of mathematical theory that starts to explain why there are substantial differences in global behavior of diffusively coupled cyclic feedback systems. We define Nf-Ns (negative feedback, negative sensing) systems where the global behavior is characterized by a unique (synchronous) equilibrium which can destabilize only via a Hopf Bifurcation. These results apply to models with n genes and do not depend on the number of cells N in the quorum. Moreover, since the Garcia-Ojalvo *et. al.* [12] repressilator model with quorum sensing is an Nf-Ns system, the same results hold true for it.

The proof of the stability of equilibria in such systems relied heavily on Theorem 3.1 which effectively block diagonalizes the Jacobian. In Theorem 3.1 the associated characteristic polynomial $P(\lambda) = Q(\lambda)R(\lambda)^{N-1} > 0$ hence the (unique) synchronous equilibria can destabilize only via a Hopf bifurcation. The polynomial $Q(\lambda)$ depends on the quorum sensing parameter q whereas $R(\lambda)$ does not. The (sole) imaginary roots of these polynomials characterize two fundamentally different types of Hopf bifurcations. Using symmetry arguments we show that only from one of these, called HB_1, can a branch of synchronous oscillations emerge.

Our analysis also leads to a new method of numerically computing Hopf bifurcation branches in such models. We applied this method to locate these branches for a coupled repressilator model [12], which is one particular example an Nf-Ns system.

In Figure 4, the loci for the Hopf bifurcations in the (ρ_1, ρ_2)-parameter space was found for the Garcia-Ojalvo *et. al.* [12] model. There the Hopf branch HB_1 divides the space into two regions, one where only the synchronous equilibria is stable and one where only the emergent oscillations are stable. Thus, the system is only monostable.

We also note that the Hopf locus HB_1 separating different regions of stability [3] was the only branch whose position in the parameter space depends on the quorum sensing parameter q and the emergent periodic orbits represent synchronous oscillations.

In Section 3 we examined $K = 3$ variants of [12] with $\Omega = B$ and $\Omega = C$ providing feedback to the autoinducer. As these variants were not Nf-Ns systems, multiple equilibria are possible. For both variants, the existence of system equilibria reduced to finding roots of a scalar function F_x. For some parameter values $F_x(S)$ had a cubic shape allowing for multiple equilibria. This is clearly evident in Figure 6a)-b) where multiple roots exist only for $S \in (S_-, S_+)$ where S is the average autoinducer concentration S. Individual system equilibria are neatly portrayed in Figure 7 as intersection points. Such points yield the S values where equilibria must satisfy respective consistency conditions.

Though no analytical results for equilibria stability were presented, subsequent numerical results in Figure 8 indicate that two or more such equilibria can be stable and coexist. It is for this reason such systems are referred to as bistable. In reality such systems are multi-stable and can have a plethora of Hopf and saddle node bifurcations as well as synchronous and asynchronous equilibria. In these cases the global dynamics are extremely complicated and have numerous different (asymmetric) stable solutions. These are hard to categorize since their basins of attraction are not known apriori (see Ulner *et. al.* [34] and Koseska *et. al.* [18] for a couple of examples of studies in this regard). We should stress that such systems are also subject to threshold behavior, as with other bistable systems. For instance, in Figure 8 we demonstrate that interval (S_-, S_+) of S for which the system has multiple equilibria disappears in a cusp bifurcation at $\alpha = \alpha^*$. For $\alpha < \alpha^*$ the system is monostable and complex system dynamics can therefore exist only if $\alpha > \alpha^*$.

[3] of equilibria and periodic orbits

It remains an open question as to why there is such a fundamental difference in the behavior of Nf-Ns and Nf-Ps systems, i.e., those where the diffusive coupling is mediated through a positive loop. This paper presents an extension of work done more than two decades ago that characterized global dynamics of both positive and negative feedback systems [13, 14, 20]. While the numerical results suggest that the complete characterization of the global dynamics of Nf-Ps systems may not be possible, our results on monostability of Nf-Ns systems represents a first step in characterization of global dynamics of these systems.

REFERENCES CITED

[1] E. Abbe, *Community detection and stochastic block models: recent developments*, ArXiv e-prints (2017).

[2] Vadim S Anishchenko, Tatyana E Vadivasova, and Galina I Strelkova, *Deterministic nonlinear systems: a short course*, Springer Series in Synergetics, Springer, Cham, 2014.

[3] Albert-Laszlo Barabasi and Reka Albert, *Emergence of scaling in random networks*, Science **286** (1999), no. 5439, 509–512.

[4] Yuxin Chen and Theodore Kolokolnikov, *A minimal model of predator–swarm interactions*, Journal of The Royal Society Interface **11** (2014), no. 94.

[5] H. Chiba and G. S. Medvedev, *The mean field analysis for the Kuramoto model on graphs I. The mean field equation and transition point formulas*, ArXiv e-prints (2016).

[6] Y.-P. Choi, S.-Y. Ha, and Z. Li, *Emergent dynamics of the Cucker-Smale flocking model and its variants*, ArXiv e-prints (2016).

[7] Silvia De Monte, Francesco d'Ovidio, Sune Danø, and Preben Graae Sørensen, *Dynamical quorum sensing: Population density encoded in cellular dynamics*, PNAS **104** (2007), no. 47, 18377.

[8] Ana Paula S Dias and Ana Rodrigues, *Hopf bifurcation with s_n-symmetry*, Nonlinearity **22** (2009), 627–666.

[9] P. Erdős and A. Renyi, *On the evolution of random graphs*, Publication of the Mathematical Institute of the Hungarian Academy of Sciences (1960).

[10] K. Fellner and G. Raoul, *Stable stationary states of non-local interaction equations*, Math. Models Methods Appl. Sci (2010), no. 20, 2267–2291.

[11] Santo Fortunato, *Community detection in graphs*, Physics Reports **486** (2010), 75–174.

[12] Jordi Garcia-Ojalvo, Michael Ellowitz, and Steven Strogatz, *Modeling a synthetic multicellular clock: repressilators coupled by quorum sensing*, PNAS **101** (2004), no. 30, 10955–10960.

[13] Tomáš Gedeon, *Cyclic feedback systems*, Memoirs of AMS **134** (1998), 637.

[14] Tomáš Gedeon and Konstantin Mischaikow, *Structure of the global attractor of cyclic feedback systems*, J. Dynamics Di. Eq. **7** (1995), 141–190.

[15] Tomas Gedeon, Mark Pernarowski, and Adam Wilander, *Cyclic feedback systems with quorum sensing coupling*, Bulletin of mathematical biology **78** (2016), no. 6, 1291–1317.

[16] Martin Golubitsky, Ian Stewart, and David Schaeffer, *Singularities and groups in bifurcation theory*, Appl. Math. Sci. 69, vol. II, Springer, New York.

[17] T. Kolokolnikov, Y. Huang, and M. Pavlovski, *Singular patterns for an aggregation model with a confining potential*, Physica D (2012).

[18] Aneta Koseska, Ekkehard Ullner, Evgenii Volkov, Juergen Kurths, and Jordi García-Ojalvo, *Cooperative differentiation through clustering in multicellular populations*, J. Theor. Bio. **263** (2010), 189–202.

[19] J. D. Lambert, *Computational methods in ordinary differential equations*, John Wiley & Sons, Inc., 1973.

[20] John Mallet-Paret and Hal Smith, *The poincare-bendixson theorem for monotone cyclic feedback systems*, J. Dynamics and Diff. Equations **2** (1990), 367–421.

[21] S. G. McCalla, M. B. Short, and P. J. Brantingham, *The Effects of Sacred Value Networks Within an Evolutionary, Adversarial Game*, Journal of Statistical Physics **151** (2013), 673–688.

[22] Georgi S Medvedev, *The nonlinear heat equation on dense graphs and graph limits*, SIAM J. Math. Analysis **46** (2014), no. 4, 2743–2766.

[23] C. Milling, C. Caramanis, S. Mannor, and S. Shakkottai, *Distinguishing Infections on Different Graph Topologies*, ArXiv e-prints (2013).

[24] Lawrence Page, Sergey Brin, Rajeev Motwani, and Terry Winograd, *The pagerank citation ranking: bringing order to the web.*, Technical Report 1999-66, Stanford InfoLab, November 1999, Previous number = SIDL-WP-1999-0120.

[25] Louis Pecora and Thomas Carroll, *Master stability functions for synchronized coupled systems*, Phys. Rev. Letters **80** (1998), no. 10, 2109–2112.

[26] Ilya Potapov, Evgenii Volkov, and Alexey Kuznetsov, *Dynamics of coupled repressilators: the role of mrna kinetics and transcription cooperativity*, Phys. Rev. E. **83** (2011), no. 031901.

[27] Albert N. Shiryaev, *Probability*, 2 ed., Graduate Texts in Mathematics, no. 95, Springer.

[28] Ian Stewart, *Symmetry methods in collisionless many-body problems*, J. Nonlinear Sci. **6** (1996), 543–563.

[29] Hui Sun, David Uminsky, and Andrea Bertozzi, *Stability and clustering of self-similar solutions of aggregation equations*, **53** (2012).

[30] Annette Taylor, Mark. Tinsley, Fang Wang, Zhaoyang Huang, and Kenneth Showalter, *Dynamical quorum sensing and synchronization in large populations of chemical oscillators*, Science **323** (2009), 614–619.

[31] C. D. Thron, *The secant condition for instability in biochemical feedback control: Parts i and ii*, Bull. Math. Biol. **53** (1991), 383–424.

[32] John J Tyson and Hans G Othmer, *The dynamics of feedback control circuits in biochemical pathways*, Progress in Theoretical Biology, vol. 5, Academic Press, New York, 1978.

[33] E. Ullner, A. Zaikin, E. Volkov, and J. Garcia-Ojalvo, *Multistability and clustering in a population of synthetic genetic oscillators via phase-repulsive cell-to-cell communication*, Phys. Rev. Letters **99** (2007), 148103.

[34] Ekkehard Ullner, Aneta Koseska, Jürgen Kurths, Evgenii Volkov, Holger Kantz, and Jordi Garcia-Ojalvo, *Multistability of synthetic genetic networks and repressive cell-to-cell communication*, Phys. Rev. E. **78** (2008), 031904.

[35] James von Brecht, Theodore Kolokolnikov, Andrea L Bertozzi, and Hui Sun, *Swarming on random graphs*, Journal of Statistical Physics **151** (2013), no. 1-2, 150–173.

[36] James von Brecht, Benny Sudakov, and Andrea L Bertozzi, *Swarming on random graphs ii*, Journal of Statistical Physics **158** (2014), no. 3, 699–734.

[37] Y. Yang, Y. Li, and A. Kuznetsov, *Characterization and merger of oscillatory mechanisms in an artificial genetic regulatory network*, Chaos **19** (2009), 033115.

[38] George F. Young, Luca Scardovi, Andrea Cavagna, Irene Giardina, and Naomi E. Leonard, *Starling flock networks manage uncertainty in consensus at low cost*, PLOS Computational Biology **9** (2013), no. 1, 1–7.

[39] Zahari Zlatev, István Faragó, and Ãgnes Havasi, *Stability of the richardson extrapolation applied together with the θ-method*, Journal of Computational and Applied Mathematics **235** (2010), no. 2, 507–517, Special Issue on Advanced Computational Algorithms.

APPENDICES

APPENDIX A

DERIVATION OF LIMITING EQUATION

In this section of the Appendix, we seek to establish the limiting equations from Remark 2.0.35, seen in (2.41)–(2.42).

We provide some work here for the two-community case, but we will note that it extends in an obvious way to three or more communities. First, by definition of m_i

$$\begin{aligned}\frac{\mathrm{d}m_i}{\mathrm{d}t} &= \frac{1}{n_i}\sum_{x_j\in C_i}\frac{\mathrm{d}x_j}{\mathrm{d}t}\\ &= \frac{1}{Nn_i}\sum_{x_j\in C_i}\left(\sum_{k=1}^{N} e_{Njk}F(|x_j-x_k|)\frac{x_j-x_k}{|x_j-x_k|}\right).\end{aligned}$$

For a particular i, we split the inner sum into two components; the first is the sum over indices belonging to C_i, whereas the second is the sum over all other indices – the ones not belonging to C_i. With two communities, this yields

$$\begin{aligned}\frac{\mathrm{d}m_1}{\mathrm{d}t} &= \frac{1}{Nn_1}\sum_{x_j\in C_1}\left(\sum_{x_k\in C_1} e_{Njk}F(|x_j-x_k|)\frac{x_j-x_k}{|x_j-x_k|} + \sum_{x_k\in C_2} e_{Njk}F(|x_j-x_k|)\frac{x_j-x_k}{|x_j-x_k|}\right),\\ \frac{\mathrm{d}m_2}{\mathrm{d}t} &= \frac{1}{Nn_2}\sum_{x_j\in C_2}\left(\sum_{x_k\in C_1} e_{Njk}F(|x_j-x_k|)\frac{x_j-x_k}{|x_j-x_k|} + \sum_{x_k\in C_2} e_{Njk}F(|x_j-x_k|)\frac{x_j-x_k}{|x_j-x_k|}\right).\end{aligned}$$

Next, we offer a remark that simplifies this sum a bit.

Remark A.0.1. *For each community C_i and an undirected graph (e_{Njk}), it is the case that*

$$\sum_{x_j\in C_i}\sum_{x_k\in C_i} e_{Njk}F(|x_j-x_k|)\frac{x_j-x_k}{|x_j-x_k|} = 0,$$

so that

$$\frac{\mathrm{d}m_i}{\mathrm{d}t} = \frac{1}{Nn_i}\sum_{x_j\in C_i}\left(\sum_{x_k\notin C_i} e_{Njk}F(|x_j-x_k|)\frac{x_j-x_k}{|x_j-x_k|}\right).$$

To see the first point, define (for fixed N) a function $G:\mathbb{Z}\cap([1,N]\times[1,N])\to\mathbb{R}$:

$$G(j,k) = e_{Njk}F(|x_j-x_k|)\frac{x_j-x_k}{|x_j-x_k|}. \tag{A.1}$$

The arguments of the function $G(j,k)$ are skew symmetric, in the sense that $G(k,j)$ is the negative of $G(j,k)$, as

$$G(k,j) = e_{Nkj}F(|x_k - x_j|)\frac{x_k - x_j}{|x_k - x_j|} = e_{Njk}F(|x_j - x_k|)\frac{-(x_j - x_k)}{|x_j - x_k|} = -G(j,k),$$

where equality of the e_{Nkj} and e_{Njk} arises due to the underlying network being undirected, and thus the graph being symmetric ($E^T = E$). Hence the sum in the remark can be rewritten as

$$\sum_{x_j \in C_i} \sum_{x_k \in C_i} G(j,k) = \sum_{x_j \in C_i} G(j,j) + \sum_{x_j, x_k \in C_i, j \neq k} G(j,k) + G(k,j).$$

Clearly, both terms are zero – the second due to the above fact. The conclusion in the Remark follows immediately.

First, as is most relevant to the system (2.7) used in the first chapter of this dissertation, we present arguments for the limiting system when its dimension is $d = 1$. To do this, suppose we have $x_j \in C_i$ for some i, j. For all such k so that $x_k \notin C_i$, let us additionally suppose that $|x_j - x_k| > (1+\kappa)^{-1}$ for all time t. In this event, for all k

$$G(j,k) = \begin{cases} e_{Njk}\left(1 - (x_j - x_k)\right) & : \quad x_j \geq x_k, \\ e_{Njk}\left((x_k - x_j) - 1\right) & : \quad x_j < x_k. \end{cases}$$

Now, for fixed i

$$\sum_{x_k \notin C_i} G(j,k) = (N - n_i)\text{mean}_k\left(G(j,k)\right) \to (N - n_i)\mathbb{E}\left(G(j,k)\right)$$

by the Law of Large Numbers as $N \to \infty$. Since the e_{Njk} are generated independently

of the value of F, we have

$$\begin{aligned}\mathbb{E}\left(G(j,k)\right) &= \mathbb{E}\left(e_{Njk}\right)\mathbb{E}\left(F(|x_j - x_k|)\frac{x_j - x_k}{|x_j - x_k|}\right)\\ &= p\mathbb{E}\left(F(x_j - x_k)\right)\\ &= pF\left(\mathbb{E}(x_j - x_k)\right) = p\left(1 - (x_j - \mathbb{E}(x_k))\right),\end{aligned}$$

assuming (without loss of generality) that $x_j - x_k > (1+\kappa)^{-1} > 0$, where the equalities in the last line come from linearity of the expected value.

Let us now suppose we have a simple two-community system, with n_1 particles in the first community and n_2 particles in the second community. Assume also that for all $x_j \in C_1, x_k \in C_2$, we have $x_k - x_j > (1+\kappa)^{-1}$. Then

$$\begin{aligned}\frac{\mathrm{d}m_2}{\mathrm{d}t} &\sim \frac{1}{Nn_2}\sum_{x_j \in C_2}\left(n_1 p(1 - (x_j - \mathbb{E}_{C_1}x_k))\right)\\ &\sim \frac{n_1 p}{N}\left(1 - (\mathbb{E}_{C_2}(x_j) - \mathbb{E}_{C_1}(x_k))\right) = \frac{n_1 p}{N}\left(1 - (m_2 - m_1)\right).\end{aligned}$$

Conversely, $\dot{m}_1$ differs by a minus sign and a coefficient of $n_2 p/N$ rather than $n_1 p/N$. Often we imagine each community's relative size as fixed in the limit $N \to \infty$; if both communities are equivalently sized, then these coefficients are $\pm 1/2$, respectively.

Note that this work can be generalized to $\mathbb{R}^d$, for $d \geq 2$. If we let

$$\Phi(z) = F(|z|)\frac{z}{|z|}, \tag{A.2}$$

we then would like to expand (A.2) about $m_1 - m_2$. As before, we typically assume the absolute value of this difference is large enough so that it exceeds the overlap region in the domain of $F(r)$. That is, we assume $|m_1 - m_2| > \frac{1-b}{1+a}$. For $d = 2$ below, we let appropriate superscripts denote the components of Φ and z, and M_0 and M_1

denote the first and second components of $M = m_1 - m_2$, respectively.

$$
\begin{aligned}
(\Phi)^0 \sim{}& \frac{M_0\left(1-|M|\right)}{|M|} + \left(\frac{1-|M|}{|M|} - \frac{\left(M_0\right)^2\left(1-|M|\right)}{|M|^3} - \frac{\left(M_0\right)^2}{|M|^2}\right)\left(z^0 - M_0\right) \\
&- \left(\frac{M_0 M_1}{|M|^2} + \frac{M_0 M_1\left(1-|M|\right)}{|M|^3}\right)\left(z^1 - M_1\right). \\
(\Phi)^1 \sim{}& \frac{M_1\left(1-|M|\right)}{|M|} + \left(\frac{1-|M|}{|M|} - \frac{\left(M_1\right)^2\left(1-|M|\right)}{|M|^3} - \frac{\left(M_1\right)^2}{|M|^2}\right)\left(z^1 - M_1\right) \\
&- \left(\frac{M_0 M_1}{|M|^2} + \frac{M_0 M_1\left(1-|M|\right)}{|M|^3}\right)\left(z^0 - M_0\right).
\end{aligned}
$$

Though considerably less concise than our usage in Equations (2.41)–(2.42), this offers similar value to the system for $d = 2$ and, more broadly, analogs for $d > 2$. We note that in higher dimensions, for which many-clustered stable states are prevalent, we may desire an approximation of Equation (2.7) with *more* than two clusters. We suggest, though it is beyond the scope of our work here, that this can be accomplished by decomposing the interaction terms of this equation by community, and then expanding each about $m_i - m_j$, for an appropriate community index i and j, respectively.

APPENDIX B

COMPUTATION OF CLOSED-FORM SOLUTION FOR $\tilde{M}_I$, $I = 1, 2$.

In this section of the Appendix, we seek to establish an explicit solution for the limiting equations of Remark 2.0.35.

Here, we consider the equations (2.41)–(2.42):

$$\begin{aligned}\frac{\mathrm{d}m_1}{\mathrm{d}t} &\sim -\frac{n_2 p}{N}(1+(m_1-m_2)),\\ \frac{\mathrm{d}m_2}{\mathrm{d}t} &\sim \frac{n_1 p}{N}(1+(m_1-m_2)).\end{aligned}$$

Note that this is a linear, first-order system in $\mathbf{m} = (m_1, m_2)^T$. We rewrite the above in the form $\dot{\mathbf{m}} = A\mathbf{m} + \mathbf{f}$:

$$\frac{\mathrm{d}\mathbf{m}}{\mathrm{d}t} = \begin{bmatrix} \frac{-n_2 p}{N} & \frac{n_2 p}{N} \\ \frac{n_1 p}{N} & -\frac{n_1 p}{N} \end{bmatrix} \mathbf{m} + \begin{bmatrix} -\frac{n_2 p}{N} \\ \frac{n_1 p}{N} \end{bmatrix}.$$

We set the characteristic equation $|A - \lambda I| = 0$ and solve for λ to find the eigenvalues $\lambda_1 = 0, \lambda_2 = -p(n_1+n_2)/N = -p$. Then, we find our eigenvectors by determining the nullspaces of $A - \lambda_1 I$ and $A - \lambda_2 I$, respectively:

$$\mathbf{x}_1 = \begin{bmatrix} 1 \\ 1 \end{bmatrix} \quad , \quad \mathbf{x}_2 = \begin{bmatrix} -n_2/n_1 \\ 1 \end{bmatrix}.$$

Our homogeneous solution is thus $\mathbf{m}_{\text{hom}} = C_1 e^{\lambda_1 t}\mathbf{x}_1 + C_2 e^{\lambda_2 t}\mathbf{x}_2$ for arbitrary constants C_i. To find our particular solution, we substitute a constant vector into the system to determine

$$\mathbf{m}_{\text{part}} = \begin{bmatrix} 0 \\ 1 \end{bmatrix}.$$

Combining these into a general solution, we have

$$\mathbf{m}(t) = \begin{bmatrix} 1 & -\frac{n_2}{n_1}e^{-pt} \\ 1 & e^{-pt} \end{bmatrix} \begin{bmatrix} C_1 \\ C_2 \end{bmatrix} + \begin{bmatrix} 0 \\ 1 \end{bmatrix}.$$

As a result, it is the case that

$$|\tilde{m}_1(t) - \tilde{m}_2(t)| = 1 + C_2 e^{-pt}\left(\frac{n_2}{n_1} + 1\right) = 1 + e^{-pt}\left(\frac{NC_2}{n_1}\right).$$

If we initialize $\tilde{m}_1$ and $\tilde{m}_2$ at a separation of S, this implies $C_2 = (S-1)n_1/N$, which forces the difference between approximate centers of mass to be $1+e^{-pt}(S-1)$. Hence, $|\tilde{m}_1(t) - \tilde{m}_2(t)| = 1 + \epsilon$ where

$$e^{-pt}(S-1) = \epsilon.$$

Equivalently, this is satisfied for

$$t = -\ln\left(\frac{\epsilon}{S-1}\right)/p.$$

Again, we stress that $\epsilon \in (0, S-1]$ is the separation tolerance – how close we desire to get to a difference between centers of mass of 1, $S \in (1, \infty)$ is the initial separation, and $p \in (0, 1]$ is the outer connection probability between communities.

APPENDIX C

COMMUNITIES OF DIFFERENT SIZE

Throughout this work, we have generally assumed all communities are sized equivalently; this was indeed a simplifying assumption. Even with the bare minimum of two communities, allowing each community's size to vary independently is like adding another parameter $\gamma = |C_1|/|C_2|$ (the community-to-community size ratio) to the system. Still, to cover all our bases, we offer a brief look into how varying community sizes may affect the dynamics of the system (2.7).

To do this, as a heuristic we consider the motion of a single particle p. This p is subject to an average of forces, generated from its interactions with the system's many other particles, stemming from each cluster's center of mass, and weighted by the number of particles at the cluster. As such, the direct impact of increasing the proportion of our particles at one cluster location, thereby decreasing the proportion of system particles at the second, is to increase the relative strength of the force felt from the first cluster while diminishing the force felt from the second. This occurs because the averaging that occurs in (2.7) will more heavily weight particles in the first location. Hence, an increase in the ratio γ increases the repulsion exhibited by the kernel F over short distances and decreases the repulsive force over long distances, provided the particle is immediately adjacent to the first cluster to begin with. Provided this shift in the balance of first and second cluster forces eventually results in the first dominating, it is thus clear that this secular increase in community size can only drive the system *away* from stability.

We illustrate this point with a simple example; we take both inner and outer connection probabilities to be 1 (yielding the system in which every particle interacts with every other particle) and $\kappa = 1/2$. We allow γ, the first-to-second-community size ratio, to vary between 1 (communities of the same size) and 10 while holding $N = 200$ fixed. Clearly, the proportion of system particles in the first and second community, for a given γ, must satisfy

$$\tau_1 = \frac{\gamma}{\gamma + 1} \quad , \quad \tau_2 = \frac{1}{\gamma + 1}.$$

As $\tau_i N$ for $i = 1, 2$ need not be an integer, there is some imprecision here. However, we conclude it is negligible; the smallest value of τ_i is attained when $\gamma = 10$. Here, $\tau_2 = 1/11$, and rounding in either direction so that we achieve an integer value of particles leads to an effective proportion of either 0.09 or 0.095 – both rather close to $1/11 = .0909\ldots$. The relative error here would of course decrease as $N \to \infty$. Finally, we run the system until we determine it has converged and record the ultimate separation between each community's centers of mass, providing us with valuable information on the degree of mixing that has taken place. We present the data below.

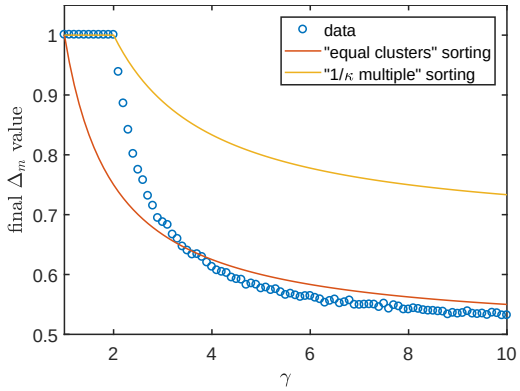

Figure C.1: A plot of community 1 to community 2 size ratio (γ) against the difference in centers of mass at large t (Δm_{final}) with two approximation schemes. All-to-all connections were used for the network structure; that is, $E = \mathbf{1}_{N,N}$. Initial conditions were a small uniform noise profile atop the point-source initial conditions with community 1 being placed at $x = -100$ and community 2 being placed at $x = 100$; results for each data point were averaged over 100 such initializations. Repulsion parameter $\kappa = 1/2$.

As seen here, the unmixed two-cluster state appears stable up to the precise threshold of $\gamma = 2$. This occurs when the size of the first community is two times the size of the other community. The location of this "bifurcation" is as we might expect: the stable state can only destabilize if the repulsive small-r force overwhelms the repulsive large-r force. As each particle p is connected to every member of both clusters, the bifurcation we are referring to here occurs when the cluster-to-cluster

size ratio exceeds $\frac{1}{\kappa}$ (in this case, 2).

After this point, we surmise the clusters equalize their masses as $t \to \infty$. This seems to, in practice, imply the larger cluster sheds particles to the smaller cluster until the two are equivalent; this is because (from the perspective of a particle near the larger cluster), the repulsive force of the larger cluster overpowers the repulsive force felt from the smaller cluster — at least assuming the particle is fully connected to both.

Hence, if we have $\tau_1 = \gamma/(\gamma+1)$ of the total system particles at the first cluster location and $\tau_2 = 1/(\gamma+1)$ at the second, we seek α, a proportion of total system particles to subtract from cluster 1 and add to cluster 2. Clearly, α must satisfy the following equation to bring the clusters into equilibrium:

$$\frac{\gamma}{\gamma+1} - \alpha = \frac{1}{\gamma+1} + \alpha.$$

Solving for α, we find a shift of particles from the first to second cluster of $\alpha = (\gamma-1)/(2\gamma+2)$ is necessary.

If the aforementioned assumption holds, our next question is perhaps "how does this affect the center of mass separation, $|m_1(t) - m_2(t)|$, as $t \to \infty$?" Without loss of generality, we assume the first and second cluster locations are at $x = 0$ and $x = 1$, respectively. Correspondingly,

$$\hat{p}_{1,2} = \frac{\alpha(\gamma+1)}{\gamma} \quad , \quad \hat{p}_{2,2} = 1,$$

are the proportions of particles belonging to community 1 and community 2 at the second cluster location (respectively). As such, $m_1 \to \hat{p}_{1,2}$ and $m_2 \to \hat{p}_{2,2} = 1$. We find that

$$|m_1(t) - m_2(t)| \to 1 - \frac{(\gamma-1)}{2\gamma} = \frac{\gamma+1}{2\gamma}$$

after some simplification, denoting this quantity Δm_{final}. As we take $\gamma \in [1, \infty)$ ($\gamma = 1/2$, for instance, is equivalent to $\gamma = 2$ with a relabeling of communities 1 and

2), the quantity Δm_{final} is monotone decreasing over its domain, attaining a maximum of 1 at $\gamma = 1$ — same-size communities — and tending to 1/2 as $\gamma \to \infty$, that is when the second community becomes vanishingly small relative to the first community.

Upon reflection, it might seem like the more logical assumption is that the larger community bleeds particles until a $|C_1|/|C_2|$ size ratio of $1/\kappa$ is met. This is indeed because the maximum 'load'' the larger cluster can bear is that of $1/\kappa$ the particles of the smaller community. For instance, if $\kappa = 1/2$, then short-distance repulsive forces from F are half as strong as long-distance repulsive forces. As the motion of each particle is a simple average of all individual forces, then the first community retains and *gains* stability by shedding as many particles as it needs to — in the latter case, up to a ratio of $1/\kappa$.

If we carry out the same process as before to find Δm_{final} we will instead set $\gamma/(\gamma+1) + \alpha$ equal to $1/\kappa$ times $(1/(\gamma+1) + \alpha)$. This leads to

$$\alpha = \frac{\gamma k - 1}{(\gamma+1)(\kappa+1)},$$

which yields

$$\Delta m_{\text{final}} = \begin{cases} 1 & : \quad 1 \leq \gamma \leq \frac{1}{\kappa}, \\ \frac{(\gamma+1)}{\gamma(\kappa+1)} & : \quad \gamma > \frac{1}{\kappa}. \end{cases}$$

Note that the first piece of this equation arises from the observation that the first community need not lose any particles if $\gamma < 1/\kappa$. We plot this relationship (solid line) in the same figure. Of the two schemes – which we denote as "equal clusters" sorting and "$1/\kappa$ multiple" sorting – only the latter captures the threshold between stability of the unmixed state and instability thereof (evidenced by the difference between centers of mass remaining at 1 until $\gamma = 1/\kappa$). However, after this point it is woefully inadequate, appearing to capture the rate of change in Δm_{final} well for γ large but not its magnitude. Of course, under this assumption

$$\lim_{\gamma \to \infty} \Delta m_{\text{final}} = \frac{1}{\kappa+1},$$

which is equivalent to 2/3 if $\kappa = 1/2$. Conversely, while the "equal clusters" assumption implicitly posits the unmixed two-cluster state as *never* attractive when $\gamma \neq 1$ (which is obviously not the case here), within some error it captures the rate of change in Δm_{final} and remains close to these actual values as γ gets large. It appears to share a common limit of $\frac{1}{2}$ as $\gamma \to \infty$, additionally; for $\gamma = 100$ and parameters as before, except for $N = 1000$, the (averaged) actual and approximate values of Δm_{final} are both within 1% of 1/2.

APPENDIX D

HEURISTIC FOR NECESSARY CONDITION FOR STABILITY OF UNMIXED TWO-CLUSTER STATE

We offer an explanation for the stability (resp. instability) of the two-cluster steady state (2.6) with no mixing. Recall the definition of F (in the system with dimension $d = 1$) in (2.5):

$$F(r) = \min(\kappa r, 1 - r).$$

Again, it is typically assumed that $\kappa > 0$, so the first piece is used when $r < (\kappa + 1)^{-1} < 1$, and the second is used for $r \geq (\kappa + 1)^{-1}$. Somewhat informally, we consider the behavior of a single particle relative to a small perturbation of the aforementioned state (2.6). We denote this particle by p, and the two clusters' centers of mass at time t by $m_1(t)$ and $m_2(t)$, respectively. Without loss of generality, we also assume $m_1(t) < m_2(t)$ for all time t.

Of course, the clusters often contain many particles, yet we need not assume they are all precisely at m_1 or m_2. Provided the particles in each cluster do not stray too far from the center of mass at time t, we may pass the cluster-interaction terms to a simple expected value computation over the total p-to-m_1 and p-to-m_2 interactions. Using C_1 and C_2 as a partition of our node set into the two clusters, this is the condition that

$$\begin{aligned} |p - x_i| &< (\kappa + 1)^{-1} \quad , \quad i \in C_1 \\ |p - x_j| &> (\kappa + 1)^{-1} \quad , \quad j \in C_2 \end{aligned}$$

The particle p feels a repulsive force κ-proportional to its distance from a particle located at m_1. As $F(1 - r) = r$ for this p, it feels a repulsive force 1-proportional to the same distance and directed away from a particle located at m_2. Given this, a straightforward computation yields (here i is the index of the particle p, the a_{ij} are

generated independently, and $\sum_j a_{ij}$ is large)

$$\sum_{x_j \in C_1} a_{ij} F(|p - x_j|) \frac{p - x_j}{|p - x_j|} \sim \kappa\varphi(p - m_1),$$

where $\alpha = \sum_j a_{ij}$. We perform the same computation with the second cluster to find

$$\sum_{x_k \in C_2} a_{ik} F(|p - x_k|) \frac{p - x_k}{|p - x_k|} \sim -\beta(p - m_1),$$

where $\beta = \sum_k a_{ik}$. Hence p is attracted to the stable first cluster provided $\frac{\varphi}{\beta} < \frac{1}{\kappa}$. What if, for instance, p is on the "outside" of m_1, so that $p < m_1 < m_2$? In this case, p is repelled κ-proportional to its distance from a hypothetical particle located at m_1. Similarly, $F(1 + r) = -r$ implies p is *attracted* (1-proportional to this same distance) to a particle located at m_2. Again, as the balance of forces is identical to the previous case, we arrive at p being attracted to the stable first cluster provided the same inequality holds.

An important part of the above heuristic was that $\sum_j a_{ij}$ is large. Again we are motivated by the idea of the Law of Large Numbers; if, for instance, $\varphi \sum_j a_{ij}$ is small, that is there are very few nonzero terms in a particular row sum, then $\sum_j a_i j x_j$ may be a rather poor asymptotic approximation to φm_j. Unfortunately, in this case our logic above falls through, as it obviously would not make sense to replace the weighted sums over each community's particles with a simpler quantity only dealing with the community's center of mass. In practice this caveat does not seem to hold much relevance; when we are trying to ascertain whether or not a particle will be attracted to the nearer community (stable), or shoot off in the direction of the other community, we consider a small perturbation of the steady state solution. Hence the perturbation can always be restricted sufficiently small so that individual particles do not deviate beyond a prescribed distance from the center of mass; even here a "loaded die" selection of particles on one of the extreme ends of the community will have a center of mass resembling that of the broader community.

How do we reconcile φ and β with the parameters p and q used for inner and outer connection probabilities? The above characterization offers a useful litmus test for a given, initialized system with random matrix A already specified; our more general question relates to the likelihood of randomly arriving at a stable system given probabilities p, q. To properly frame this question, we first define two random variables: X_p, to be the number of links between p and the first cluster, and Y_p, to be the number of links between p and the second cluster. As the existence of each link is independent of all other links, it is clear that

$$\mathbb{P}\left\{X_p = x, Y_p = y\right\} = \binom{N_1}{x} p^x (1-p)^{N_1 - x} \binom{N_2}{y} q^y (1-q)^{N_2 - y}.$$

Accordingly,

$$\mathbb{P}\left\{\kappa X_p \leq Y_p\right\} = \sum_{x=0}^{N_1} \sum_{y=\lceil \kappa x \rceil}^{N_2} \mathbb{P}\left\{X_p = x, Y_p = y\right\} = \alpha.$$

If, for simplifying purposes we assume $N_1 = N_2 = N/2$, we believe this probability to converge to 1 if $\kappa p/q < 1$ and to 0 if $\kappa p/q > 1$ (as $N \to \infty$). Though we do not have numerical estimates that would undoubtedly be useful here, we illustrate with an example. Suppose $(p_{\text{in}}, p_{\text{out}}) = (0.8, 0.4)$, so that $p/q = 2$. In Figure D.1, data points belonging to different curves represent different $N \in \{50, 100, 250, 500, 1000\}$, and we consider the above probability as a function of κ. We stress that this curve is the probability a *given* particle has inner/outer connection density in excess of $1/\kappa$.

There is an obvious threshold here. Recalling that $p_{\text{in}}/p_{\text{out}} = 2$, we expect there to be a shift in α behavior at $\kappa = 0.5$; that appears to be what we observe in Figure (D.1). For κ values less than 0.5, we see

$$\lim_{N \to \infty} \alpha(\kappa, N) = 1. \tag{D.1}$$

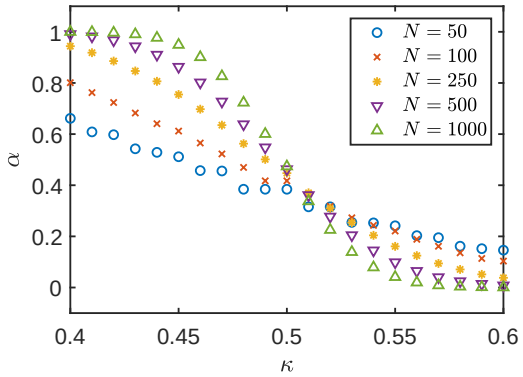

Figure D.1: A plot of α, the probability a given particle has an inner/outer connection density not exceeding $1/\kappa$, as a function of κ. Here, $(p_{\text{in}}, p_{\text{out}}) = (0.8, 0.4)$ and $N \in \{50, 100, 250, 500, 1000\}$.

For κ values in excess of 0.5, we see

$$\lim_{N\to\infty} \alpha(\kappa, N) = 0. \tag{D.2}$$

(D.1) and (D.2) suggest that, given κ so that $1/\kappa < p_{\text{in}}/p_{\text{out}}$, the steady state (2.6) cannot be asymptotically a.s. stable as $N \to \infty$, as (with probability tending to 1), there will exist a particle with inner-to-outer connection density exceeding $1/\kappa$. In this case, stronger near-repulsive forces relative to far-repulsive forces will push this particle away from the cluster it has been seeded at and towards the other cluster. Hence $\alpha \to 1$ appears to be a *necessary* (though perhaps not sufficient) condition for stability of this state.

For a (possibly) sufficient condition, we require *all* of the system's N particles to obey the given condition. Note that, with two even communities of $N/2$ particles, this is simply the N^{th} power of the previous figure's probability quantity. In Figure D.2, we explore this value, denoted $\rho = \rho(\kappa, N)$, as a function of large N values, for several fixed, equivalently-spaced κ.

We observe that each of the ρ slices in fixed κ resemble a roughly sigmoidal shape – they are monotone increasing in N, with a lower bound of $\rho = 0$ for small N, an

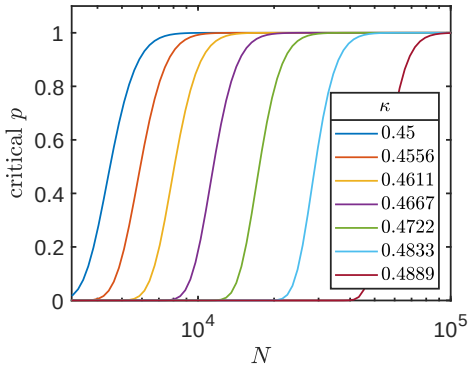

Figure D.2: A plot of the probability *all* N particles have an inner/outer connection density not exceeding $1/\kappa$ as a function of N, for $(p_{\text{in}}, p_{\text{out}}) = (0.8, 0.4)$ and various κ (listed).

upper bound of $\rho = 1$ for large N, and a thin band connecting the two in between. As κ increases, the ρ slices shift to the right (in N), with little apparent effect otherwise. As $\kappa \to p_{\text{in}}/p_{\text{out}}$, this shift (note the log scale on the N-axis) increases at a seemingly above-linear relationship, hence if $\kappa \approx p_{\text{in}}/p_{\text{out}}$, excessively large N values may be necessary to attain $\rho \approx 1$ and thus stability of the steady state (2.6). Although it is not depicted, we also note that tested values of $\kappa > 0.5$, even those ≈ 0.5, resulted in near-zero probabilities for even modestly large N.

As a final, brief aside, we suggest more extensive results along this vein may lead to a characterization of the bifurcation threshold observed in, e.g., Figures 2.6 and 2.12. Again taking $p_{\text{in}} = 0.8$ for illustrative purposes, observe that $p_{\text{out}} = 0.6$ is on the "mixed" side of the threshold, while $p_{\text{out}} = 0.65$ is on the "unmixed" side of the threshold for $N = 200$. Appropriately, our estimation for $\rho(\kappa, N) = \rho(0.5, 200)$ with the latter outer probability is 0.96 – near 1. Our estimation for ρ at the smaller p_{out} value (on the "mixed" side) is 0.04 – near 0. This implies we have crossed the threshold at which ρ' is large somewhere in between, and thus we might suspect the threshold between mixing and well-separated behaviors for (2.7) lies in between.